

**SECRET**

CENTRAL RESEARCH LIBRARY  
DOCUMENT COLLECTION

ORNL-2221, Part 6 134-A  
C-85 - Reactors-Aircraft Nuclear Propulsion Systems

**AEC RESEARCH AND DEVELOPMENT REPORT**

*ANP*

CENTRAL RESEARCH LIBRARY  
DOCUMENT COLLECTION

**LIBRARY LOAN COPY**

DO NOT TRANSFER TO ANOTHER PERSON

If you wish someone else to see this document,  
send in name with document and the library will  
arrange a loan.

MARTIN MARIETTA ENERGY SYSTEMS LIBRARIES



3 4456 0251025 4

AIRCRAFT NUCLEAR PROPULSION PROJECT

QUARTERLY PROGRESS REPORT

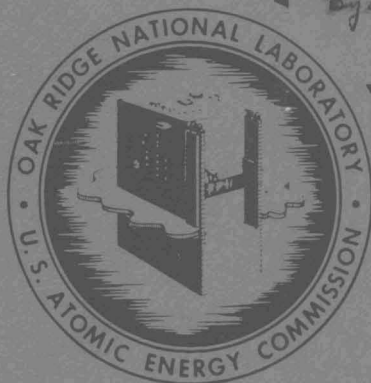
FOR PERIOD ENDING DECEMBER 31, 1956

**DECLASSIFIED**

Classification Changes To:

By University of AEC 1-25-66

By Edward 11/26/67



This document contains Restricted Data as defined in the Atomic Energy Act of 1954. Its transmittal or the disclosure of its contents in any manner to an unauthorized person is prohibited.

**OAK RIDGE NATIONAL LABORATORY**

OPERATED BY

**UNION CARBIDE NUCLEAR COMPANY**

A Division of Union Carbide and Carbon Corporation



POST OFFICE BOX X · OAK RIDGE, TENNESSEE

**RESTRICTED DATA**

This document contains Restricted Data as defined in the Atomic Energy Act of 1954. Its transmittal or the disclosure of its contents in any manner to an unauthorized person is prohibited.

**SECRET**

107  
57

107  
57

107  
57

107  
57

ORNL-2221, Part 6  
C-85 - Reactors-Aircraft Nuclear Propulsion Systems

This document consists of 68 pages.  
Copy 34 of 229 copies. Series A.

Contract No. W-7405-eng-26

**AIRCRAFT NUCLEAR PROPULSION PROJECT**

**QUARTERLY PROGRESS REPORT**

For Period Ending December 31, 1956

W. H. Jordan, Director  
S. J. Cromer, Co-Director  
A. J. Miller, Assistant Director

DATE ISSUED

MAR 26 1957

OAK RIDGE NATIONAL LABORATORY  
Operated by  
UNION CARBIDE NUCLEAR COMPANY  
A Division of Union Carbide and Carbon Corporation  
Post Office Box X  
Oak Ridge, Tennessee

**RESTRICTED DATA**

This document contains Restricted Data as defined in the Atomic Energy Act of 1954. Its transmission or the disclosure of its contents in any manner to an unauthorized person is prohibited.

**SECRET**

MARTIN MARIETTA ENERGY SYSTEMS LIBRARIES



3 4456 0251025 4

ORNL-2221, Part 6  
C-85 - Reactors-Aircraft Nuclear Propulsion Systems

INTERNAL DISTRIBUTION

1. R. G. Affel
2. C. J. Barton
3. M. Bender
4. D. S. Billington
5. F. F. Blankenship
6. E. P. Blizard
7. C. J. Borkowski
8. W. F. Boudreau
9. G. E. Boyd
10. M. A. Bredig
11. E. J. Breeding
12. W. E. Browning
13. F. R. Bruce
14. A. D. Callihan
15. D. W. Cardwell
16. C. E. Center (K-25)
17. R. A. Charpie
18. R. L. Clarke
19. C. E. Clifford
20. J. H. Coobs
21. W. B. Cottrell
22. D. D. Cowen
23. S. Cromer
24. R. S. Crouse
25. F. L. Culler
26. D. R. Cuneo
27. J. H. DeVan
28. L. M. Doney
29. D. A. Douglas
30. E. R. Dytko
31. W. K. Eister
32. L. B. Emlet (K-25)
33. D. E. Ferguson
34. A. P. Fraas
35. J. H. Frye
36. W. T. Furgerson
37. R. J. Gray
38. A. T. Gresky
39. W. R. Grimes
40. A. G. Grindell
41. E. Guth
42. C. S. Harrill
43. E. E. Hoffman
44. H. W. Hoffman
45. A. Hollaender
46. A. S. Householder
47. J. T. Howe
48. W. H. Jordan
49. G. W. Keilholtz
50. C. P. Keim
51. F. L. Keller
52. M. T. Kelley
53. F. Kertesz
54. J. J. Keyes
55. E. M. King
- 56-57. J. A. Lane
58. R. B. Lindauer
59. R. S. Livingston
60. R. N. Lyon
61. H. G. MacPherson
62. R. E. MacPherson
63. F. C. Maienschein
64. W. D. Manly
65. E. R. Mann
66. L. A. Mann
67. W. B. McDonald
68. J. R. McNally
69. F. R. McQuilkin
70. R. V. Meghreblian
71. R. P. Milford
72. A. J. Miller
73. R. E. Moore
74. J. G. Morgan
75. K. Z. Morgan
76. E. J. Murphy
77. J. P. Murray (Y-12)
78. M. L. Nelson
79. G. J. Nettle
80. R. B. Oliver
81. L. G. Overholser
82. P. Patriarca
83. R. W. Peelle
84. S. K. Penny
85. A. M. Perry
86. C. Pigg
87. P. M. Reyling
88. A. E. Richt
89. M. T. Robinson
90. H. W. Savage
91. A. W. Savolainen
92. R. D. Schultheiss
93. D. Scott
94. J. L. Scott
95. E. D. Shipley



- 96. A. Simon
- 97. O. Sisman
- 98. J. Sites
- 99. M. J. Skinner
- 100. A. H. Snel
- 101. C. D. Susan
- 102. J. A. Swartou
- 103. E. H. Taylor
- 104. R. E. Thoma
- 105. D. B. Trauger
- 106. D. K. Trubey
- 107. G. M. Watson

- 108. A. M. Weinberg
- 109. J. C. White
- 110. G. D. Whitman
- 111. E. F. Wagner (consultant)
- 112. G. C. Williams
- 113. J. C. Wilson
- 114. C. E. Winters
- 115-124. ORNL - Y-12 Technical Library,  
Document Reference Section
- 125-131. Laboratory Records Department
- 132. Laboratory Records, ORNL R.C.
- 133-135. Central Research Library

EXTERNAL DISTRIBUTION

- 136. AF Plant Representative, Baltimore
- 137. AF Plant Representative, Burbank
- 138. AF Plant Representative, Clifton
- 139. AF Plant Representative, Long Beach
- 140. AF Plant Representative, Marietta
- 141-143. AF Plant Representative, Santa Monica
- 144-145. AF Plant Representative, Seattle
- 146. AF Plant Representative, Wichita
- 147. Air Research and Development Command (RDGN)
- 148. Air Technical Intelligence Center
- 149. Air University Library
- 150-152. ANP Project Office, Fort Worth
- 153. Argonne National Laboratory
- 154. Armed Forces Special Weapons Project, Sandia
- 155. Armed Forces Special Weapons Project, Washington
- 156. Assistant Secretary of the Air Force, R&D
- 157-162. Atomic Energy Commission, Washington
- 163. Bureau of Aeronautics
- 164. Bureau of Aeronautics General Representative
- 165. Chicago Operations Office
- 166. Chicago Patent Group
- 167. Chief of Naval Research
- 168. Convair-General Dynamics Corporation
- 169. Curtiss-Wright Corporation
- 170-174. General Electric Company (ANPD)
- 174. Hartford Area Office
- 175. Headquarters, Air Force Special Weapons Center
- 176. Idaho Operations Office
- 177. Lockland Area Office
- 178. Los Alamos Scientific Laboratory
- 179. Marquardt Aircraft Company
- 180. National Advisory Committee for Aeronautics, Cleveland
- 181. National Advisory Committee for Aeronautics, Washington
- 182-184. Naval Air Development and Material Center
- 185. Naval Research Laboratory



- 
186. North American Aviation, Inc. (Missile Development Division)
  187. Nuclear Development Corporation of America
  188. Office of Chief of Naval Operations (OP-361)
  189. Patent Branch, Washington
  - 190-193. Pratt & Whitney Aircraft Division (Fox Project)
  194. San Francisco Operations Office
  195. Sandia Corporation
  196. Sandia Corporation, Livermore
  197. School of Aviation Medicine
  198. USAF Headquarters
  199. USAF Project RAND
  200. University of California Radiation Laboratory, Livermore
  - 201-218. Wright Air Development Center (WCOS-1)
  - 219-228. Technical Information Service Extension, Oak Ridge
  229. Division of Research and Development, AEC, ORO

~~SECRET~~

#### FOREWORD

This portion, Part 6. Aircraft Shielding, of the Aircraft Nuclear Propulsion Project Quarterly Progress Report falls in AEC category C-85, Reactors – Aircraft Nuclear Propulsion Systems, and is therefore being issued separately in order not to further limit distribution of the material that falls in AEC category C-84, Reactors – Special Features of Aircraft Reactors, which has been issued as ORNL-2221, Parts 1–5.

~~SECRET~~



**CONTENTS**

FOREWORD .....	v
SUMMARY .....	ix
PART 6. AIRCRAFT SHIELDING	
6.1 SHIELDING THEORY .....	3
A Monte Carlo Calculation of Multiple Scattering of Neutrons in Air .....	3
6.2 TOWER SHIELDING FACILITY .....	5
Preliminary Differential Gamma-Ray Shielding Tests .....	5
Gamma-Ray Dose Rate Measurements .....	5
Thermal-Neutron Flux Measurements .....	7
Comparison of Thermal-Neutron Detectors .....	8
Effect of Air and Ground Scattering of Fast Neutrons on the Dose Rates Measured in Air and in a Crew-Compartment Mockup .....	8
Measurements in Air .....	12
Measurements in a Crew-Compartment Mockup .....	18
Determination of Scattering Probabilities .....	18
Fast-Neutron Dose Rates in a Crew-Compartment Mockup Resulting from Radiation from a Compartmentalized Reactor Shield Tank .....	31
Description of Reactor Shield and Crew-Compartment Mockup .....	37
Experimental Measurements .....	38
Comparison of Experimental Data with Calculations .....	38
Analysis of the Experimental Data .....	44
Future Experiments .....	50
Determination of Gamma-Ray Dose Rates and Spectra from Soil and Concrete Samples After Irradiation at the TSF .....	51



# ANP PROJECT QUARTERLY PROGRESS REPORT

## SUMMARY

### 6.1. Shielding Theory

A Monte Carlo calculation has been performed to determine the energy flux and angular distribution of air-scattered neutrons from a monodirectional beam at a source-detector separation distance of 64 ft. The source was assumed to be located on an absorbing sphere of diameter  $D_0$ . The diameter was assigned two different values: 0, which resulted in a point source, and 12 ft. Isotropic scattering in the center-of-mass system was taken as the scattering law. The source energies included in the calculations were 0.55, 1.2, 2, 3, and 5 Mev, and the angle of radiation emission from the source was considered to be 2, 15, 30, 60, 90, 135, and 180 deg. The problem was idealized in that the source-detector system was considered as suspended in an infinite body of air.

### 6.2. Tower Shielding Facility

The preliminary differential gamma-ray shielding tests which have been under way for some time have been concluded. The final tests included measurements of the total gamma-ray dose rate inside the G-E crew compartment mockup with the side lead and water shielding removed and measurements of the dose rate at one of the legs of the TSF structure with no shielding around the detector. In addition, thermal-neutron flux measurements were made in air at distances of 25 and 50 ft from the reactor as a function of  $\theta$  (the angle between the reactor beam and the reactor-detector axis) for various values of  $\rho$  (the thickness of the reactor shielding). Thermal-neutron flux measurements were also made along a line normal to the front face of the TSF reactor at several distances varying from 5 to 1000 cm. For these measurements, the reactor was positioned at  $\rho = 16$  cm. A comparison of the response of the three thermal-neutron detectors used throughout the tests was also made.

An experiment designed to study the effects of air and ground scattering of fast neutrons in a typical shielding geometry has been performed. A highly collimated beam of neutrons was obtained for the experiment by placing either of two air-

filled cylindrical aluminum pipes (8- and 15-in. ID) adjacent to the TSR in the reactor tank. Fast-neutron dose rate measurements were made with an unshielded detector at a distance of 64 ft from the reactor tank while both the direction of the beam and the height above the ground were varied. The measurements made as a function of altitude showed a maximum intensity at an altitude varying between 20 and 40 ft. There was a decrease in intensity as higher altitudes were approached, which resulted from a decrease in ground scattering that was larger than the small increase in air scattering. In addition to the in-air measurements, measurements were made inside a compartmentalized crew-compartment mockup with various rear and side shield thicknesses. The resulting data were used to determine the probabilities of fast neutrons scattering into the sides of the crew-compartment mockup. A comparison of the results with values of probabilities determined in earlier experiments with a much more diffuse beam showed good agreement for the region outside the horizontal beam angles of 0 and 30 deg, as was expected.

In order to confirm a calculational procedure developed for the optimization of a divided neutron shield, an experiment was performed which utilized a reactor-shield mockup and a crew-shield mockup whose thicknesses could be varied. The reactor shield, which is spherical in shape, contains many small compartments which can be filled and drained remotely with liquids of densities as high as 2.5. By varying the position of the liquid the shape of the shield, as well as the thickness, could be varied. The crew-shield mockup consists of 33 cylindrical compartments surrounding a central air-filled cylinder. The TSF reactor was placed inside the reactor shield 64 ft from the outside rear of the crew-compartment mockup, and measurements of the neutron dose rate were made inside the crew-compartment mockup as a function of the thickness of water (neutron shield) at the reactor or crew-shield mockup. Relaxation lengths resulting from the experimental data have been compared with those predicted in a calculation.

**SECRET**

Samples of concrete and soil from Marietta, Georgia were irradiated at the TSF in order to determine the degree of activation to be expected at the Lockheed Radiation Facility. The concrete samples consisted of plain concrete, barytes concrete, and one sample of each containing an admixture of 1% boron. All the samples were exposed for 20 hr to the TSF reactor operating at a power of 400 kw. The dose rate at the positions of the concrete samples was 0.725 ergs/g·hr·w, while that at the position of the soil sample was 0.896 ergs/g·hr·w. Subsequent to irradiation the intensity

of the gamma-ray dose rate from the samples was determined as a function of time after irradiation. In addition to the dose rate measurements, pulse-height spectra of gamma rays from the samples were determined. For barytes and soil samples a large part of the dose rate 4 hr after irradiation was due to a thermal  $n$ - $\gamma$  reaction in  $Mn^{55}$ ; between 24 and 100 hr after irradiation the main contribution was from the same reaction in  $Na^{23}$ . For the plain concrete samples the gamma-ray dose rate throughout the first 100 hr after irradiation was essentially due to the thermal  $n$ - $\gamma$  reaction in  $Na^{23}$ .

**SECRET**

Part 6

**AIRCRAFT SHIELDING**

E. P. Blizard

## 6.1. SHIELDING THEORY

### A MONTE CARLO CALCULATION OF MULTIPLE SCATTERING OF NEUTRONS IN AIR

C. D. Zerby

Quantities of importance in the design of the crew-compartment shield of a nuclear-powered aircraft are the angular distribution and energy spectra of radiation incident on the exterior surfaces of the shield. In an effort to provide some fundamental information about this radiation a neutron air-scattering problem to be computed by using the Monte Carlo method was coded for solution on the Oracle at ORNL.

The problem was idealized to have the source and a point detector suspended in an infinite body of air. The source-detector geometry selected for the computation is shown in Fig. 6.1.1. The source was located on an absorbing sphere of diameter  $D_0$  where the axis of symmetry of the radiation leaving the sphere had an angle  $\theta_0$  with respect to the source-detector axis. The distribution of source radiation about the symmetry axis was taken as  $[(J + 1)/2] \cos^J \theta$  per unit solid angle. The values of  $D_0$ ,  $\theta_0$ ,  $J$ , and the separation distance  $g$  were assigned arbitrarily. In particular  $D_0$  was assigned the values 0 ft, which resulted in a point source, and 12 ft;  $J$  was assigned a value of infinity to give a monidirectional beam; and  $g$  was considered to be 64 ft. The values of the density of the air and the amount of moisture in the air were allowed to vary.

The cross sections used for oxygen, nitrogen, and hydrogen were taken from BNL-325.<sup>1</sup> The

<sup>1</sup>D. J. Hughes and J. A. Harvey, *Neutron Cross Sections*, BNL-325 (July 1, 1955).

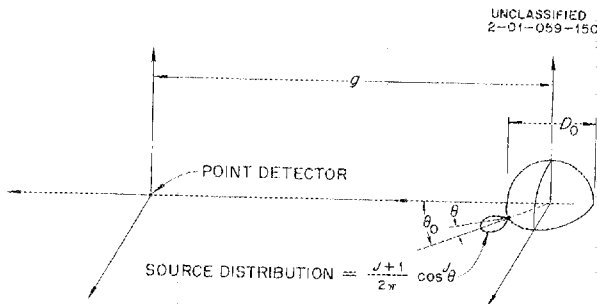


Fig. 6.1.1. Geometry Used for Neutron Air-Scattering Problem.

scattering was considered to be isotropic in the center-of-mass system.

The Monte Carlo method used for this computation differed from the straight analog procedure in that a process of statistical estimation was incorporated. This amounted to summing the probabilities that a neutron would pass through the detector after each of its collisions. The distribution of collisions after the first collision was generated by using standard Monte Carlo methods. The contribution of first-scattered particles to the detector response was calculated systematically in order to approximate a numerical solution.

In order to test this statistical calculation against numerical solutions, the code was altered to duplicate the one-velocity transport equation for an isotropic point source in an infinite, homogeneous medium. The scattering was taken to be isotropic in the laboratory system, and test problems were run for several source-detector separation distances. The result of these test problems are shown in Fig. 6.1.2 and compared with the numerical solutions given by Case, de Hoffmann,

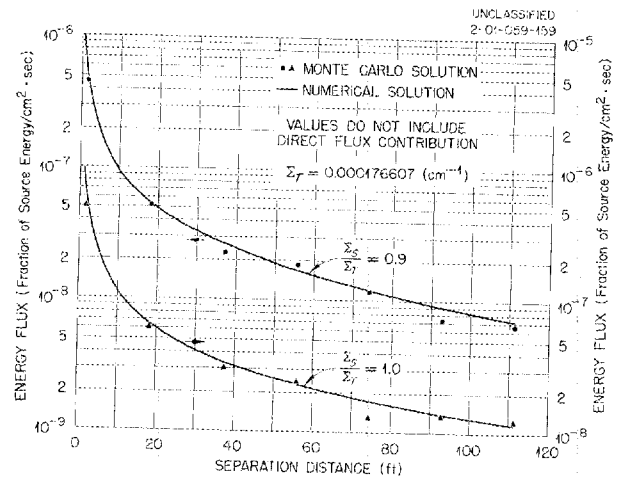


Fig. 6.1.2. Comparison of Numerical Solution of the One-Velocity Boltzmann Equation with a Monte Carlo Solution for an Isotropic Point Source of 1-Mev Neutrons in Infinite Air (Scattering Taken as Isotropic in the Laboratory System; Density of the Air = 0.001293 g/cm<sup>3</sup>).

and Placzek.<sup>2</sup> In one set of problems a ratio of the macroscopic scattering cross section to the total macroscopic cross section of 1.0 was used, while in the other set a ratio of 0.9 was used. In both cases only that portion of the flux which was contributed by particles that had made one or more collisions is presented. In almost every case the error between the statistically determined values and the numerically determined values is less than 10% out to separation distances of 0.6 mean free paths. This is of particular interest, since this error indicates the error that may be expected when a problem is calculated by using energy degradation and isotropic scattering in the center-of-mass system.

A set of problems was then calculated for a source-detector separation distance of 64 ft. These calculations included energy degradation and isotropic scattering in the center-of-mass system. In every case the source was taken as a line beam of monoenergetic neutrons. For one set of problems the diameter of the absorbing sphere was considered to be zero; that is, the source was a point source. In the other set the diameter of the sphere on which the point source was located was considered to be 12 ft. The source energies included in the calculation were 0.55, 1.2, 2, 3, and 5 Mev. For the point source,  $\theta_0$  was considered to be 2, 15, 30, 60, 90, 135, and 180 deg. For the point source on the 12-ft-dia sphere,  $\theta_0$  was considered to be 15, 90, 135, and 180 deg. The results of these calculations included the energy and angular distribution of the neutrons at the detector.

The energy flux at the detector for a source energy of 3 Mev is shown in Fig. 6.1.3. In this figure the flux values do not include the direct flux. The lower curve shows the marked depression in the energy flux caused by the absorbing sphere shielding the detector. It is to be noted that at  $\theta_0 = 180$  deg, the scattered energy flux for the point source was  $0.2324 \times 10^{-8}$  when normalized to a unit energy source. The results of the calculation showed that the single scattering contribution for the point source was only  $0.1217 \times 10^{-8}$ . This is to be compared with the value of  $0.915 \times 10^{-9}$  for the sources on the absorbing sphere.

<sup>2</sup>K. M. Case, F. de Hoffmann, and K. M. Placzek, *Introduction to the Theory of Neutron Diffusion*, vol. 1, U.S. Government Printing Office, Washington 25, D.C., 1953.

Figure 6.1.4 shows the fractional contribution to the scattered energy flux by neutrons which have scattered one, two, and three times. This set of data was obtained from the 3-Mev point source cases shown in Fig. 6.1.3.

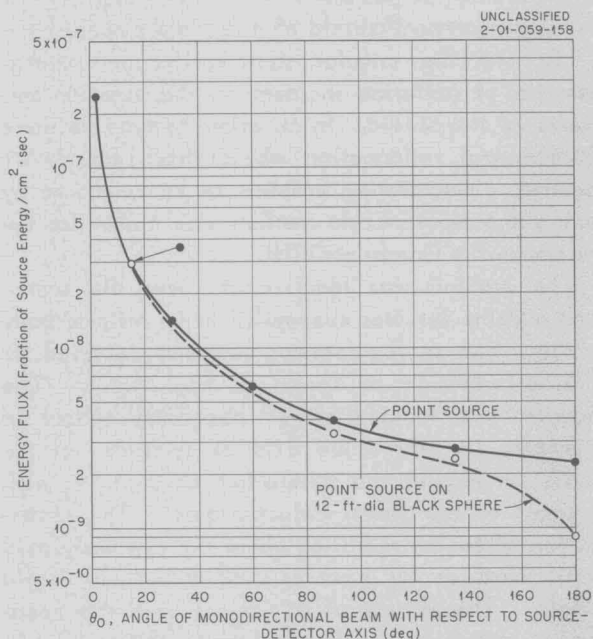


Fig. 6.1.3. Energy Flux of Air-Scattered Neutrons from a Monodirectional Beam of 3-Mev Neutrons at a Source-Detector Separation Distance of 64 ft (Density of the Air =  $0.001250 \text{ g/cm}^3$ ).

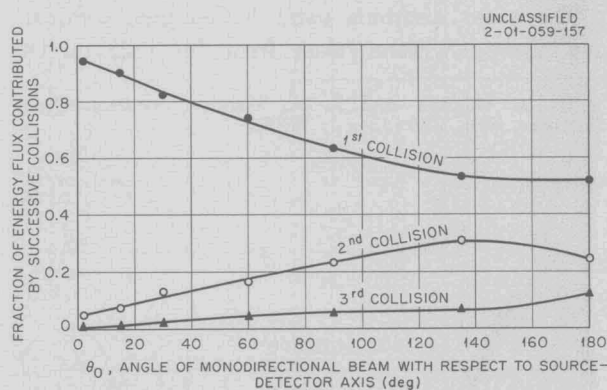


Fig. 6.1.4. Fraction of Energy Flux of Air-Scattered Neutrons from a Point, Monodirectional Beam of 3-Mev Neutrons Contributed by Successive Collisions at a Source-Detector Separation Distance of 64 ft (Density of the Air =  $0.001250 \text{ g/cm}^3$ ).



ANP PROJECT PROGRESS REPORT

thicknesses ( $\rho$ ) of 16 and 45 cm. (In this figure  $x, y, z = 0$  at the center of the inside rear wall of the crew compartment.) The difference in the shapes of the two curves as they approach  $\theta = 180$  deg demonstrates the effect of the thermal-neutron capture gamma rays and air-scattered gamma rays in a geometry where the emergent radiation is sharply peaked away from the detector.

A number of gamma-ray dose rate measurements were made as a function of the distance between the reactor and a detector by fixing an unshielded detector on a TSF leg (No. 1) and varying the position of the reactor tank. The effect of the tower leg on the measured dose rates is assumed to be negligible. Figure 6.2.2 presents these data as a function of separation distance for  $\rho = 45$  cm

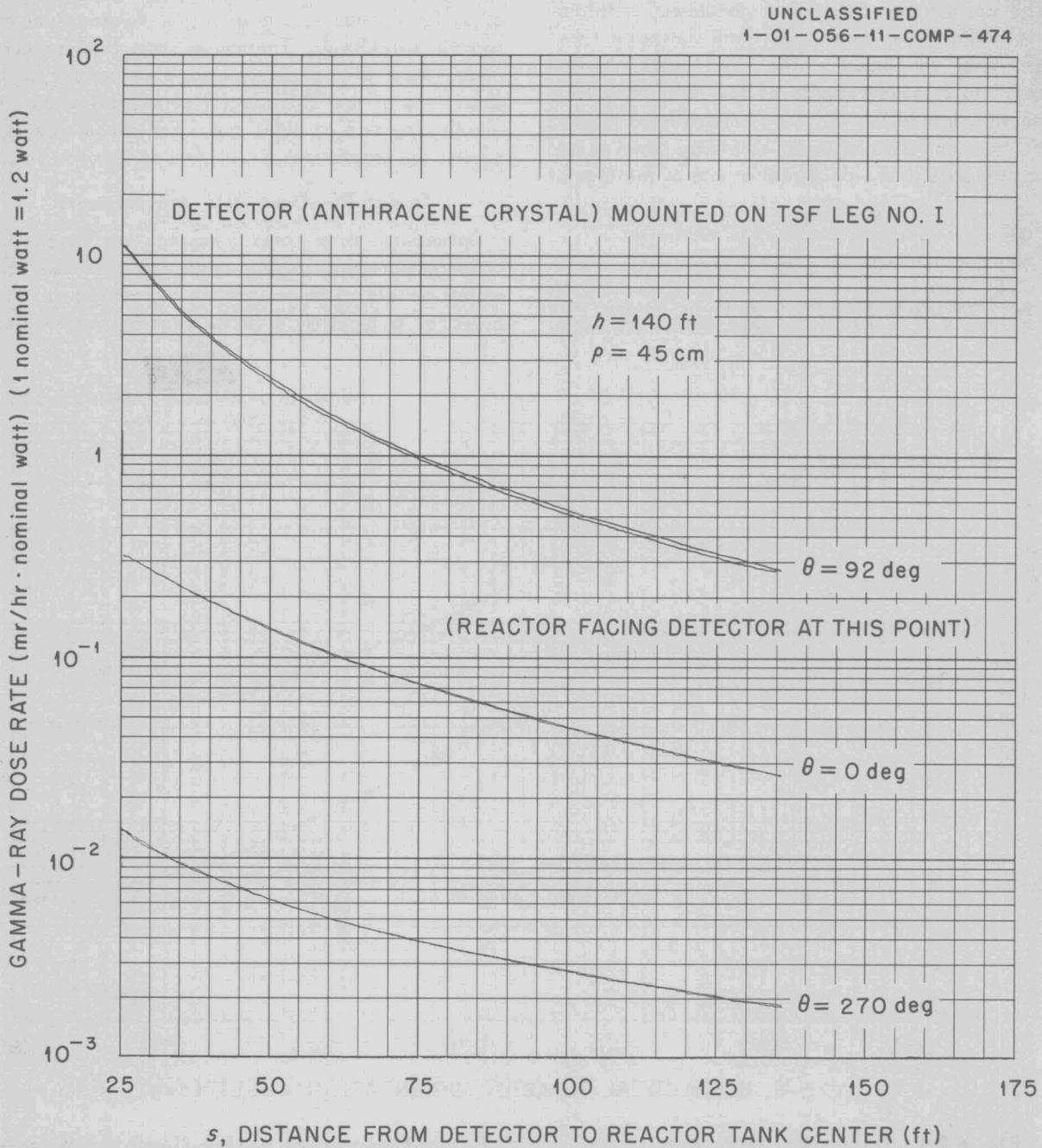


Fig. 6.2.2. Gamma-Ray Dose Rate in Air as a Function of Reactor-Detector Separation Distance for Various Values of  $\theta$ .

and for  $\theta = 0, 92,$  and  $270$  deg. At  $\theta = 92$  deg the reactor is facing the detector. Figure 6.2.3 presents the gamma-ray dose rate at the TSF leg as a function of  $\rho$  for a fixed separation distance of 100 ft.

Examination of the data in Fig. 6.2.2 indicates that the direct-beam dose rate ( $\theta = 92$  deg) follows the inverse distance-squared law to a close approximation. The dose rate with the beam of radiation pointed directly away from the detector ( $\theta = 270$  deg) decreases more rapidly than the inverse distance law but much more slowly than the inverse distance-squared law. As was expected, the dose rate as a function of distance with the beam of radiation directed at 90 deg from the detector ( $\theta = 0$  deg) falls somewhere between the other two curves.

**Thermal-Neutron Flux Measurements**

Measurements have been taken from which a profile of the thermal-neutron flux in the TSF

reactor tank water and in the air normal to the front face of the reactor could be established. Bare and cadmium-covered gold foils, previously calibrated with the ORNL Standard Pile, were exposed at various distances from the reactor, and the thermal-neutron flux as a function of distance from the reactor was determined. The results are shown in Fig. 6.2.4, where the relative position of the reactor tank wall is indicated. The flux in water at various distances from the BSF reactor is also plotted for comparison.<sup>4</sup> From the reactor face to within 5 cm of the tank wall the agreement between the TSF reactor and BSF reactor data is within 10%. Immediately outside the tank wall the thermal-neutron flux is approximately 7% of that predicted from the BSF reactor curve.

Thermal-neutron flux measurements were also made at distances of 25 and 50 ft as a function of

<sup>4</sup>H. E. Hungerford, *Bulk Shielding Facility Water Data Work Sheet*, ORNL CF-52-2-37 (Feb. 1, 1952).

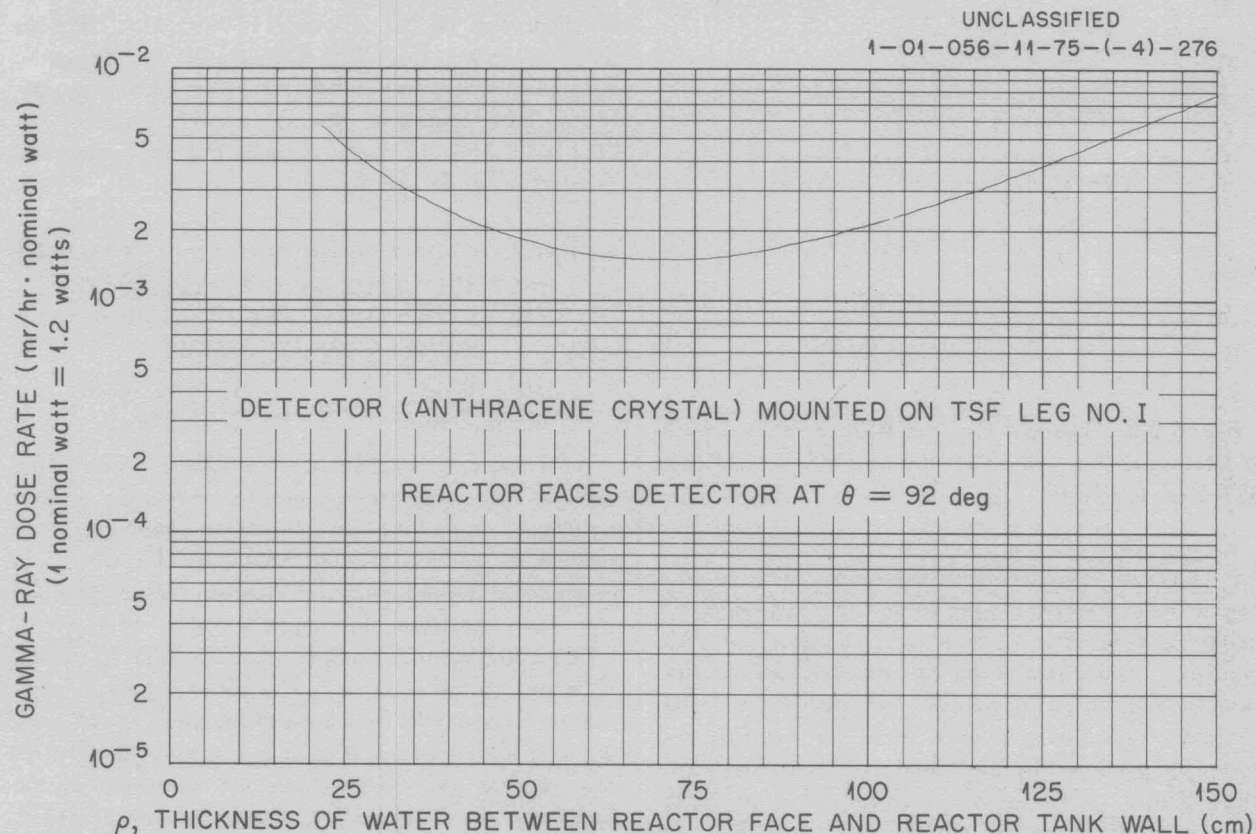


Fig. 6.2.3. Gamma-Ray Dose Rate in Air at a Point 100 ft from the Center of the Reactor Tank as a Function of the Reactor Shield Thickness for  $\theta = 270$  deg.

UNCLASSIFIED  
2-01-056-11-COMP-498

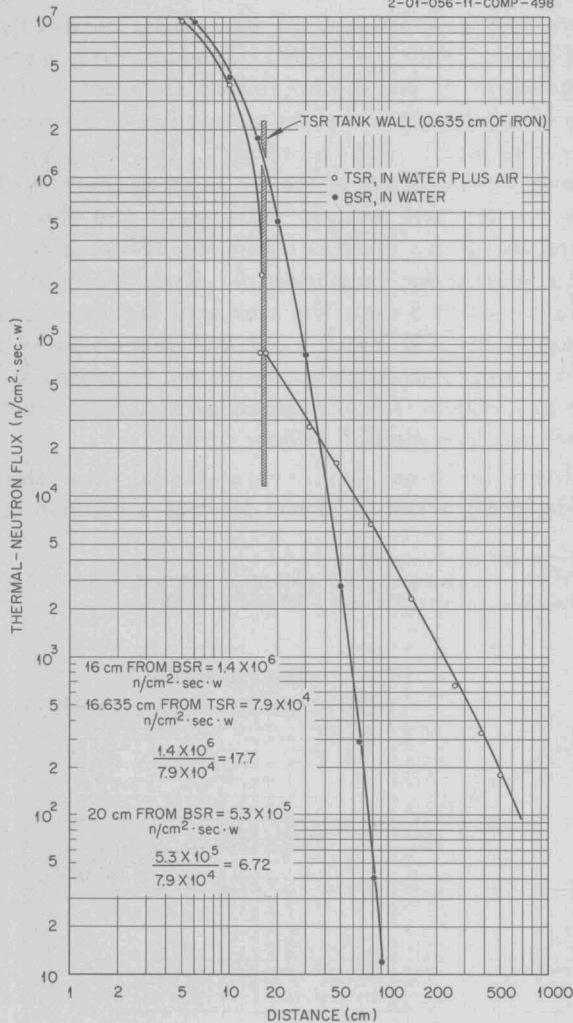


Fig. 6.2.4. Thermal-Neutron Flux as a Function of Distances from the TSF Reactor (TSR) and the BSF Reactor (BSR).

$\theta$  for several values of  $\rho$  in the range 16 to 90 cm. These measurements were also accomplished by mounting a detector (a bare  $\text{BF}_3$  chamber) on TSF leg No. 1 and positioning the reactor tank at the desired separation distance. No cadmium-covered detector measurements were made, so the flux reported is governed by the boron  $1/v$  cross section. The results of these measurements for the 25-ft separation distance are shown in Figs. 6.2.5 and 6.2.6. It is interesting to note that these curves are almost identical in shape. The reason for this is not immediately obvious. A plot of the data

for the 50-ft separation distance (Fig. 6.2.7) shows curves with the same shapes, although the slopes of the curves vary more slowly than the slopes of the curves for the 25-ft separation distance. It is felt that this is an indication that the ratio of direct-to-scattered flux is changing, with the scattered component becoming more predominant.

Comparison of Thermal-Neutron Detectors

The responses of three detectors used at the TSF to measure thermal-neutron flux have been compared in a series of tests. The measurements were made with the reactor-detector center line 6 ft above ground level. The results are plotted as a function of the reactor-detector separation distance,  $s$ , in Fig. 6.2.8. It is to be noted that these data follow an inverse distance-squared relationship if the effective position of the source is considered to be at a point inside the reactor 3 cm from the front face. Some of the discrepancy in the results for the different detectors can be attributed to the lack of cadmium-difference data for the fission chamber and the  $\text{BF}_3$  counter. The fission chamber may indicate a high flux because it was designed for use in water and is backed up by a thick plastic block that returns, to the sensitive portion of the counter, both the thermal and the fast neutrons slowed down in the block.

EFFECT OF AIR AND GROUND SCATTERING OF FAST NEUTRONS ON THE DOSE RATES MEASURED IN AIR AND IN A CREW-COMPARTMENT MOCKUP

M. J. Welch                      W. J. McCool<sup>6</sup>  
R. M. Davis<sup>5</sup>                      C. R. Fink<sup>5</sup>

An experiment designed for obtaining information on the effects of air and ground scattering of fast neutrons in a typical shielding geometry was performed at the Tower Shielding Facility. A highly collimated beam of neutrons was obtained for the experiment by placing either of two air-filled cylindrical aluminum pipes (8- and 15-in.-ID) adjacent to the reactor in the reactor tank. Fast-neutron dose rate measurements were made with an unshielded detector at a distance of 64 ft from the reactor tank while both the direction of the beam and the height above the ground were varied.

<sup>5</sup>On assignment from The Glenn L. Martin Co.

<sup>6</sup>On assignment from Pratt & Whitney Aircraft.

UNCLASSIFIED  
1-01-056-11-129-(3)-336

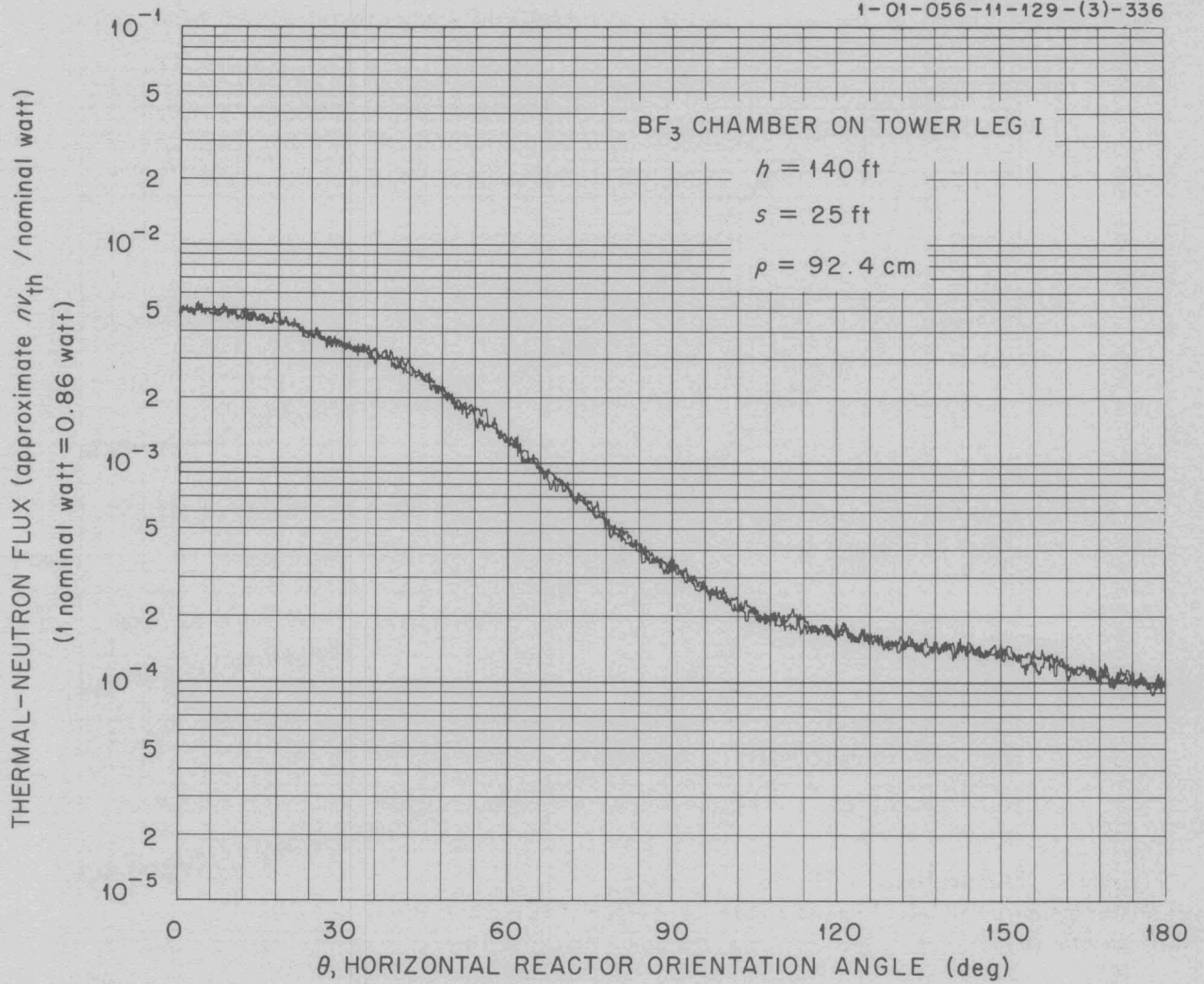


Fig. 6.2.5. Thermal-Neutron Flux in Air at a Point 25 ft from the Center of the Reactor Tank as a Function of  $\theta$  for  $\rho = 92.4$  cm.

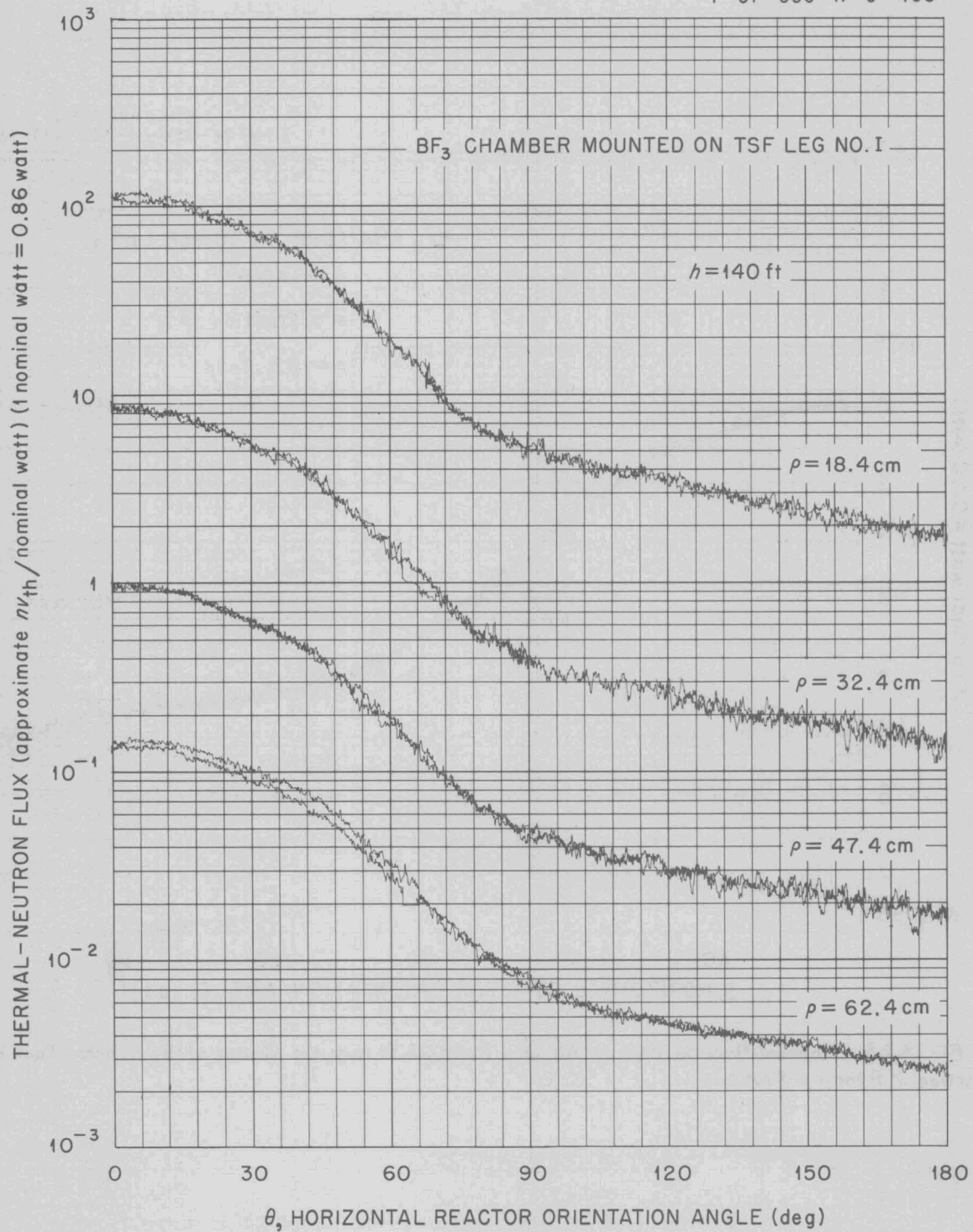


Fig. 6.2.6. Thermal-Neutron Flux in Air at a Point 25 ft from the Center of the Reactor Tank for  $\rho = 18.4, 32.4, 47.4,$  and  $62.4 \text{ cm}$ .

UNCLASSIFIED  
4-01-056-11-C-469

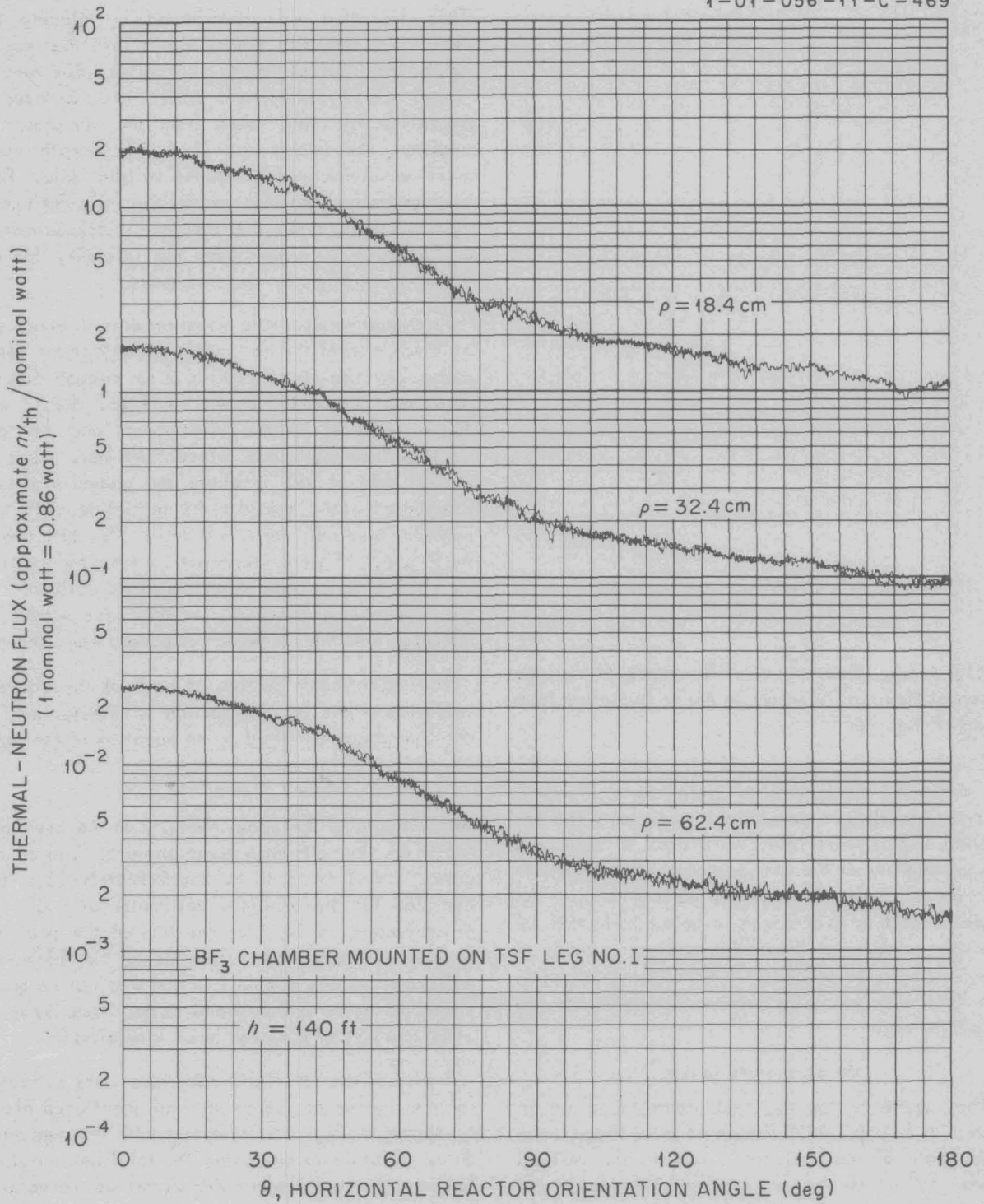
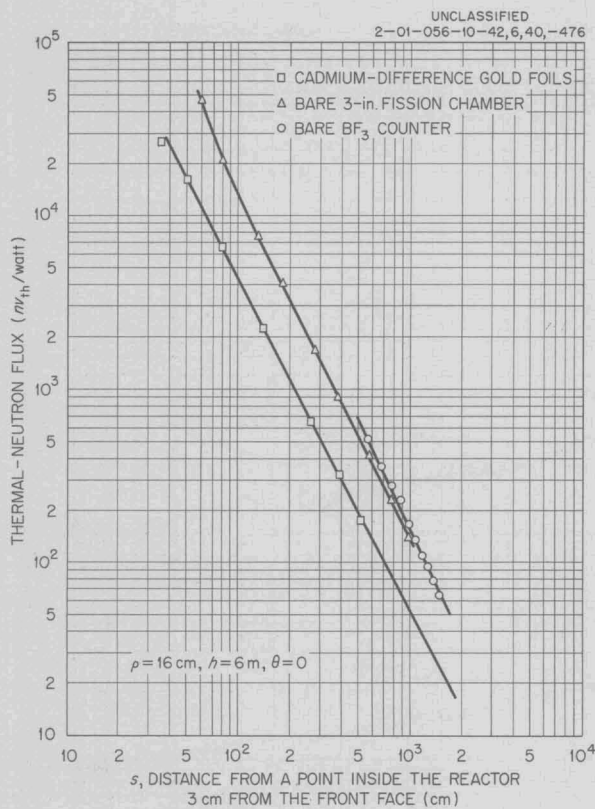


Fig. 6.2.7. Thermal-Neutron Flux in Air at a Point 50 ft from the Center of the Reactor Tank as a Function of  $\theta$  for  $\rho = 18.4, 32.4, \text{ and } 62.4$  cm.



**Fig. 6.2.8. Comparison of Response of Various Thermal-Neutron Detectors in Air to Radiation from the TSF Reactor.**

In addition, measurements were made inside a compartmentalized crew-shield mockup. The resulting experimental data were used to determine the probability of the fast neutrons scattering into the sides of the crew-compartment mockup. An analysis of this experiment is being performed by Convair personnel. Since this analysis is now in progress, only the procedures, experimental results, and a comparison with previous experiments are presented here.

**Measurements in Air**

The geometry for the measurements in air is shown in Fig. 6.2.9a. The angle  $\phi$  is the orientation angle of the collimator axis in the vertical plane and  $\theta$  is the corresponding angle in the horizontal plane. At  $\phi = 0$  deg and  $\theta = 0$  deg the collimator is directed at the detector. The collimator assemblies are shown in Figs. 6.2.9b and 6.2.9c.

The asymmetries in the reactor and the tank wall cause the source strength to vary with  $\phi$  and  $\theta$ . This variation was determined by placing the detector in the direct beam 64 ft from the reactor center for different values of  $\theta$  and  $\phi$ . The results (Figs. 6.2.10, 6.2.11, and 6.2.12) must be used to normalize all data taken from the variplot. In addition, the background ( $2 \times 10^7$  mrep/hr-watt) must be subtracted from all the variplot data. This is especially important for the 8-in.-dia collimator measurements, since the intensity is approximately a factor of 10 lower than the intensity for the 15-in.-dia collimator measurements.

Fast-neutron dose rate measurements at  $\phi = 0$  deg as a function of the horizontal angle  $\theta$  of the collimator are shown in Figs. 6.2.13 through 6.2.15. The measurements shown in Figs. 6.2.13 and 6.2.14 consist of the direct-beam and the air-scattered contributions, since they were taken at an altitude of 195 ft where the ground-scattered component was assumed to be negligible. (This is probably true only for  $\phi = 0$  deg.) The data shown in Fig. 6.2.15 were taken with a detector encased in a shield which was penetrated by a collimator in the direct-beam direction. In this case some contribution from the scattered component was removed.

The direct-beam portion of each of the above  $\theta$  traverses (that is, the portion in the vicinity of  $\theta = 0$  deg) can be fitted by an equation of the form:

$$D_{\theta} = D_{\theta=0} \cos^n \theta ,$$

where  $D_{\theta=0}$  is the peak intensity of the beam and  $D_{\theta}$  is the intensity at a given angle  $\theta$ . The cosine power  $n$  was found to be approximately 181, 185, and 186 for the 8-in.-dia collimator at angles of  $\theta$  equivalent to 50, 25, and 10% of the peak intensity, respectively. The fit of the 15-in.-dia collimator to this cosine function was not so good, since the power  $n$  was found to vary from 56 to 63 at 50 and 25% of the peak beam intensity.

A plot of the 15-in.-dia collimator data corrected for the change in source strength mentioned above is shown in Fig. 6.2.16, along with the measured data. In order to determine the total neutron dose leaving the collimator, the corrected curve was resolved into the direct-beam and air-scattered components between  $\theta = 0$  and 30 deg by extrapolating the curve from the  $\theta = 30$ -deg point back to  $\theta = 0$  deg and assuming that the extrapolated curve

UNCLASSIFIED  
2-01-056-13+14-D-482

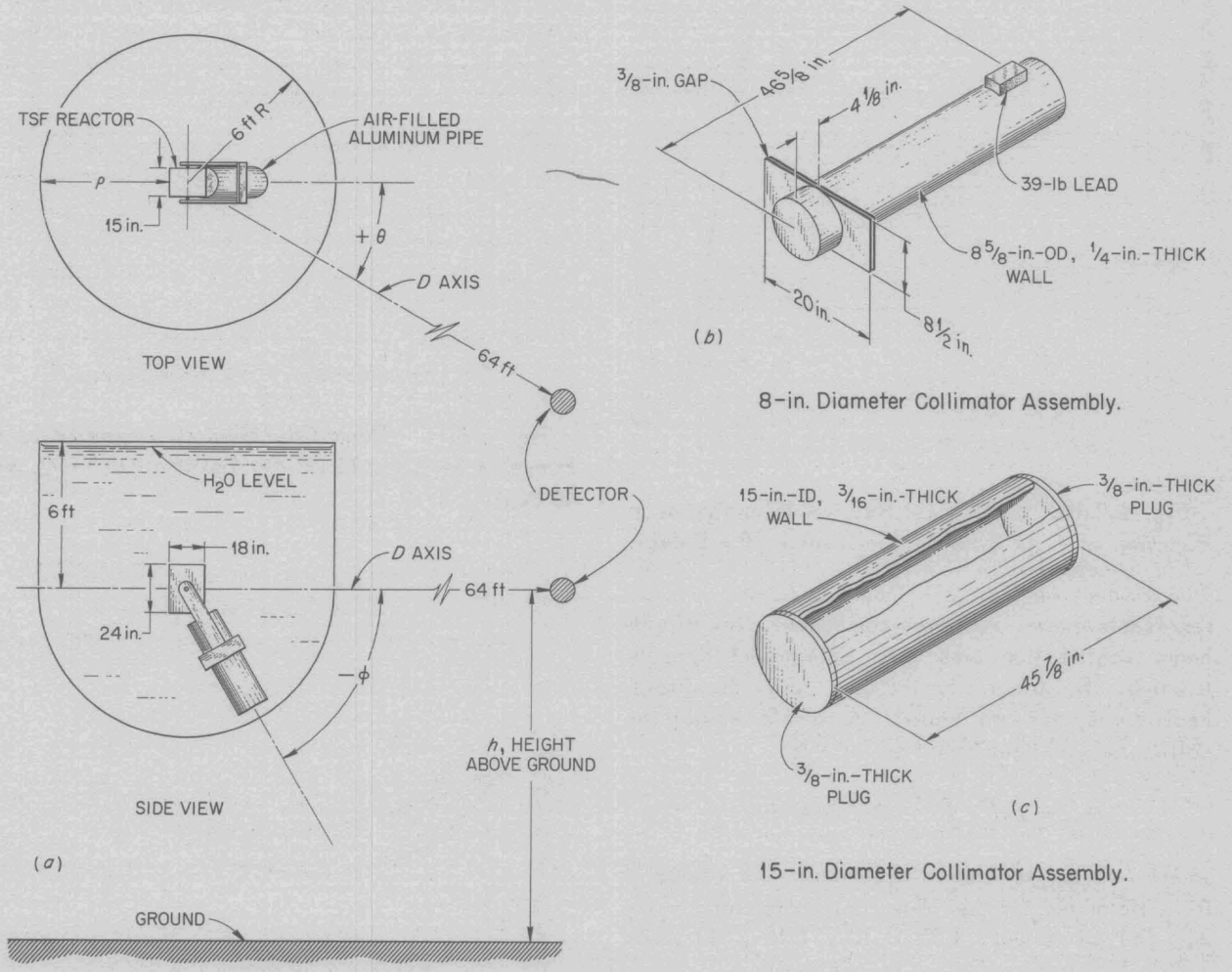


Fig. 6.2.9. Collimator Geometry in the TSF Reactor Tank.

UNCLASSIFIED  
2-01-056-13-163-479

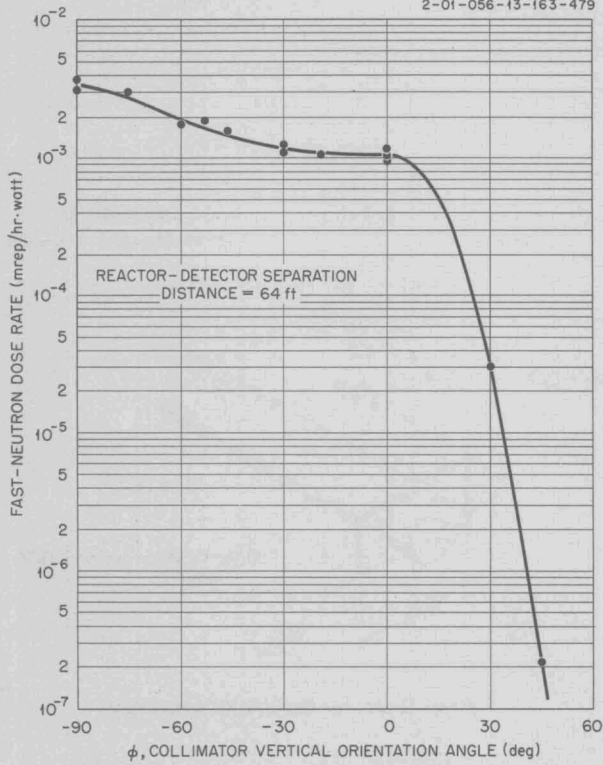


Fig. 6.2.10. Peak Fast-Neutron Intensity as a Function of  $\phi$  for 8-in.-dia Collimator ( $\theta = 0$  deg).

represents the air-scattered component. The direct-beam contribution was then determined by subtraction. By integrating the area under the direct-beam curve, the total neutron dose rate leaving the collimator was determined as follows:

$$D_T = 2\pi l^2 \int_0^{\pi/2} D_\theta \sin \theta d\theta ,$$

where  $l$  is the separation distance. The values of  $D_T$  determined for the 15-in. collimator for  $l = 15, 30,$  and  $64$  ft were  $1.32 \times 10^3, 1.16 \times 10^3,$  and  $1.26 \times 10^3$  mrep·cm<sup>2</sup>/hr·w, respectively.

Fast-neutron dose rate measurements as a function of altitude were made for various values of  $\phi$  and  $\theta$  (Figs. 6.2.17 through 6.2.24). These traverses show a maximum intensity of dose rate at an altitude of between 20 and 40 ft. There is a decrease in intensity as higher altitudes are approached. This results from decreasing ground scattering, which overrides the small increase in air scattering. The ground-scattering effects are seen at higher altitudes for greater negative values of  $\phi$ .

UNCLASSIFIED  
2-01-056-14-COMP-480

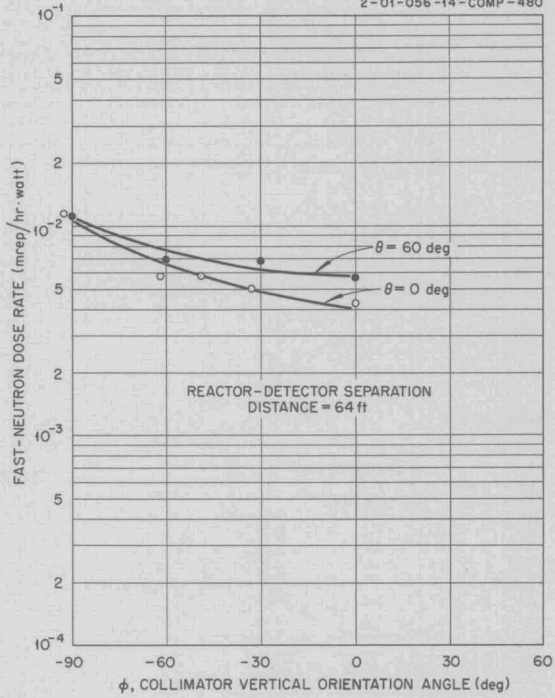


Fig. 6.2.11. Peak Fast-Neutron Intensity as a Function of  $\phi$  for 15-in.-dia Collimator ( $\theta = 0$  and 60 deg).

UNCLASSIFIED  
2-01-056-14-COMP-481

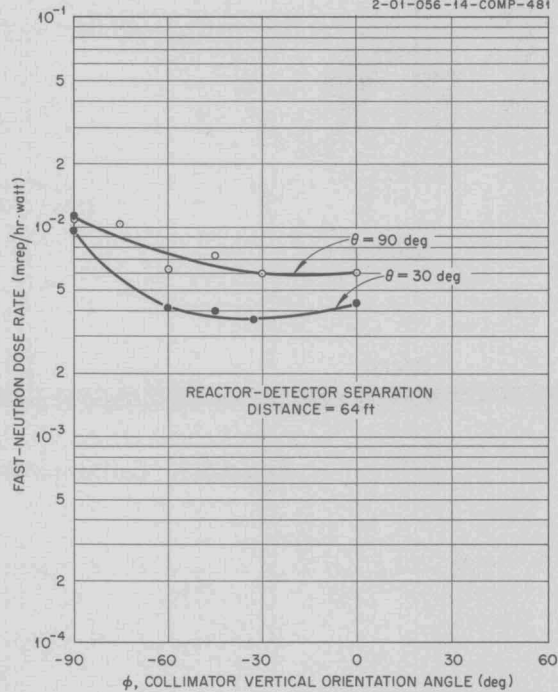


Fig. 6.2.12. Peak Fast-Neutron Intensity as a Function of  $\phi$  for 15-in.-dia Collimator ( $\theta = 30$  and 90 deg).

UNCLASSIFIED  
1-01-056-13-8-(-4)-344

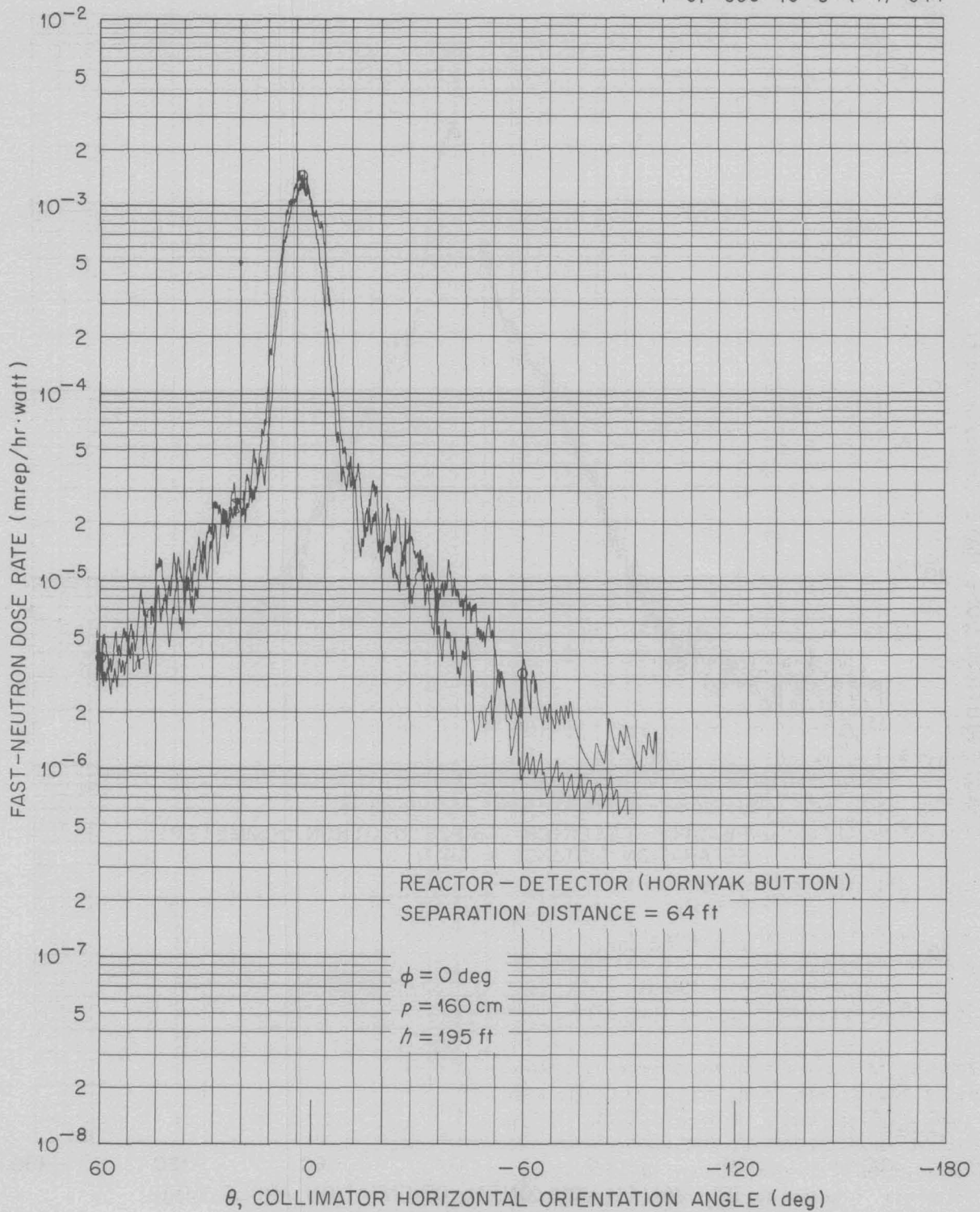


Fig. 6.2.13. Fast-Neutron Dose Rate in Air as a Function of  $\theta$  for 8-in.-dia Collimator ( $b = 195$  ft).

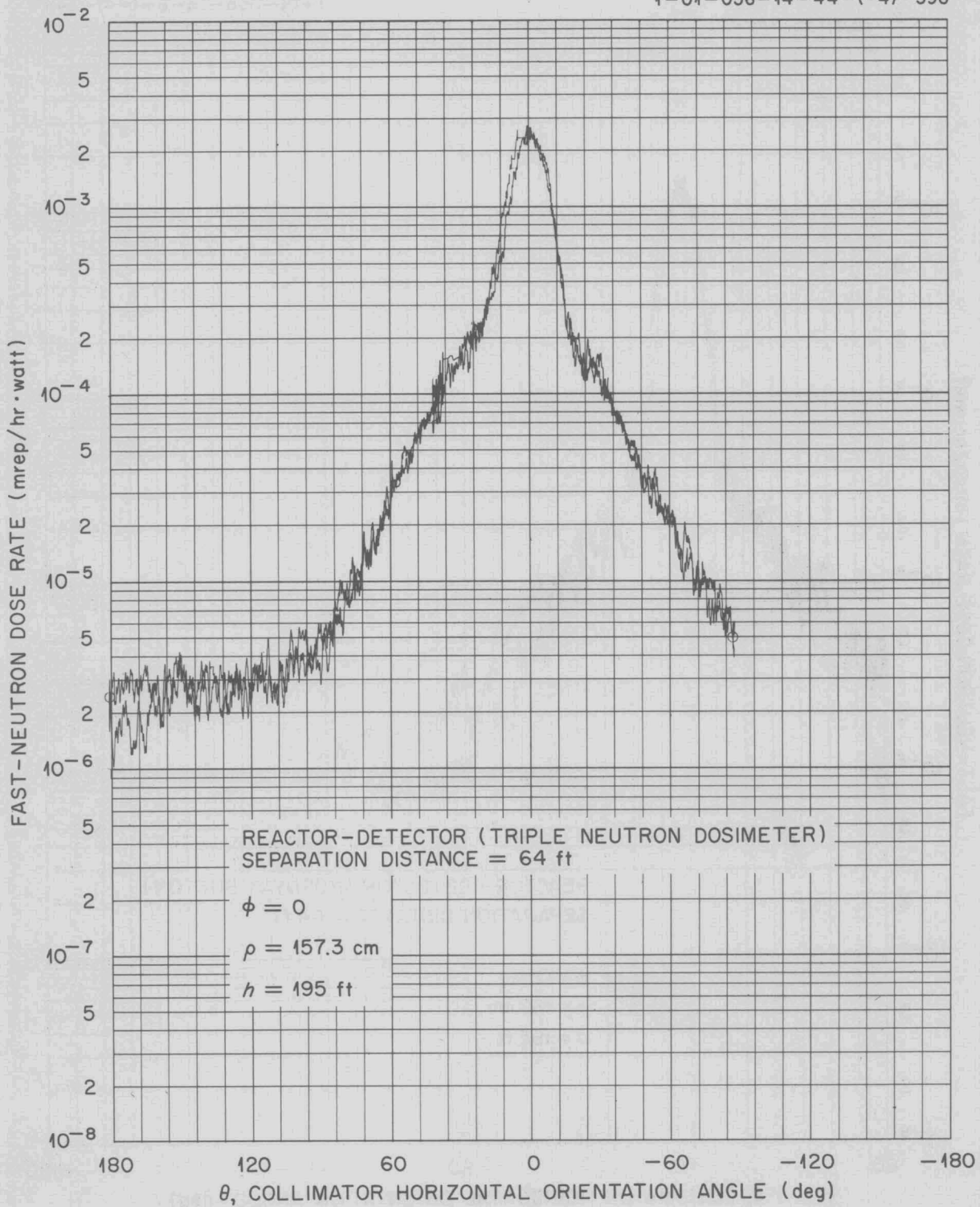


Fig. 6.2.14. Fast-Neutron Dose Rate in Air as a Function of  $\theta$  for 15-in.-dia Collimator ( $b = 195$  ft).

UNCLASSIFIED  
1-01-056-14-155-(-4)-430

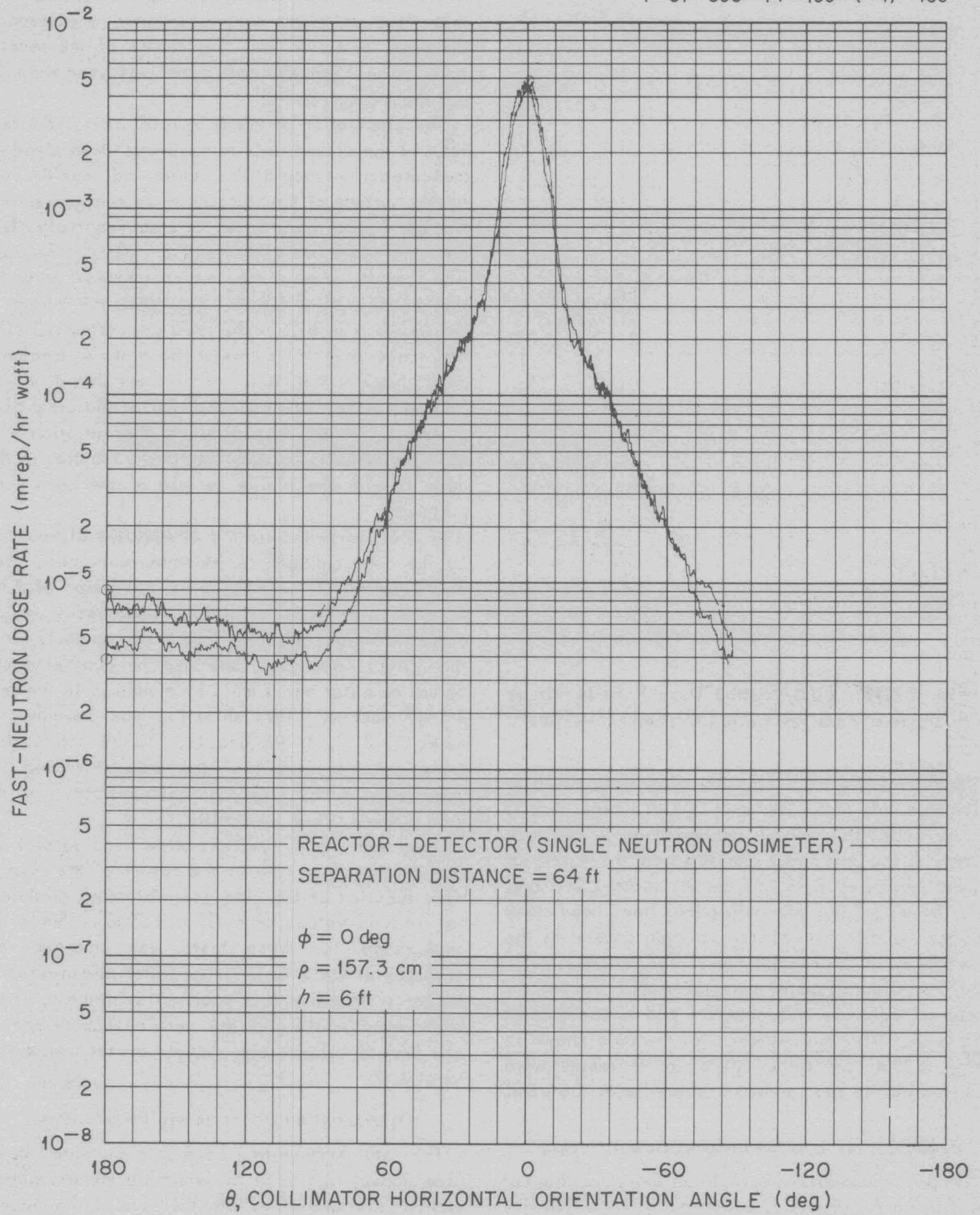


Fig. 6.2.15. Fast-Neutron Dose Rate in Partially Shielded Detector as a Function of  $\theta$  for 15-in.-dia Collimator ( $h = 6$  ft).

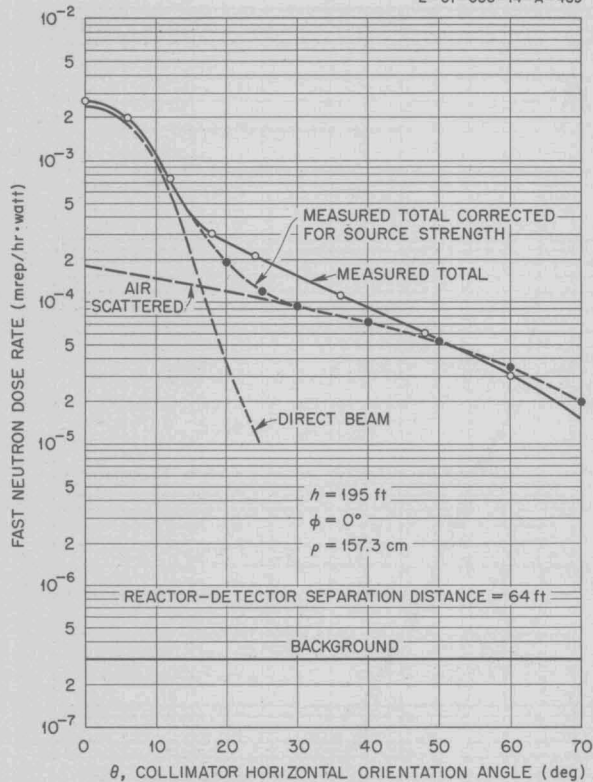
UNCLASSIFIED  
2-01-056-14-A-489

Fig. 6.2.16. Fast-Neutron Dose Rate in Air as a Function of  $\theta$  for 15-in.-dia Collimator ( $b = 195$  ft).

Measurements as a function of  $\phi$  were taken at altitudes of 12.5, 25, and 195 ft (Figs. 6.2.25 through 6.2.28). The background (that is, the dose rate with the collimator removed from the tank) has been subtracted from the results plotted in Figs. 6.2.29 and 6.2.30, and corrections have been made for the variations in source strength caused by the asymmetry in the reactor tank. The traverses with the 8-in.-dia collimator were taken with the reactor tank centered over the concrete pad to one side of the pool. With the exception of the data shown in Fig. 6.2.24, the large collimator traverses were taken with the reactor tank centered over the pool.

#### Measurements in a Crew-Compartment Mockup

A compartmentalized cylindrical tank, constructed by Boeing Airplane Co. according to an ORNL design, was used for the fast-neutron measurements in a crew-shield mockup. The water shielding in the mockup (Fig. 6.2.31) could be varied by successively filling or draining the compartments.

The detector was placed inside the mockup, the rear face of which was positioned a horizontal distance of 64 ft from the center of the reactor tank. The 15-in.-dia collimator was used throughout the measurements.

The attenuation of the dose rate through the rear face of the crew-shield mockup was determined by measurements made at the center and near the rear inside surface of the mockup while compartments 1 through 4 (each 3 in. thick) were successively filled and the sides were shielded by 20 in. of water. The results are plotted as a function of water thickness in Fig. 6.2.32. ( $y = 0$  at the center of the inside rear wall of the crew compartment.) The difference in slope between the plots of measurements made at the center of the crew shield ( $y = 38$  in.) and those made near the rear of the crew compartment ( $y = 4\frac{1}{2}$  in.) is due to the variation with shield attenuation of the angular distribution of the dose rate at the inside surface of the crew compartment.

In order to determine the attenuation of neutrons by the crew side shield, measurements were made at the center of the mockup as a function of  $\theta$  for various side wall shielding thicknesses (Figs. 6.2.33 through 6.2.37). For these measurements the direct beam was shielded by approximately 36 in. of water and 1.6 in. of aluminum in the rear of the mockup. This shielding was contained in tanks 1, 2, 3, 4, 10, and 11. Tanks 5 through 9 were considered part of the side shielding and were filled successively as adjacent tanks on the side of the mockup were filled.

Data from the  $\theta$  traverses were used to plot the fast-neutron dose rate at the center of the mockup as a function of the side wall shielding thickness for various values of  $\theta$  (Fig. 6.2.38). Since the background for these tests was unknown, the accuracy of the data for large water thicknesses or for large values of  $\theta$  is poor. A subtraction of the background would give the more customary shapes and would reduce the values of the relaxation lengths,  $\lambda$ .

#### Determination of Scattering Probabilities

The total fast-neutron dose rate measured in air (see above) was used to determine the probability of neutrons scattering into the side of the mockup as a function of the horizontal angle  $\theta$ . This scattering probability,  $l^2 P_s^S(\theta)$  ( $l$  = separation distance,  $P_s^S(\theta)$  = probability of neutrons from beam at angle  $\theta$  scattering into the sides of the mockup),

UNCLASSIFIED  
1-01-056-13-COMP-438

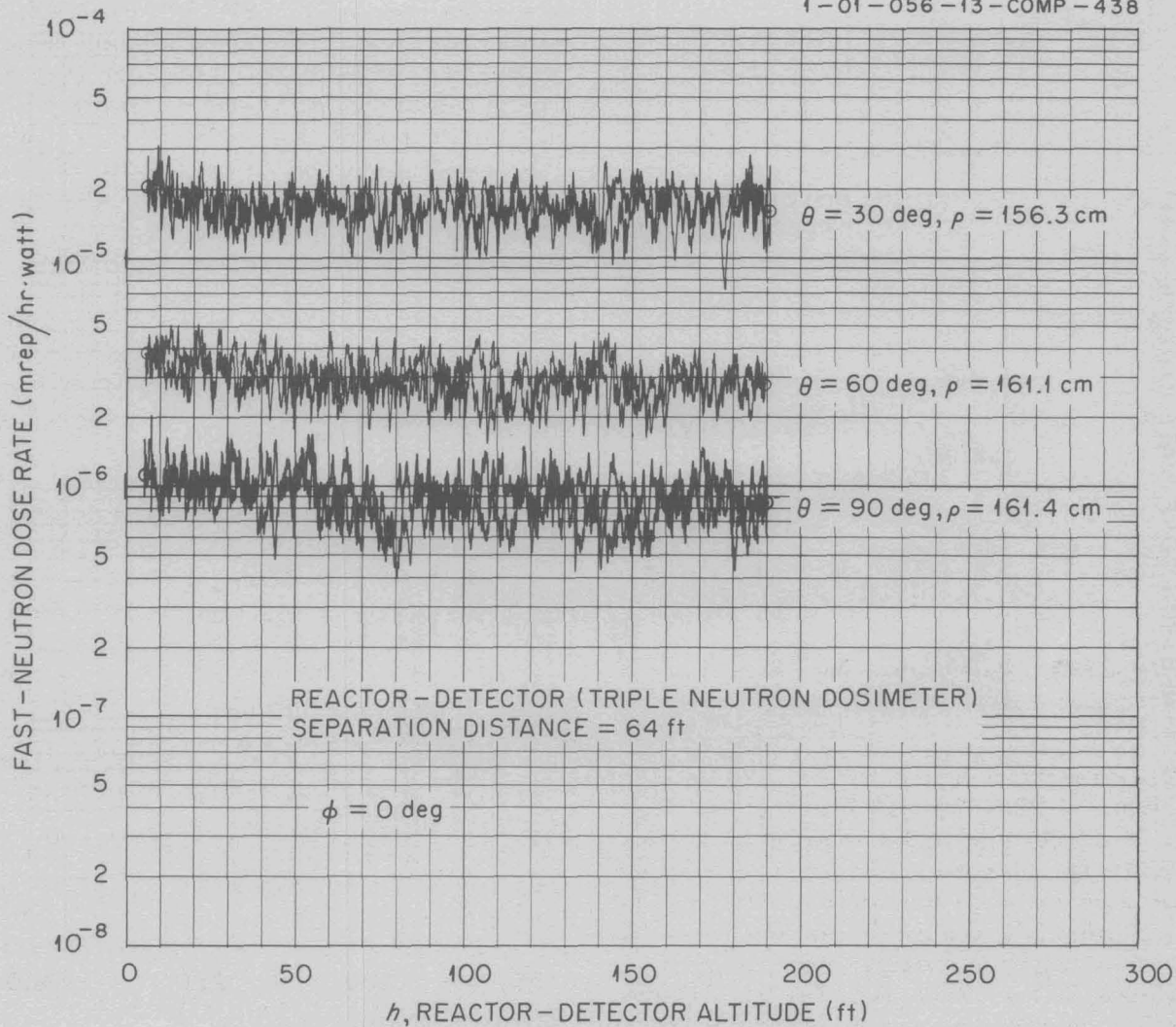


Fig. 6.2.17. Fast-Neutron Dose Rate in Air as a Function of Altitude for 8-in.-dia Collimator ( $\theta = 30, 60, \text{ and } 90 \text{ deg}; \phi = 0$ ).

UNCLASSIFIED  
1-01-056-13-COMP-439

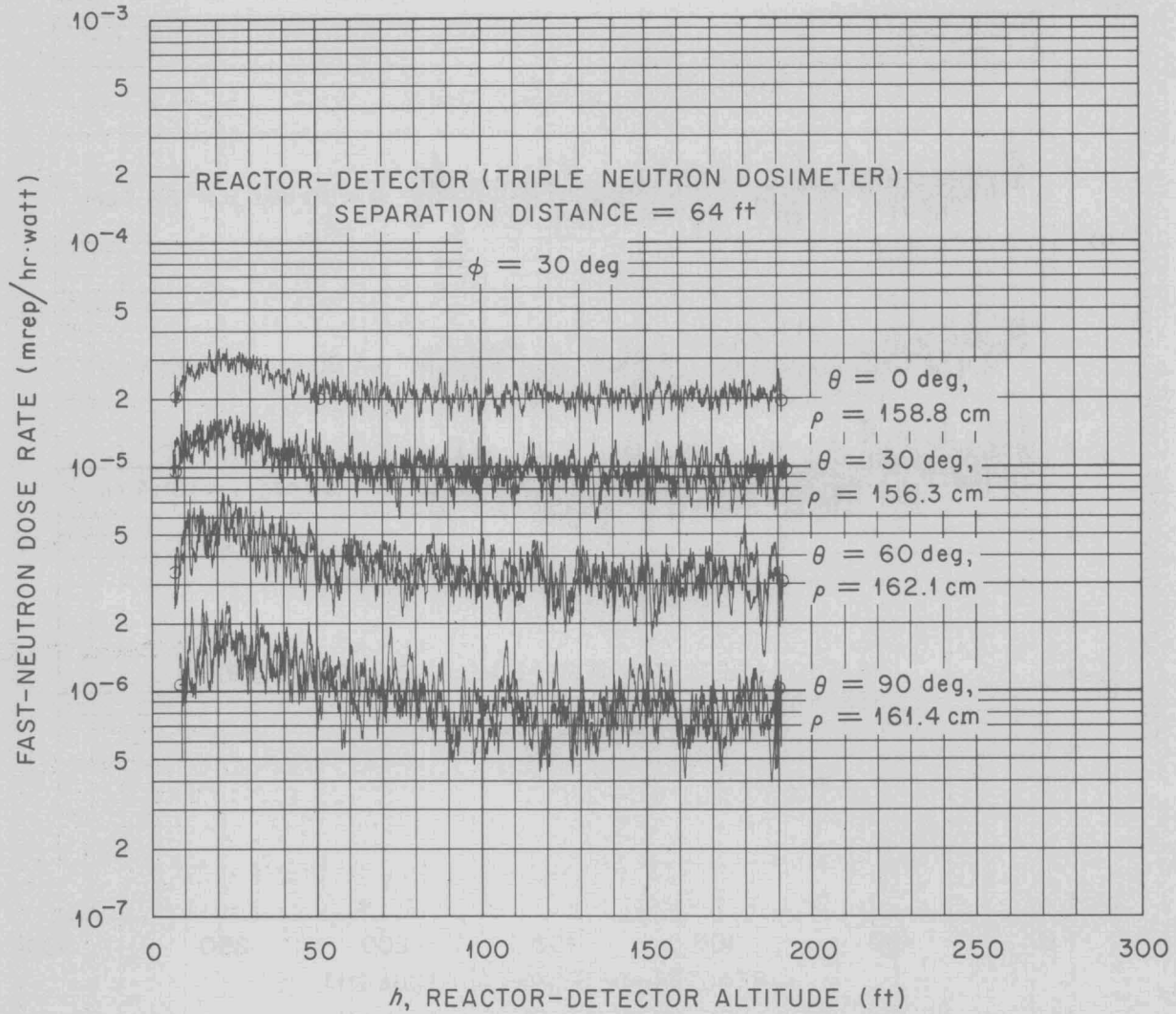


Fig. 6.2.18. Fast-Neutron Dose Rate in Air as a Function of Altitude for 8-in.-dia Collimator ( $\theta = 0, 30, 60, \text{ and } 90 \text{ deg}; \phi = 30 \text{ deg}$ ).

UNCLASSIFIED

1-01-056-13-70-(-6)-362

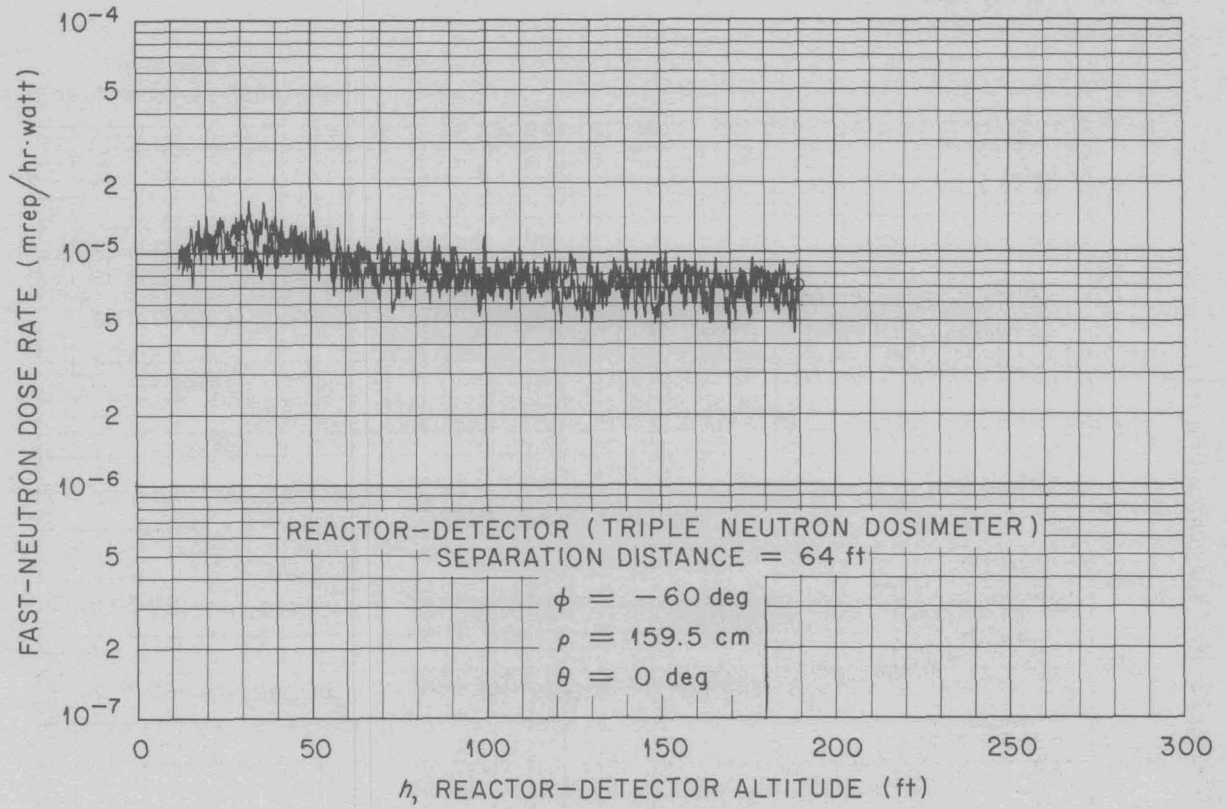


Fig. 6.2.19. Fast-Neutron Dose Rate in Air as a Function of Altitude for 8-in.-dia Collimator ( $\theta = 0$ ;  $\phi = 60 \text{ deg}$ ).

UNCLASSIFIED

1-01-056-13-COMP-437

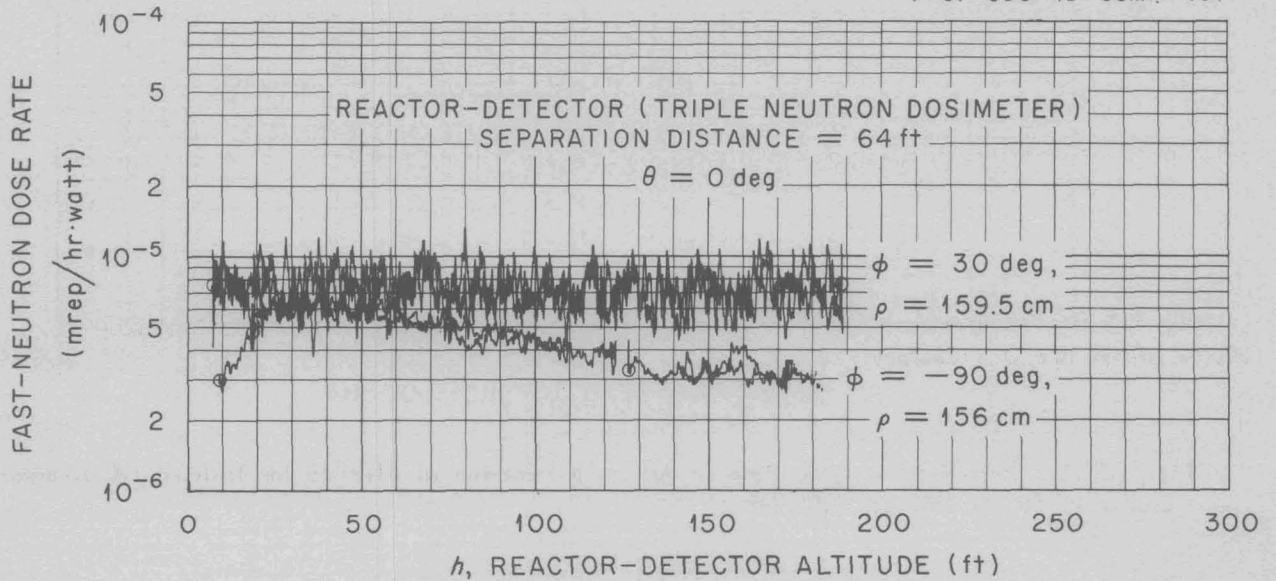


Fig. 6.2.20. Fast-Neutron Dose Rate in Air as a Function of Altitude for 8-in.-dia Collimator ( $\theta = 0$ ;  $\phi = +30$  and  $-90 \text{ deg}$ ).

UNCLASSIFIED  
1-01-056-14-COMP-443

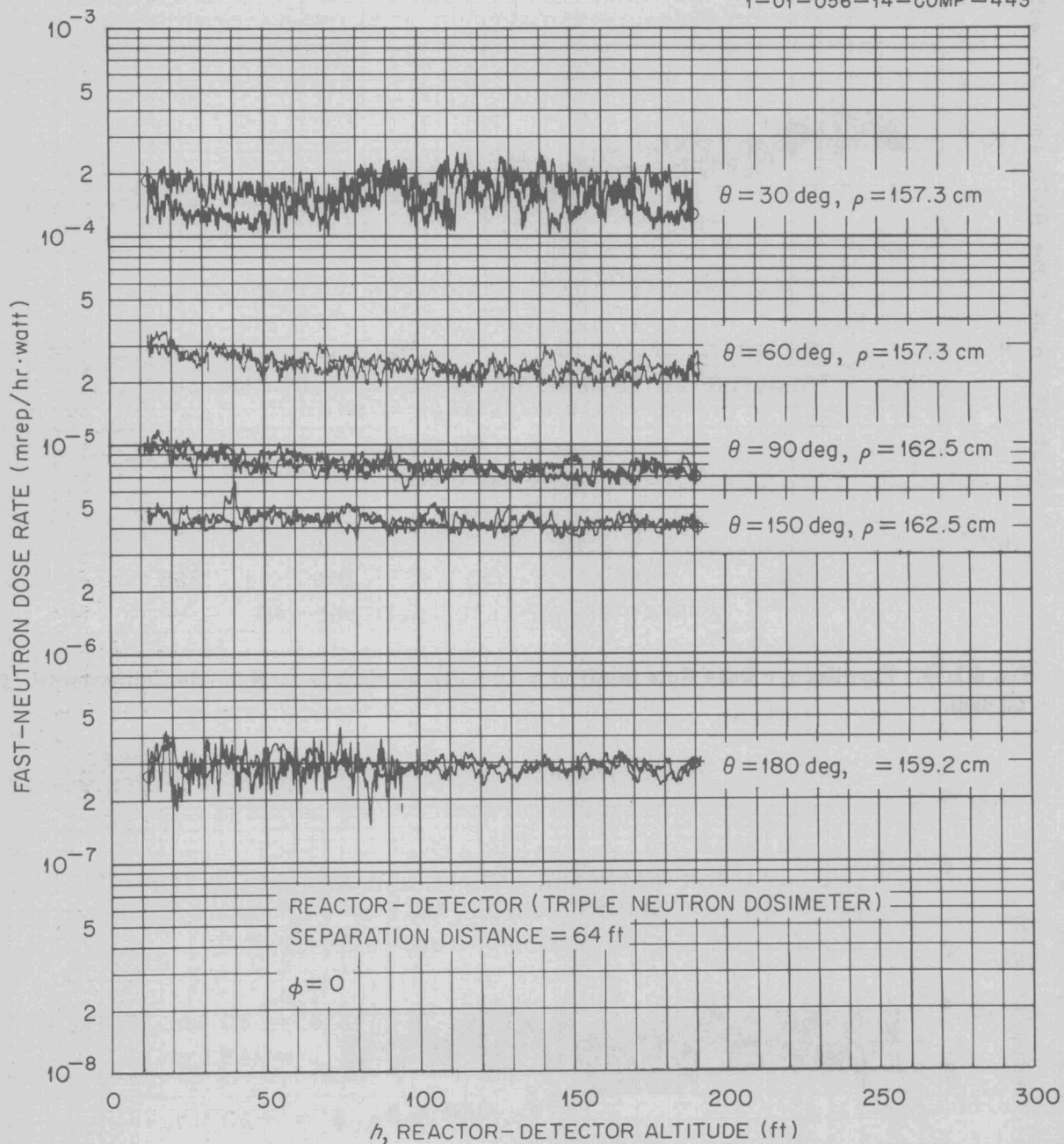


Fig. 6.2.21. Fast-Neutron Dose Rate in Air as a Function of Altitude for 15-in.-dia Collimator ( $\phi = 0$ ;  $\theta = 30, 60, 90, 150, \text{ and } 180 \text{ deg}$ ).

UNCLASSIFIED  
1-01-056-14-COMP-441

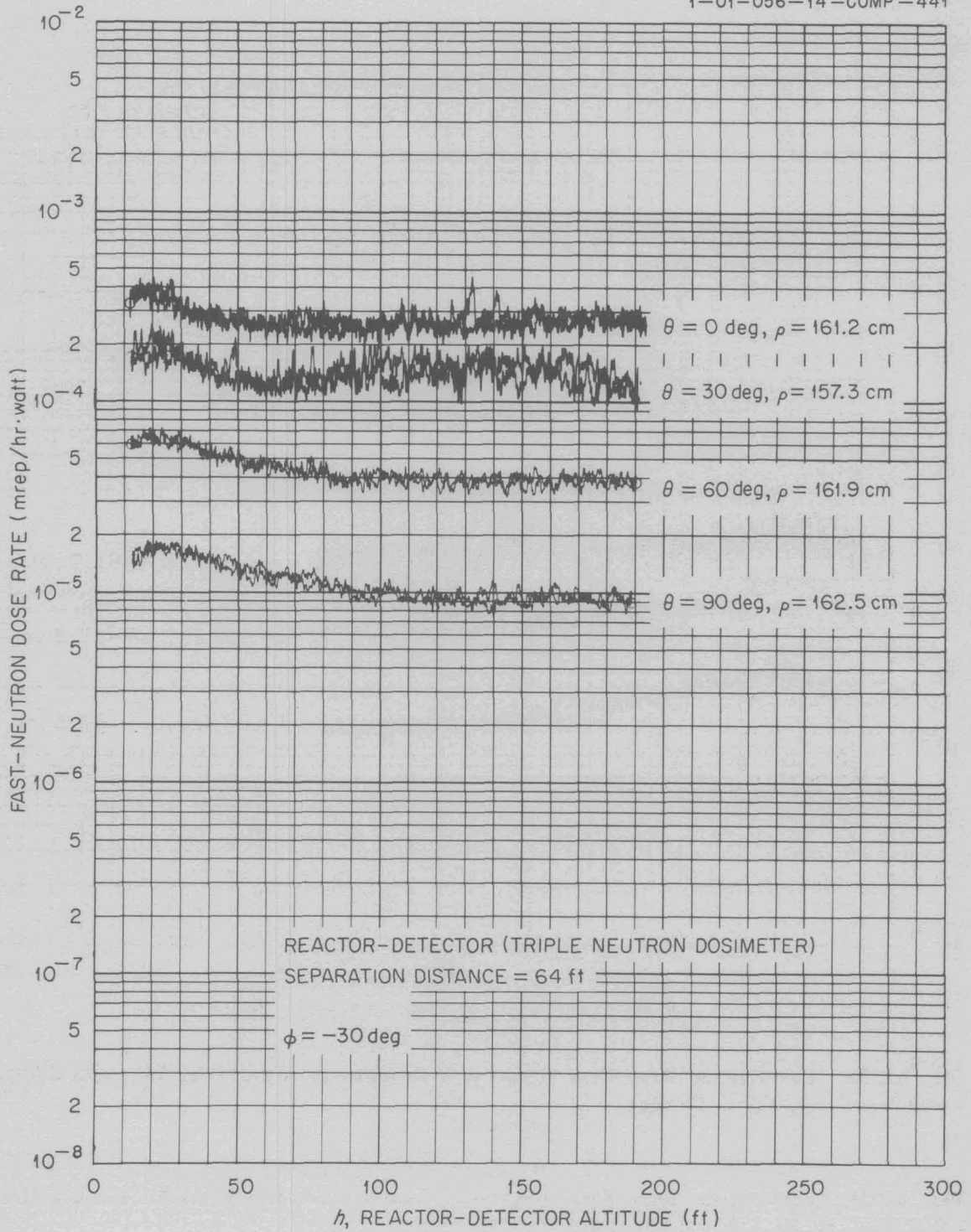


Fig. 6.2.22. Fast-Neutron Dose Rate in Air as a Function of Altitude for 15-in.-dia Collimator ( $\phi = -30 \text{ deg}; \theta = 0, -30, -60, \text{ and } -90 \text{ deg}$ ).

UNCLASSIFIED  
1-01-056-14-COMP-442

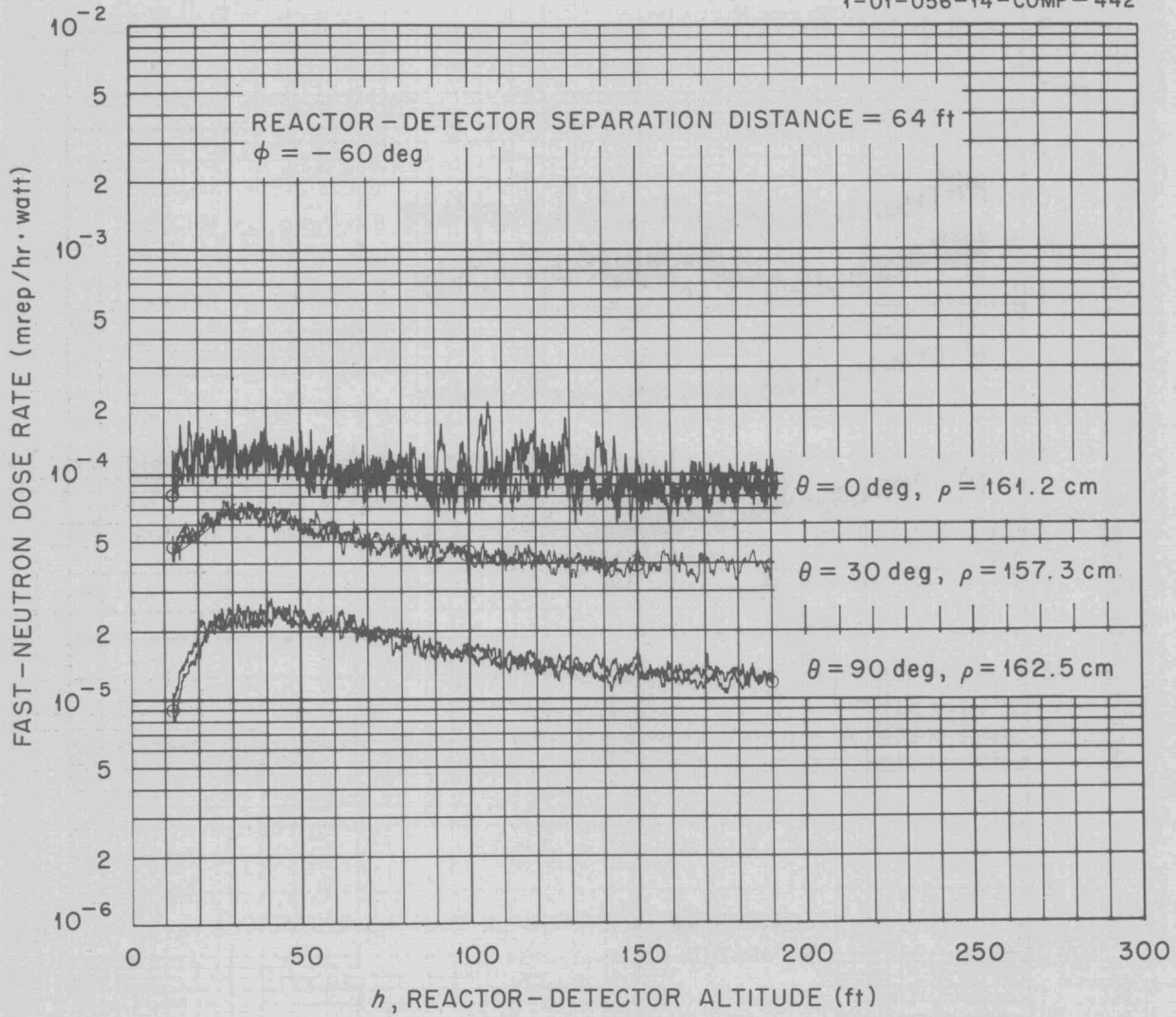


Fig. 6.2.23. Fast-Neutron Dose Rate in Air as a Function of Altitude for 15-in.-dia Collimator ( $\phi = -60 \text{ deg}; \theta = 0, 30, \text{ and } 90 \text{ deg}$ ).

UNCLASSIFIED  
1-01-056-14-139-(-5)-426

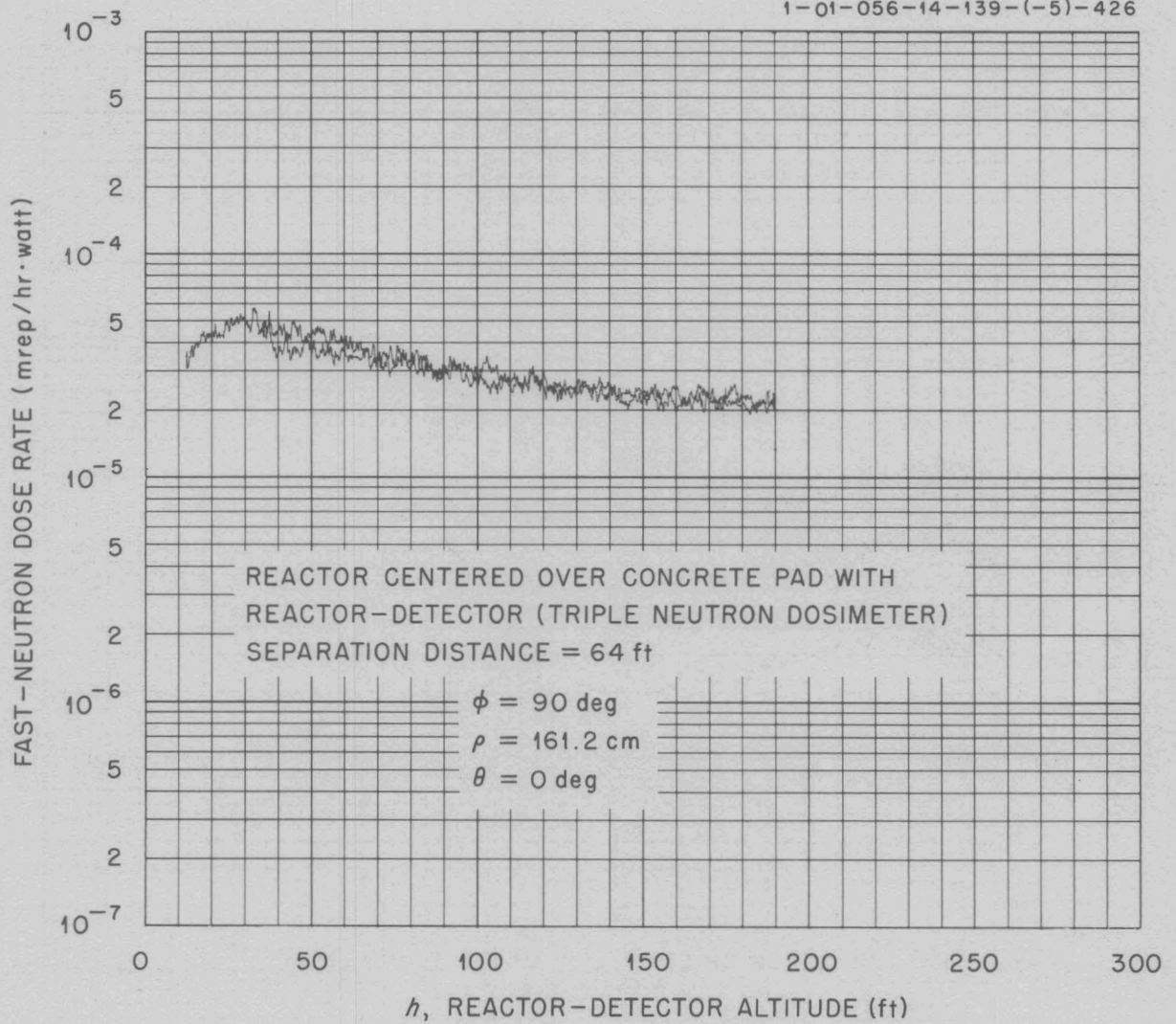


Fig. 6.2.24. Fast-Neutron Dose Rate in Air as a Function of Altitude for 15-in.-dia Collimator ( $\phi = -90$  deg;  $\theta = 0$  deg).

UNCLASSIFIED  
1-01-056-13-60-(-4)-359

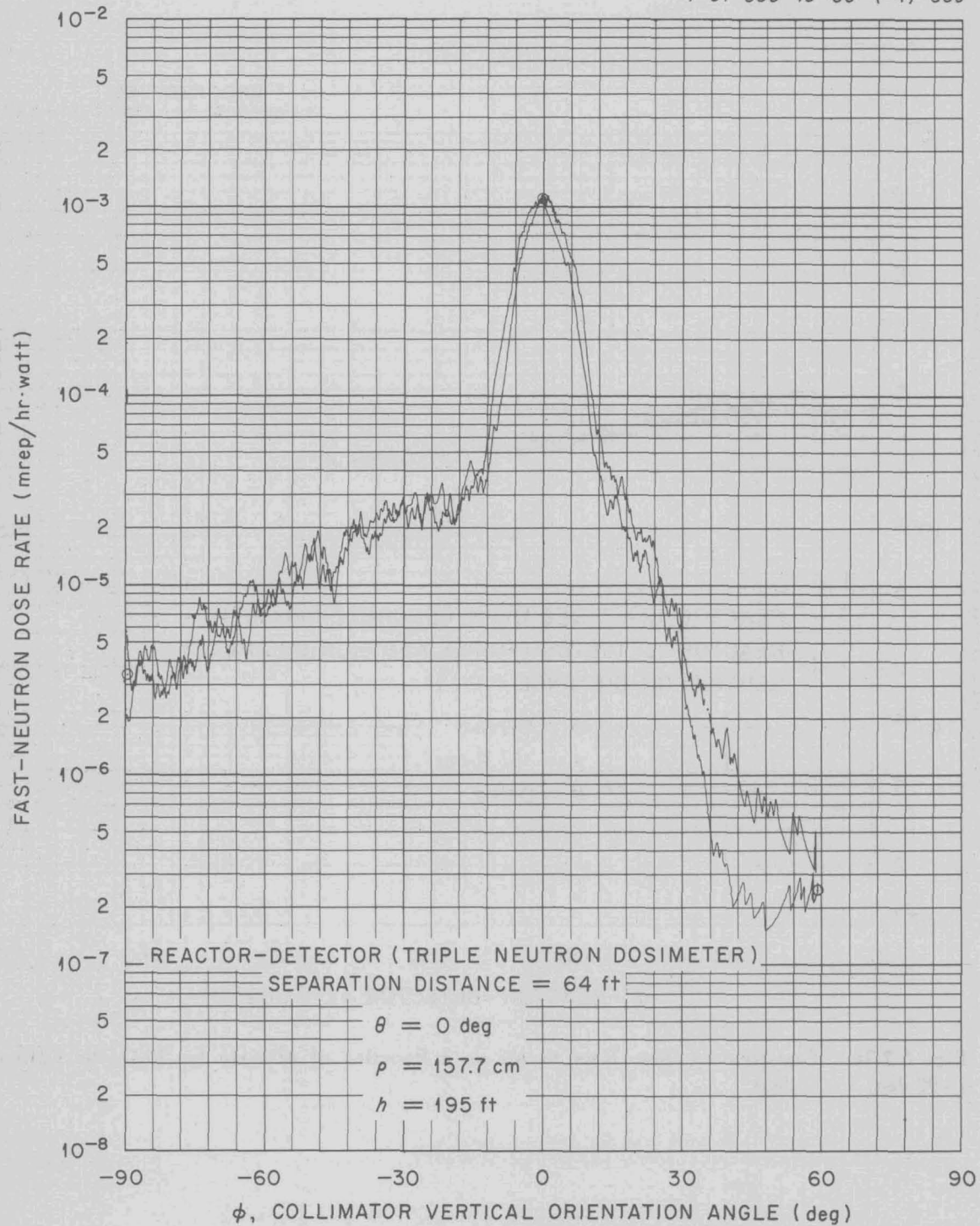


Fig. 6.2.25. Fast-Neutron Dose Rate in Air as a Function of  $\phi$  for 8-in.-dia Collimator ( $\theta = 0$  deg).

UNCLASSIFIED

1-01-056-14-67-(-4)-404

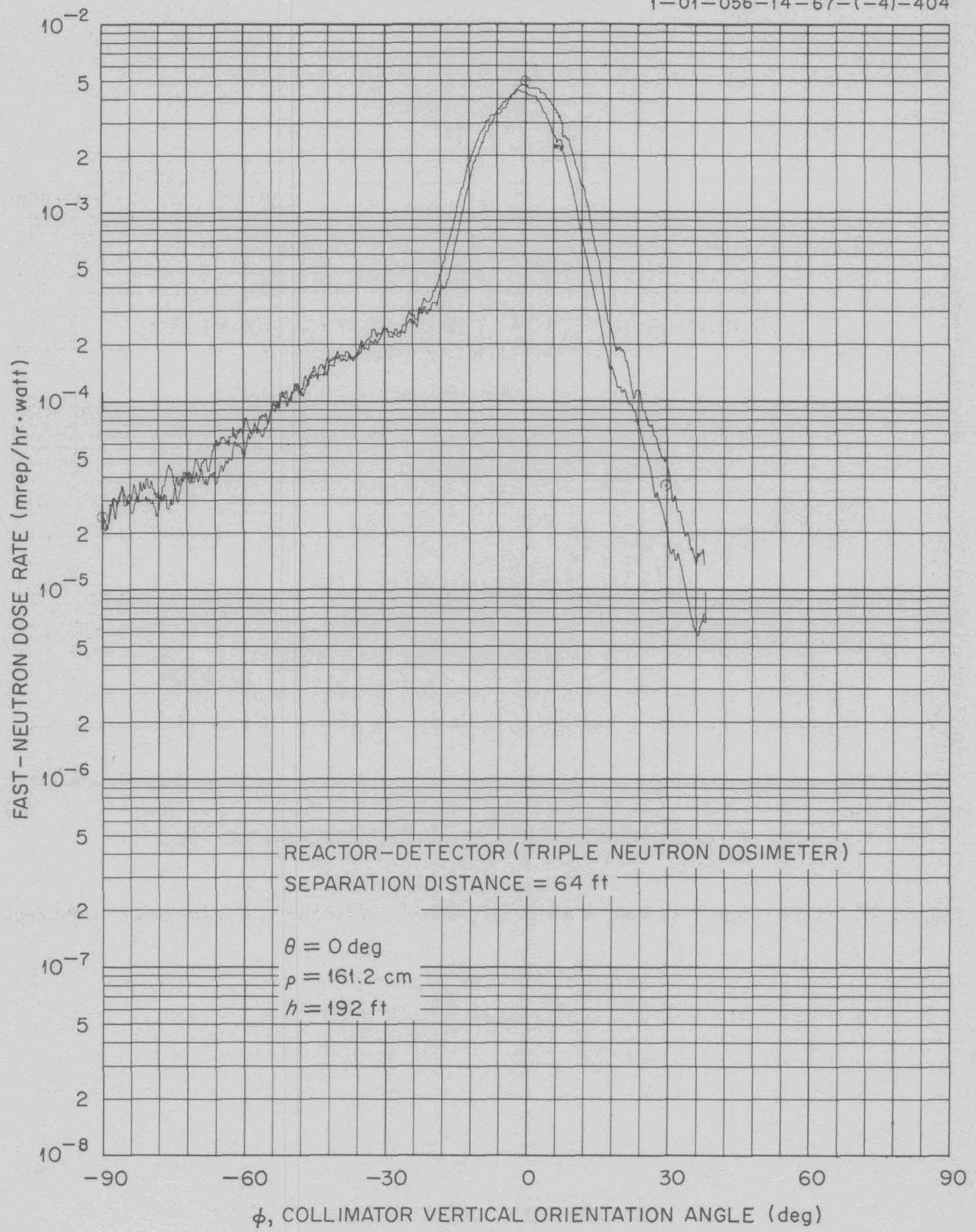


Fig. 6.2.26. Fast-Neutron Dose Rate in Air as a Function of  $\phi$  for 15-in.-dia Collimator ( $\theta = 0$  deg).

UNCLASSIFIED  
 1-01-056-13-63-(-6)-360

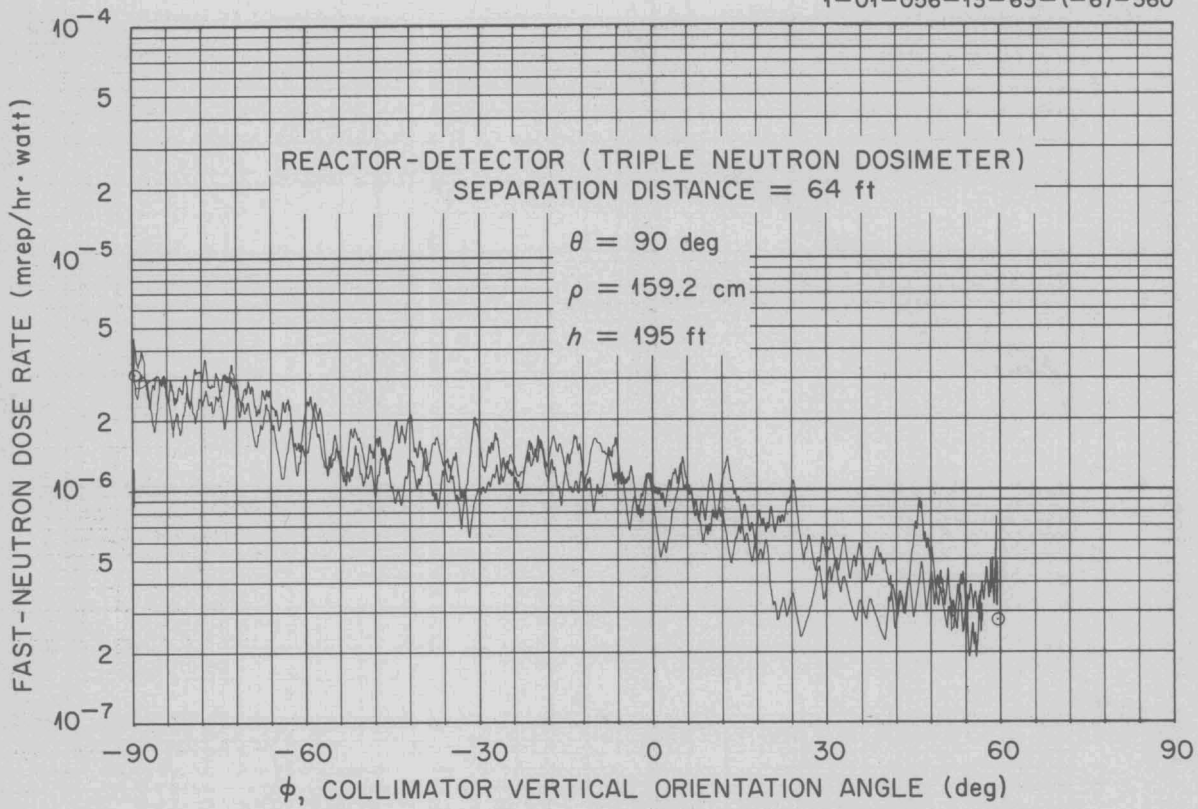


Fig. 6.2.27. Fast-Neutron Dose Rate in Air as a Function of  $\phi$  for 8-in.-dia Collimator ( $\theta = 90 \text{ deg}$ ).

UNCLASSIFIED  
1-01-056-14-88-(-6)-411

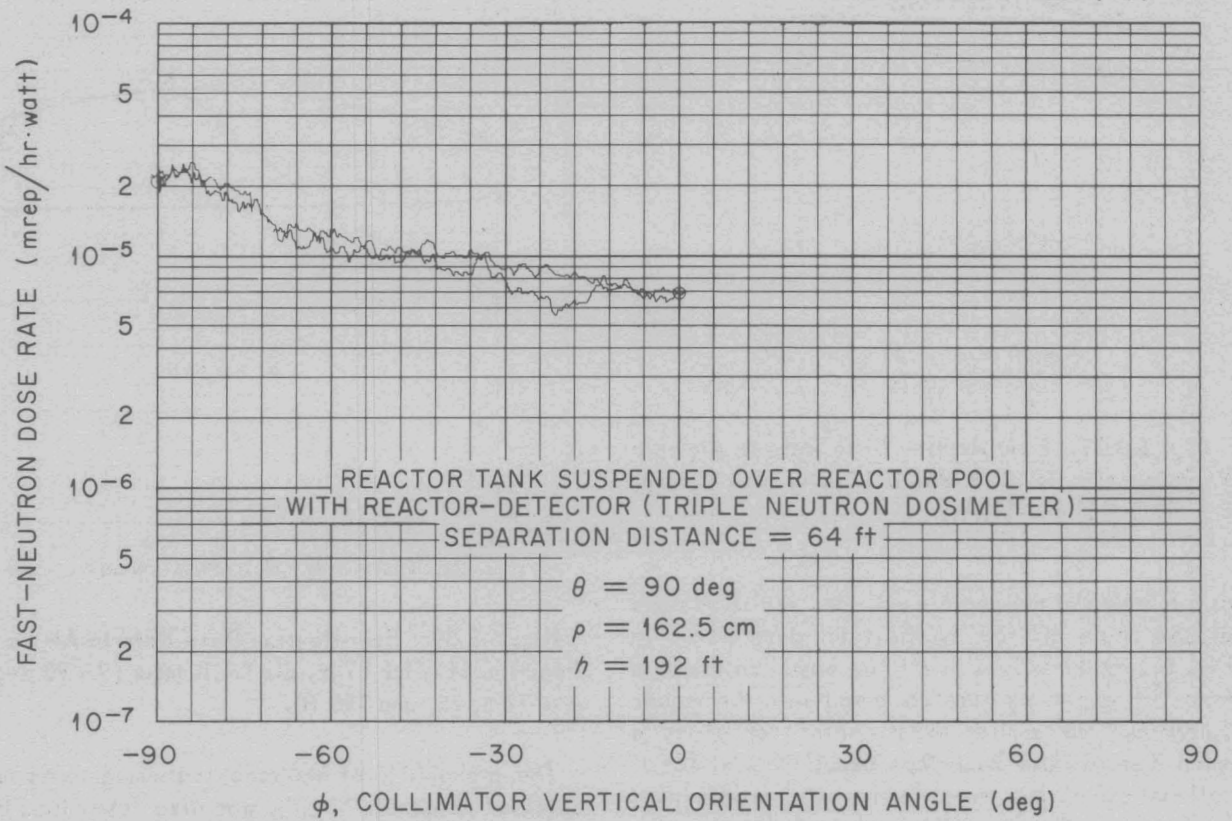
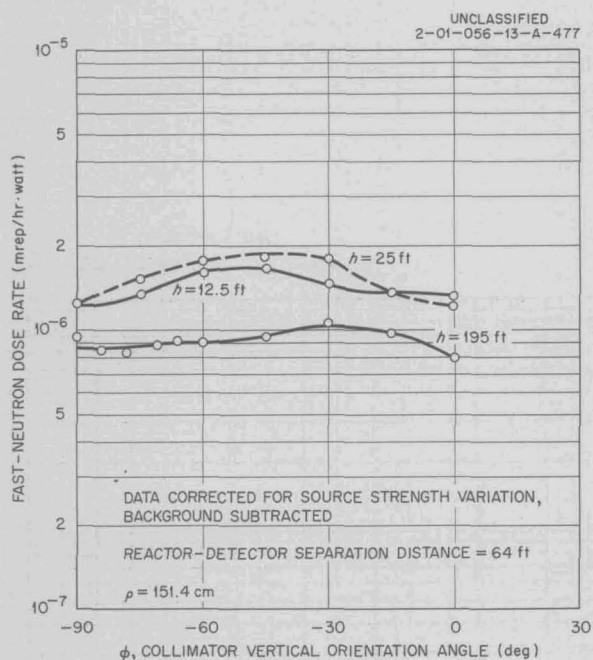


Fig. 6.2.28. Fast-Neutron Dose Rate in Air as a Function of  $\phi$  for 15-in.-dia Collimator ( $\theta = 90$  deg).



**Fig. 6.2.29. Fast-Neutron Dose Rate in Air as a Function of  $\phi$  for 8-in.-dia Collimator ( $\theta = 90$  deg;  $b = 12.5, 25,$  and  $195$  ft).**

as a function of the angle equals the scattered dose at the angle divided by the total dose rate. In Fig. 6.2.39 the values of  $I^2P_s(\theta)$  based on the data from this experiment are compared with the values determined in earlier experiments<sup>7</sup> for which a much more diffuse beam was used. The effect of collimation of the beam seems most predominant in the region  $0 < \theta < 30$  deg. Since measurements as a function of  $\theta$  were taken for each side shielding water thickness, a plot of the scattering probability as a function of the side shielding could also be made for each angle (Fig. 6.2.40). The results are compared with those obtained in an earlier experiment for which the detector tank<sup>8</sup> and a diffuse beam of neutrons was used. As in Fig. 6.2.39, there is little agreement between the angles of 0 and 30 deg for the highly collimated beam, but the agreement outside this region is very favorable, showing a maximum of about 25% error.

<sup>7</sup>M. F. Valerino and F. L. Keller, *ANP Quar. Prog. Rep.* Sept. 10, 1955, ORNL-1947, p 205.

<sup>8</sup>M. F. Valerino, *ANP Quar. Prog. Rep.* June 10, 1955, ORNL-1896, p 206.

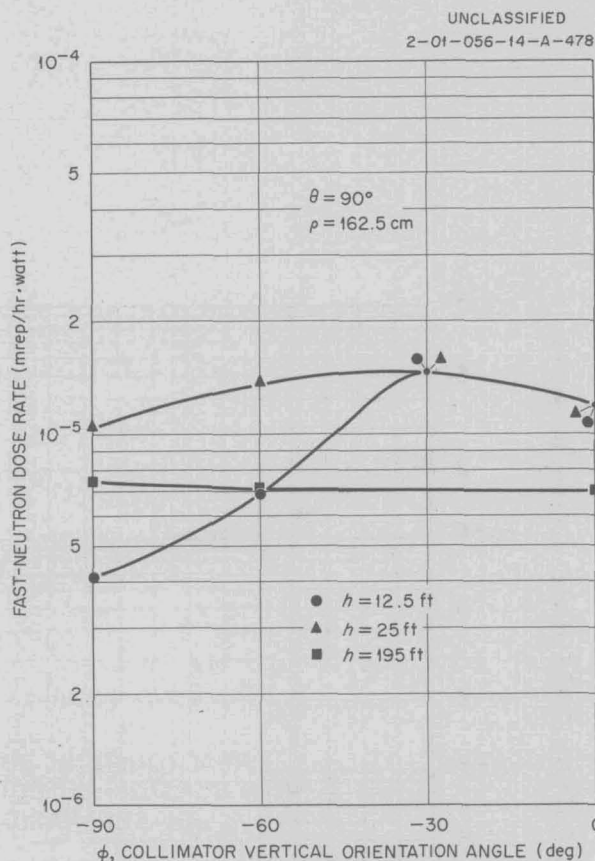


**Fig. 6.2.30. Fast-Neutron Dose Rate in Air as a Function of  $\phi$  for 15-in.-dia Collimator ( $\theta = 90$  deg;  $b = 12.5, 25,$  and  $195$  ft).**

The probability of neutrons scattering to an unshielded detector,  $I^2P_s(\theta)$ , was also determined by using the extrapolated values of the scattered dose rate shown in Fig. 6.2.16. The results as a function of  $\theta$  for a separation distance of 64 ft are shown in Fig. 6.2.41. Since measurements as a function of  $\theta$  were made for reactor-detector separation distances of 15 (not shown), 30 (not shown), and 64 ft, the scattering probability as a function of separation distance could also be determined (Fig. 6.2.42). It should be remembered that the values of  $I^2P_s(\theta)$  are dependent on the manner in which the scattered component is separated from the direct beam, and, until some method is devised for accurately separating the two components, there is no assurance that these probabilities are correct. This will also affect the scattering probabilities in the crew-compartment mockup, since the same direct beam is used to determine those values.

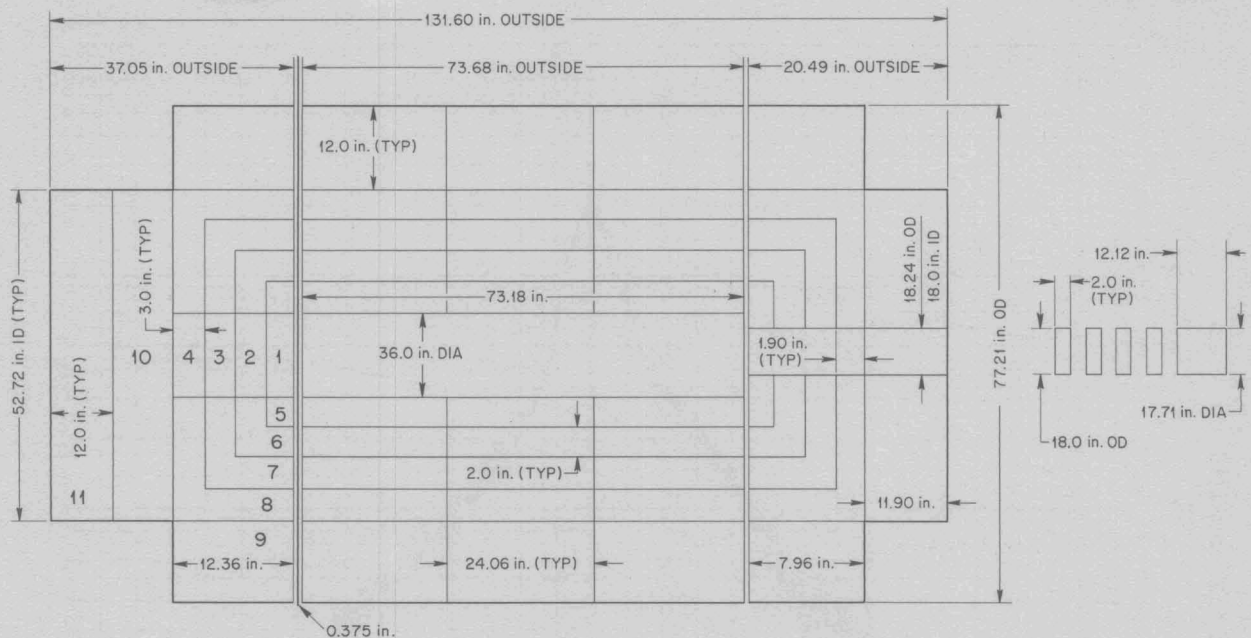


Fig. 6.2.31. Boeing Crew-Compartment Mockup.

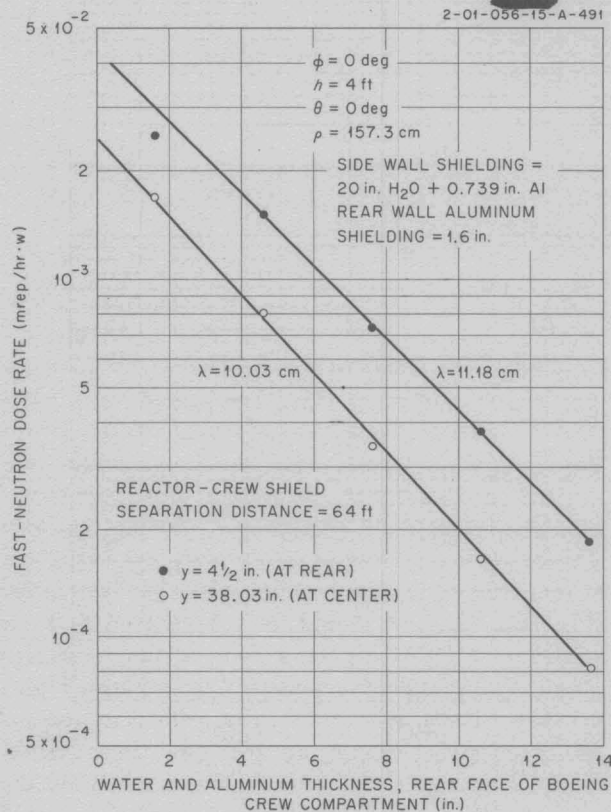


Fig. 6.2.32. Fast-Neutron Dose Rate in the Boeing Crew-Compartment Mockup as a Function of the Shielding Thickness on the Rear Wall.

The agreement with previous crew shield data indicates that the approach used is good, but it will be necessary to extend this experiment further in order to verify the results. Plans for such an extension are now being made.

**FAST-NEUTRON DOSE RATES IN A CREW-COMPARTMENT MOCKUP RESULTING FROM RADIATION FROM A COMPARTMENTALIZED REACTOR SHIELD TANK**

W. G. Blessing<sup>9</sup>                      L. A. Bowman<sup>10</sup>  
 S. K. Penny                              J. L. Hull  
 H. B. Hilgeman<sup>10</sup>

A calculation procedure for the optimization of a divided neutron shield<sup>11</sup> was developed at the TSF in which the reactor shield is divided into  $N$  conical shells whose vertexes converge at the center of the reactor. The total weight of the combined reactor and crew-compartment neutron shield is then expressed as a function of  $T_n$  (the thickness of the shielding in the conical shell),  $T_s$  (the crew-compartment side wall thickness), and  $T_r$  (the crew-compartment rear wall thickness). The method of Lagrange multipliers is used to obtain equations which  $T_n$ ,  $T_s$ , and  $T_r$  must satisfy in order for the weight to be a minimum for the specified dose rate.

<sup>9</sup>On assignment from Convair, San Diego.

<sup>10</sup>On assignment from WADC. *(Wright Air Development Center)*

<sup>11</sup>M. F. Valerino and F. L. Keller, *ANP Quar. Prog. Rep. Sept. 10, 1955, ORNL-1947, p 205.*

1-01-056-15-31-(-5)-465

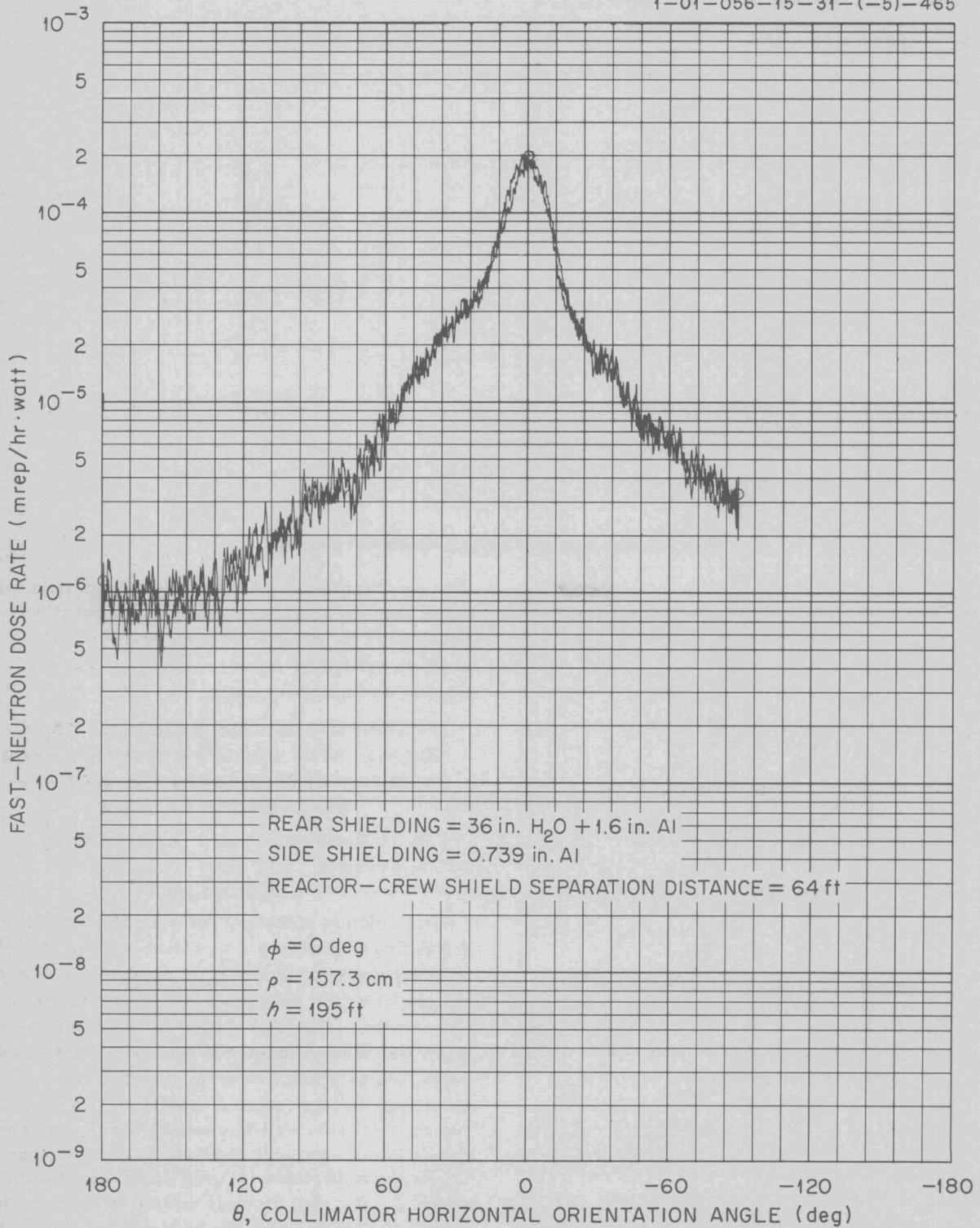


Fig. 6.2.33. Fast-Neutron Dose Rate in the Boeing Crew-Compartment Mockup as a Function of  $\theta$  for No Water Side Shielding.

1-01-056-15-29-(-5)-464

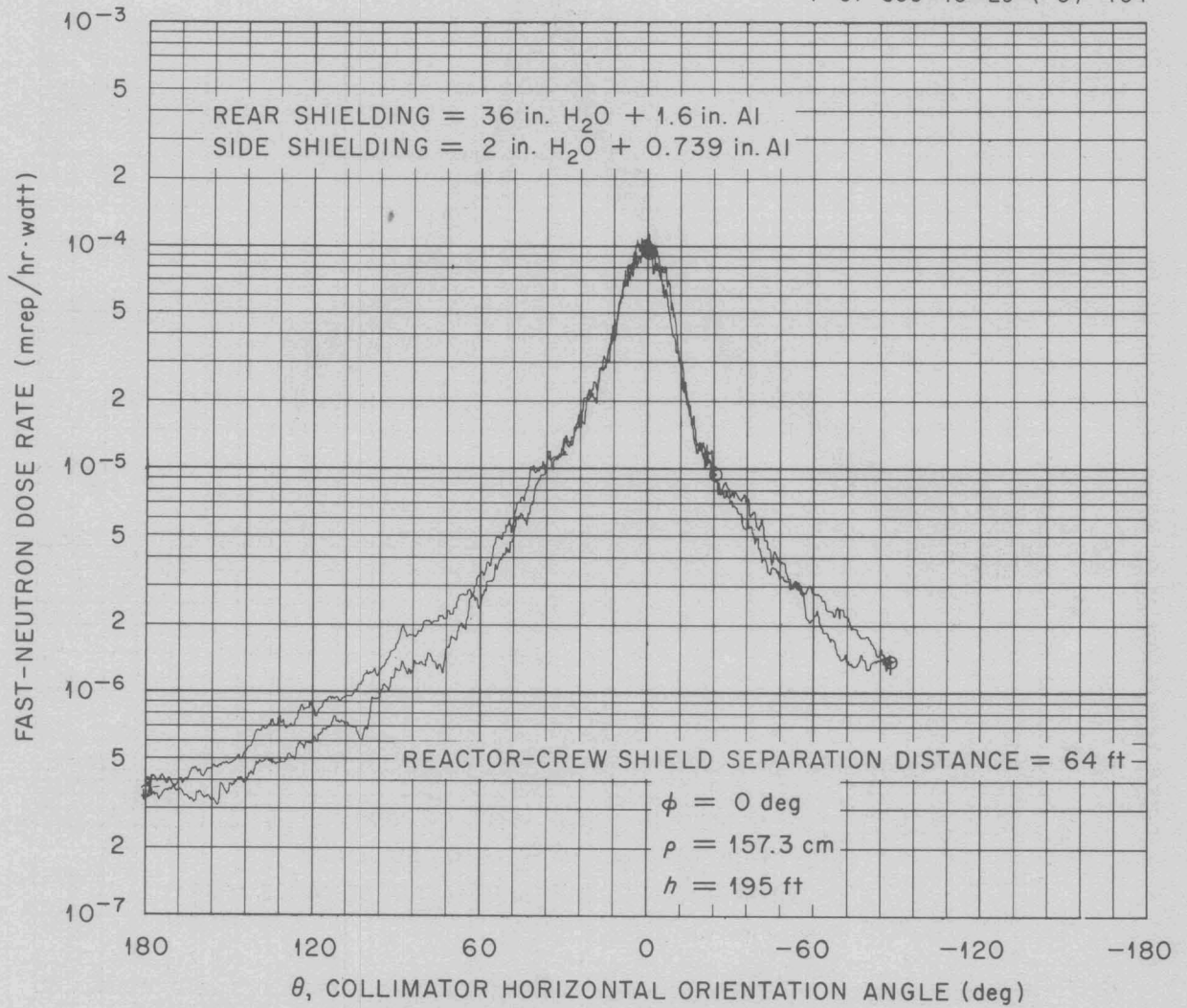


Fig. 6.2.34. Fast-Neutron Dose Rate in the Boeing Crew-Compartment Mockup as a Function of  $\theta$  for a 2-in. Water Side Shielding Thickness.

1-01-056-15-27-(-6)-463

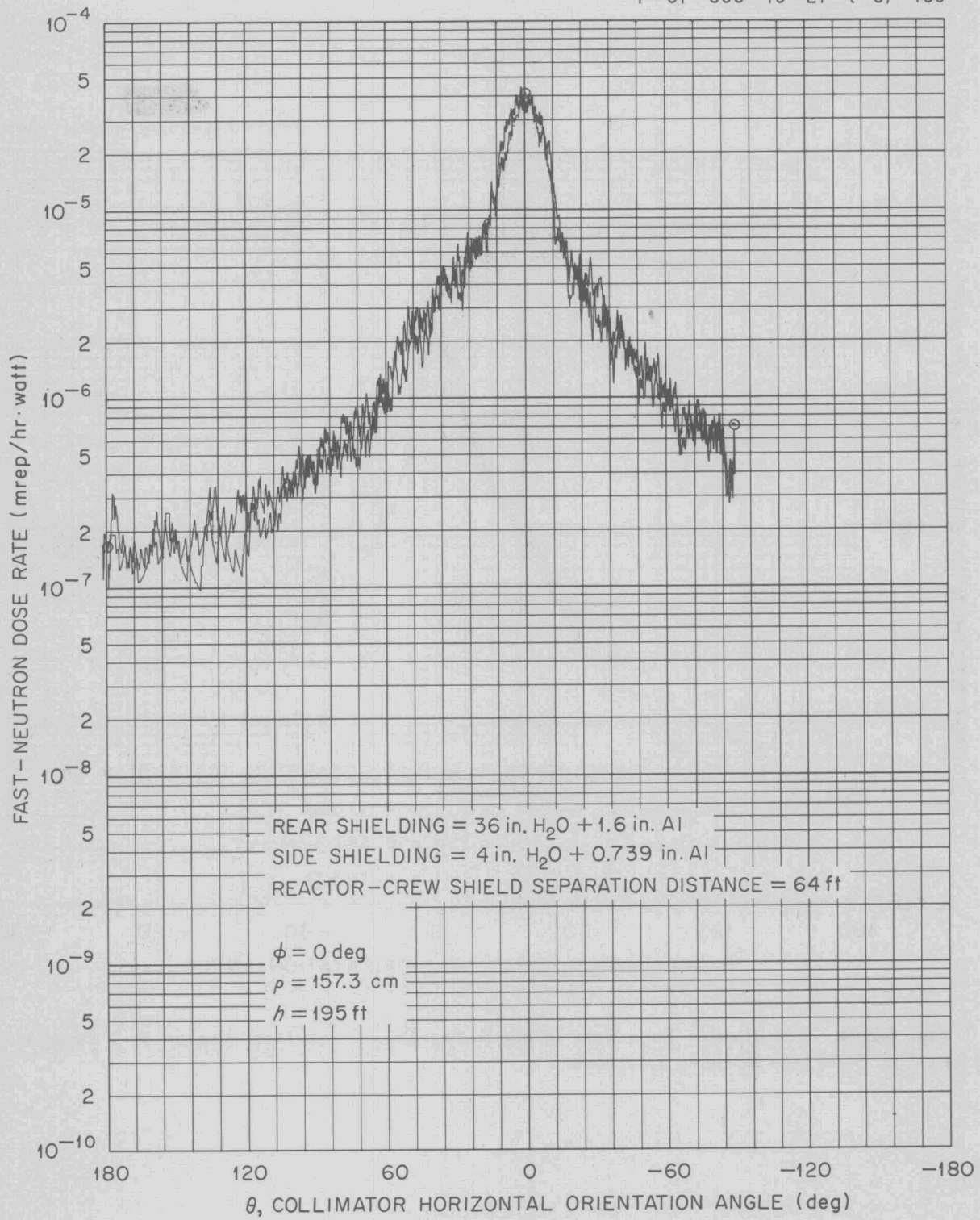


Fig. 6.2.35. Fast-Neutron Dose Rate in the Boeing Crew-Compartment Mockup as a Function of  $\theta$  for a 4-in. Water Side Shielding Thickness.

1-01-056-15-25-(-6)-462

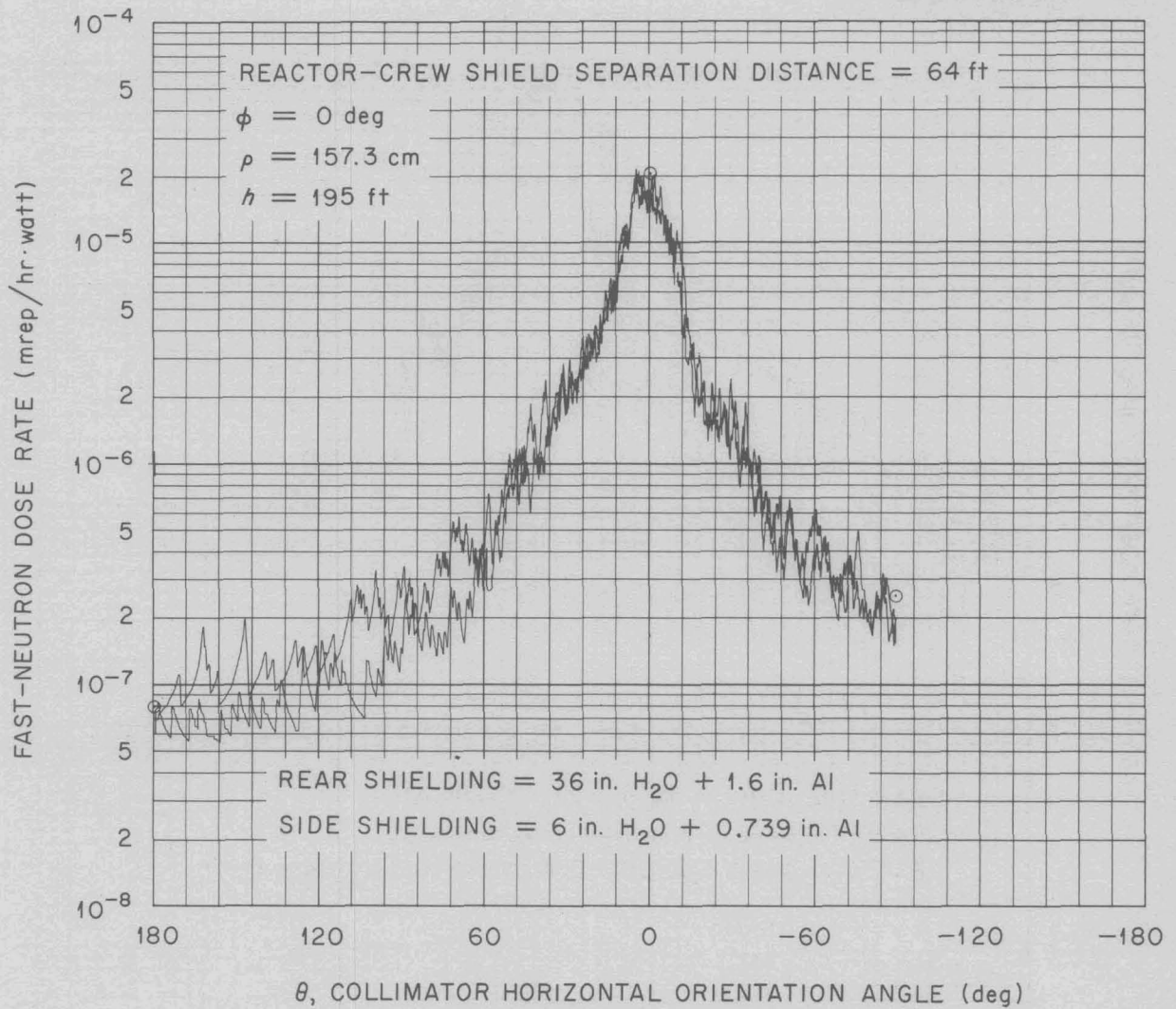


Fig. 6.2.36. Fast-Neutron Dose Rate in the Boeing Crew-Compartment Mockup as a Function of  $\theta$  for a 6-in. Water Side Shielding Thickness.

1-01-056-15-23-(-6)-461

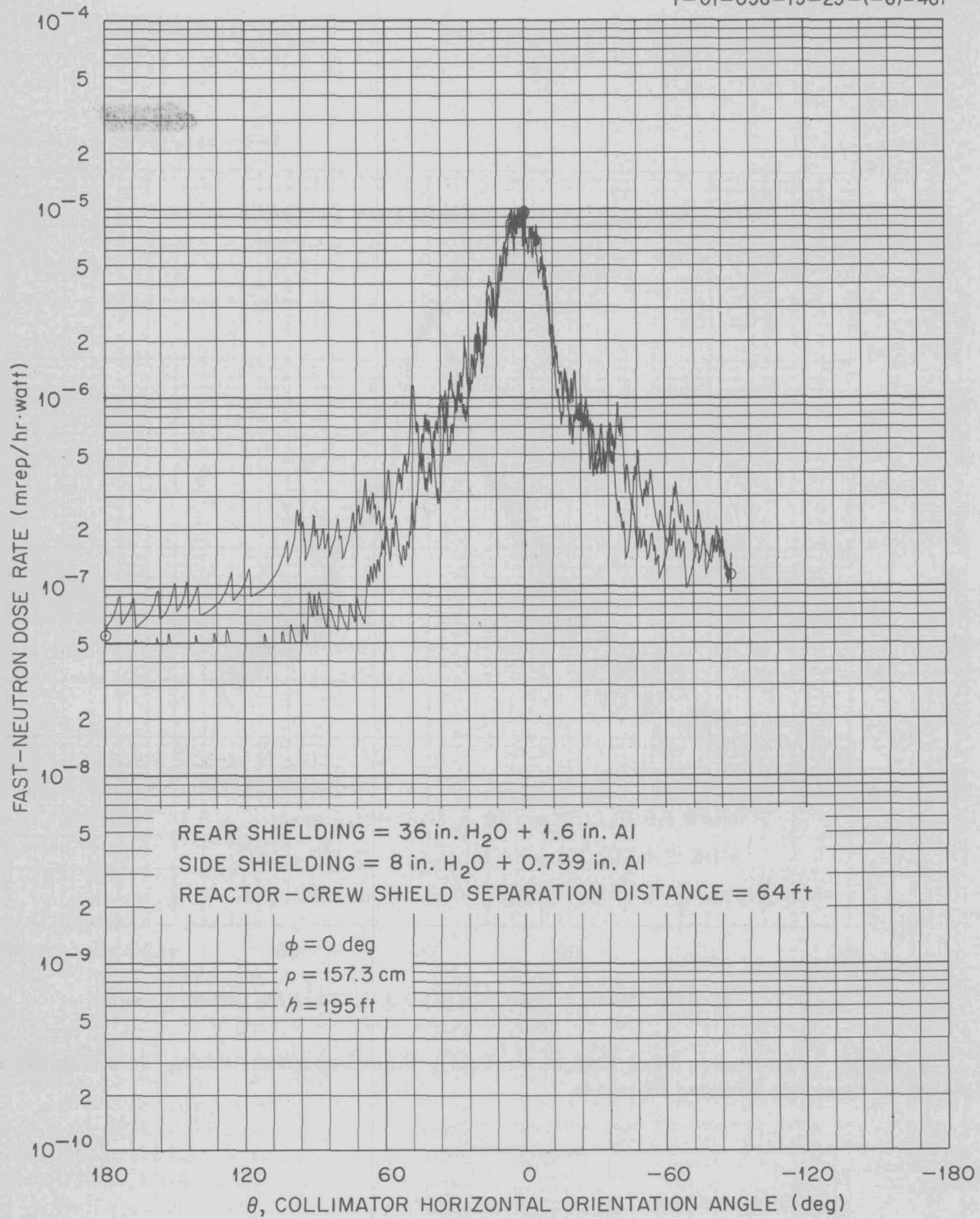


Fig. 6.2.37. Fast-Neutron Dose Rate in the Boeing Crew-Compartment Mockup as a Function of  $\theta$  for an 8-in. Water Side Shielding Thickness.

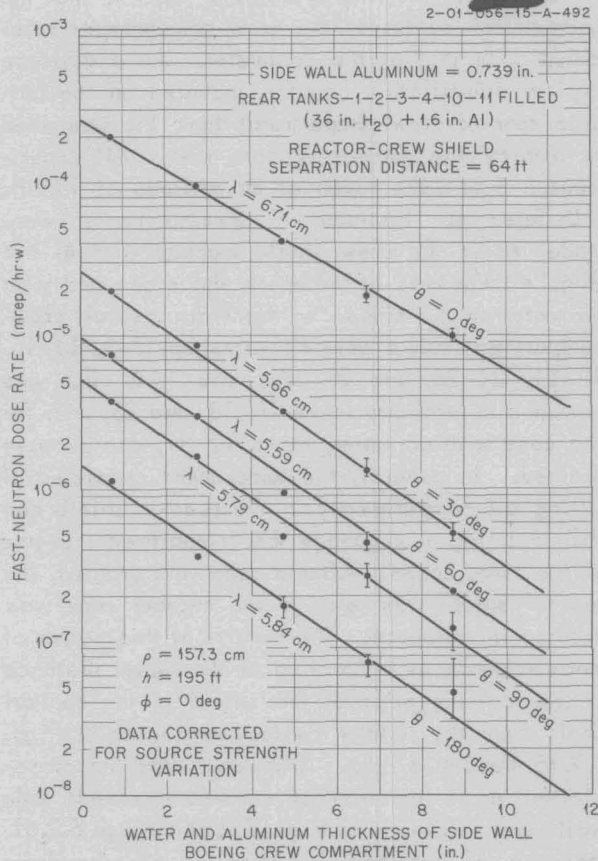


Fig. 6.2.38. Fast-Neutron Dose Rate at the Center of the Boeing Crew-Compartment Mockup as a Function of the Shielding Thickness on the Side Wall.

An iteration procedure<sup>12</sup> is used for solution of the equations.

In order to confirm the calculation procedure, a compartmentalized reactor shield tank and a compartmentalized crew-compartment mockup were obtained for use in a series of experimental tests. The compartmentalized reactor shield tank was designed by ORNL and constructed by Convair (San Diego); the crew compartment was designed and constructed by Boeing Airplane Co. according to ORNL specifications.

<sup>12</sup>S. K. Penny, *ANP Quar. Prog. Rep.* March 10, 1956, ORNL-2061, Part IV, p 54.

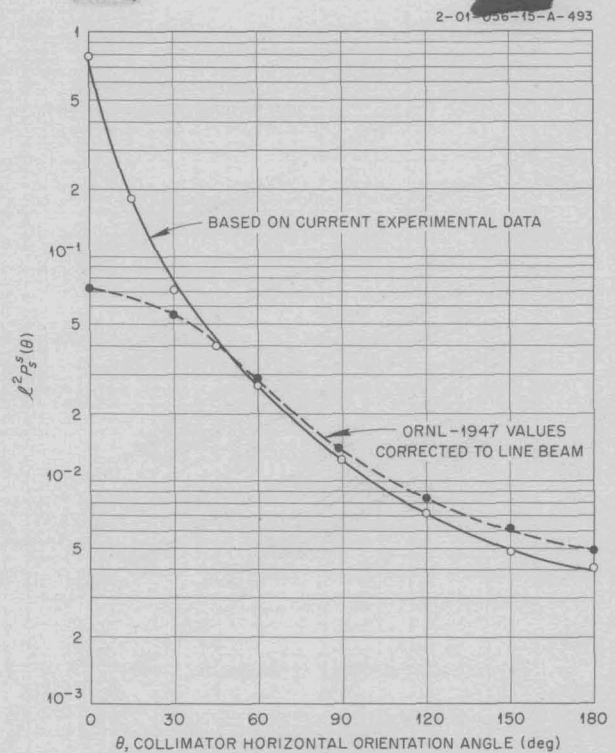


Fig. 6.2.39. Probability of Fast Neutrons Scattering into the Sides of the Boeing Crew-Compartment Mockup as a Function of  $\theta$ .

#### Description of Reactor Shield and Crew-Compartment Mockup

The reactor shield is a compartmentalized tank (Figs. 6.2.43 and 6.2.44), approximately spherical in shape, which was built to enclose the core of the TSF reactor and serve as a neutron shield. The compartments in the tank are of welded aluminum construction and can be filled and drained remotely with liquids of density as high as 2.5. By varying the location of the liquid the shape of the neutron shield can thus be changed. The tank actually consists of eight large conical shells containing a total of 44 subshells, some of which are intersected by the cylindrical reactor standpipe. The outer 1-ft compartments in each of the eight large cones are used to block out the neutron radiation from complete sections of the shield for differential beam experiments. The 2-in. compartments are used to determine the optimum neutron shield shape by trial and error filling of various tank combinations.

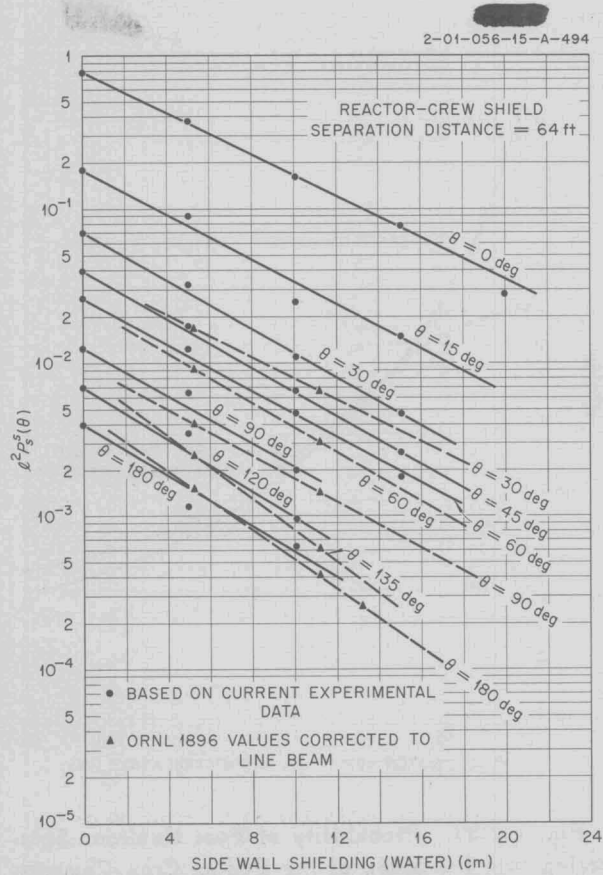


Fig. 6.2.40. Probability of Fast Neutrons Scattering into the Sides of the Boeing Crew-Compartment Mockup as a Function of the Thickness of the Side Wall Water Shielding.

The compartmentalized crew-compartment mockup (Fig. 6.2.45) consists of 33 cylindrical shells surrounding the cylindrical crew-compartment air space. When filled with water, tanks 1 through 4 and 10 and 11 are used for rear shielding, tanks 12 through 26 are used for side shielding, and tanks 27 through 33 are used for front shielding. Tanks 5 through 9 are used to investigate the effect of shielding at the "corners" of the tank.

**Experimental Measurements**

The TSF reactor was placed inside the compartmentalized reactor shield tank at a distance ( $l$ ) of 64 ft from the outside rear of tank 4 of the crew compartment. A Hurst fast-neutron dosimeter, calibrated against a Po-Be neutron source, was placed lengthwise inside the crew-compartment

mockup along the reactor-detector axis so that the geometrical center of the crew compartment coincided with that of the dosimeter. An anthracene crystal scintillation counter, mounted on the outside rear of crew-compartment tank 11, was used to monitor the gamma-ray dose rate. All experimental data were taken at an altitude of 195 ft.

Differential fast-neutron measurements were made inside the crew shield mockup with 4- and 2-in. thicknesses of water on the sides and with no water on the sides. In the 4-in. case all crew-compartment tanks were filled except 7-9, 14-16, 19-21, 24-26, and 29-31. The 2-in. case was obtained by draining tanks 13, 18, and 23, and, for the case with no water, tanks 12, 17, and 22 were drained. In general, the experiment consisted of filling all compartments in the reactor shield and then draining in sequence the compartments in one of the large cones. After a cone was drained, the reactor shield was refilled and another cone was drained in sequence. The results of this series of measurements as a function of the radial distance of the outside edge of the shield in the conical shell from the reactor center are shown in Figs. 6.2.46 through 6.2.53. The same data are cross-plotted as a function of crew-compartment side wall water thickness in Figs. 6.2.54 through 6.2.61. Because of mechanical difficulty with the drain valve, the data from cone 2 (Figs. 6.2.47 and 6.2.55) are considered to be questionable.

Integral fast-neutron dose rate measurements corresponding to several neutron shield configurations were made after draining layers of compartments around the eight cones. (A layer consists of a group of comparable compartments such as compartments 6, 12, 18, 24, 30, 36, 41, and 44.) Dose rate measurements were obtained for eight different configurations.

**Comparison of Experimental Data with Calculations**

The relaxation lengths of the fast neutrons from each conical shell in the side shielding of the crew compartment can be determined as a function of reactor shield thickness in a conical shell (that is, as a function of the number of filled tanks) from the data presented in Figs. 6.2.54 through 6.2.61. These relaxation lengths can be compared with calculated relaxation lengths based on data from earlier TSF differential shielding experiments and on an empirical relation<sup>11</sup> which was established during the analysis of those experiments.

UNCLASSIFIED  
2-01-056-14-A-495

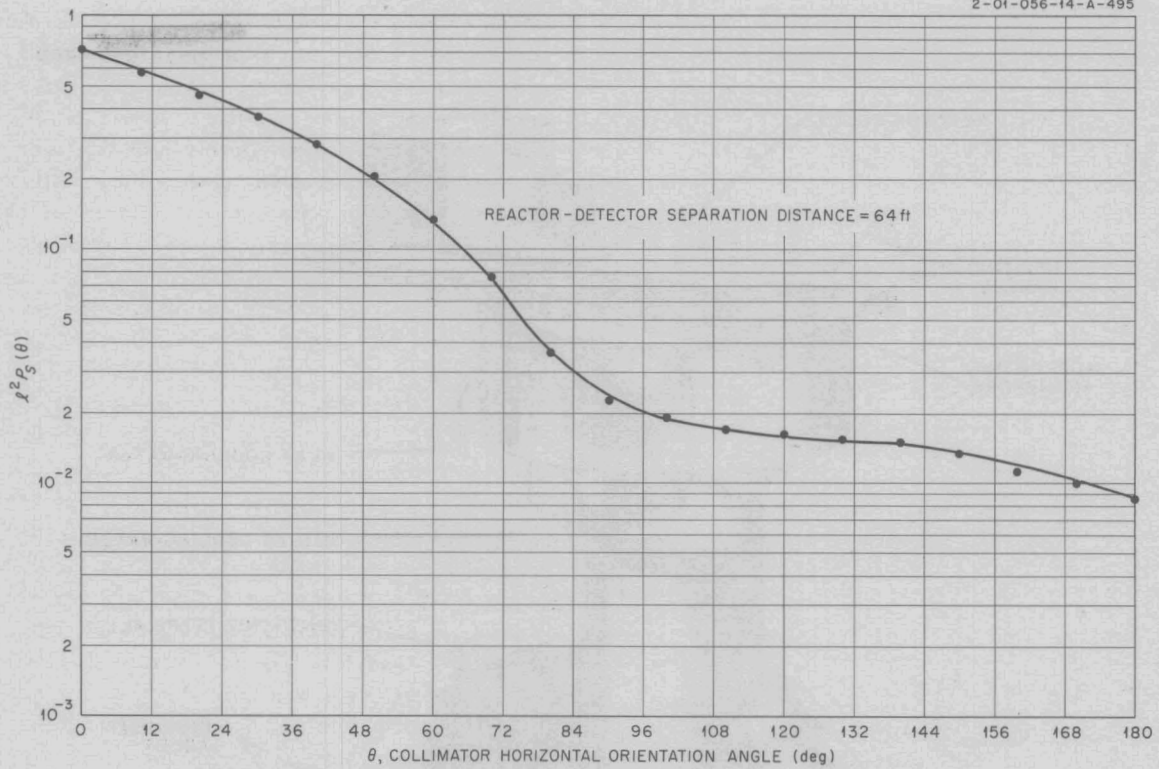


Fig. 6.2.41. Probability of Fast Neutrons Scattering to an Unshielded Detector as a Function of  $\theta$ .

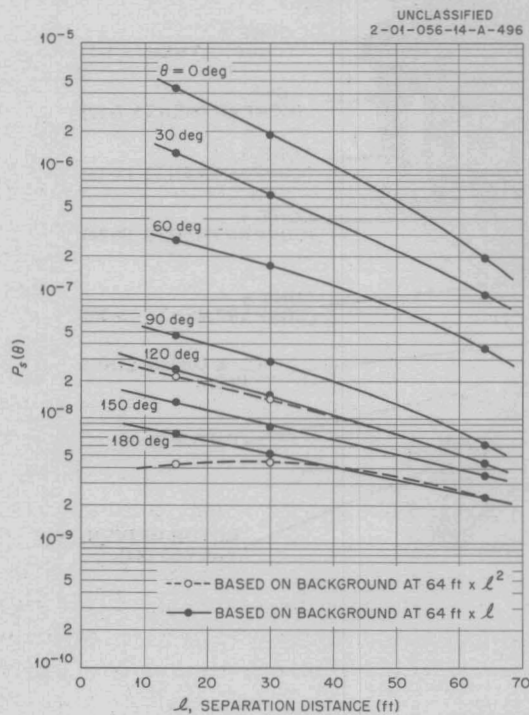


Fig. 6.2.42. Probability of Fast Neutrons Scattering to an Unshielded Detector as a Function of Reactor-Detector Separation Distance.

The relation states that

$$\lambda_s^s(T_n, T_s, \theta_n) = \lambda_s^s(45, T_s, \theta_n) \frac{\lambda_d(T_n + T_s)}{\lambda_d(45 + T_s)}$$

where

$\lambda_s^s$  = relaxation length of air-scattered fast neutrons in the side of the crew compartment,

$\lambda_d$  = relaxation length in the reactor shield,

$T_n$  = thickness of shield in the conical shell,

$T_s$  = crew-compartment side wall thickness,

$\theta_n$  = reactor shield conical shell angle.

Values of  $\lambda_d$  for reactor shield thicknesses extending to approximately 150 cm were established from earlier TSF and BSF data (Fig. 6.2.62). Values of  $\lambda_s^s$  for a reactor shield thickness of 45 cm were also determined in earlier TSF experiments (Fig. 6.2.63). With the use of these results and the above equation, it is possible to calculate values of  $\lambda_s^s$  for various reactor shield thicknesses which can be compared with those obtained from this experiment. The calculations were made for cones 1, 4, 7, and 8 and a crew-

1-01-056-16-P-488

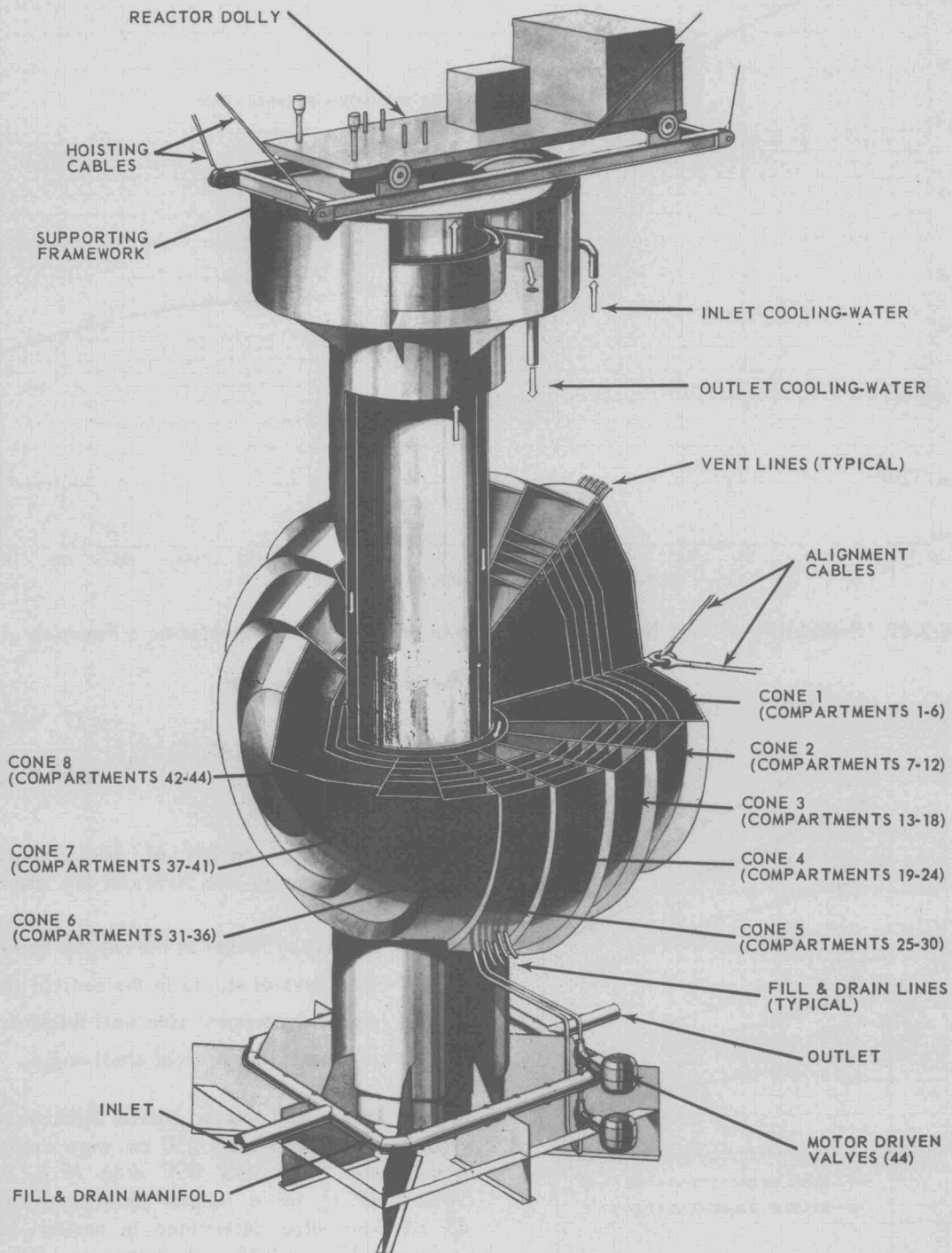


Fig. 6.2.43. Compartmentalized Reactor Shield Tank.

2-01-056-16-P-499

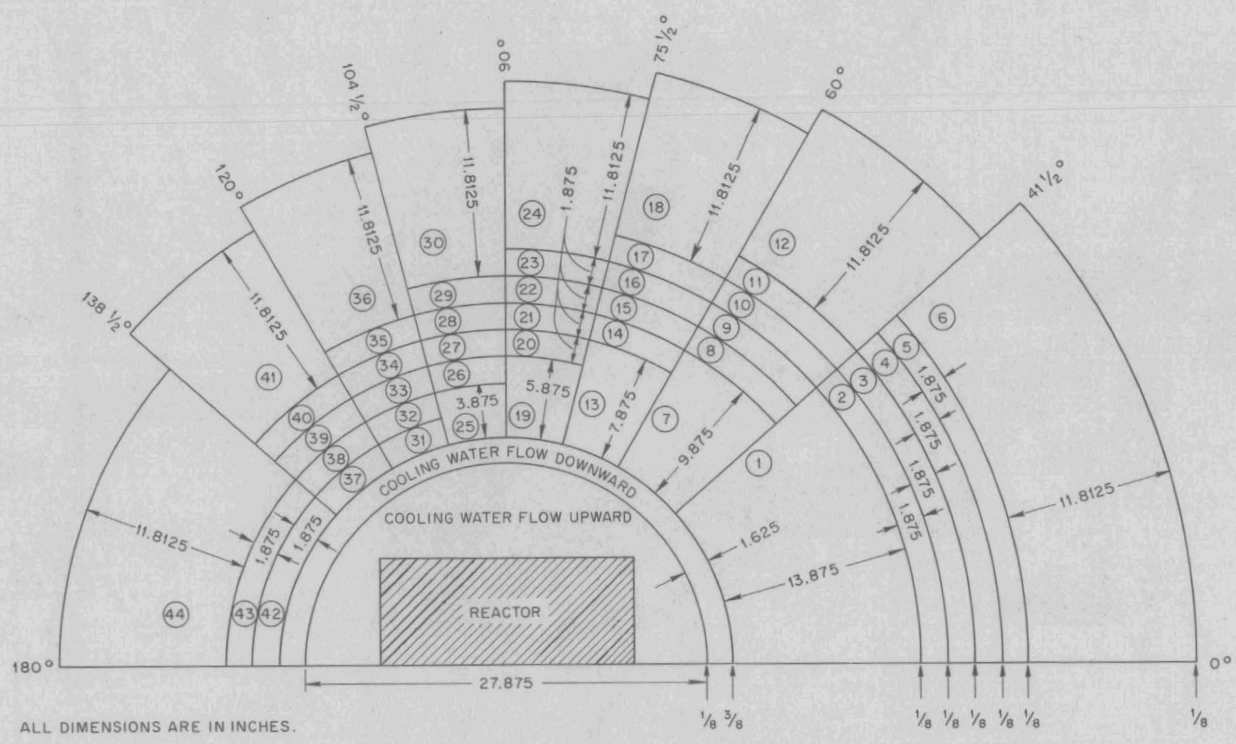
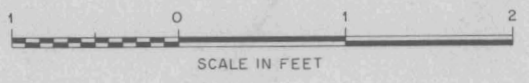


Fig. 6.2.44. Compartmentalized Reactor Tank (Horizontal Section).

PERIOD ENDING DECEMBER 31, 1956

CONFIDENTIAL  
2-01-056-16-P-523A

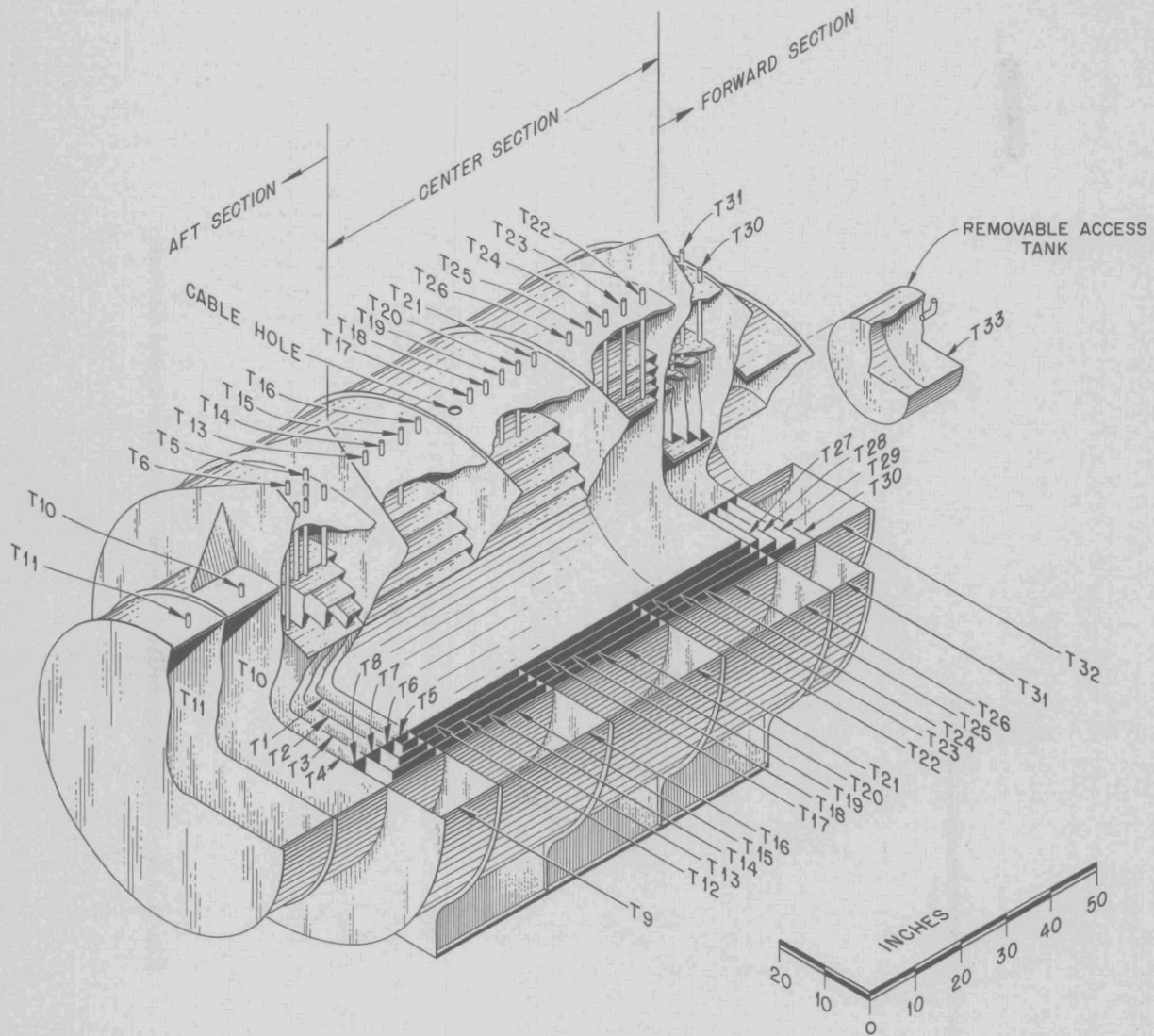
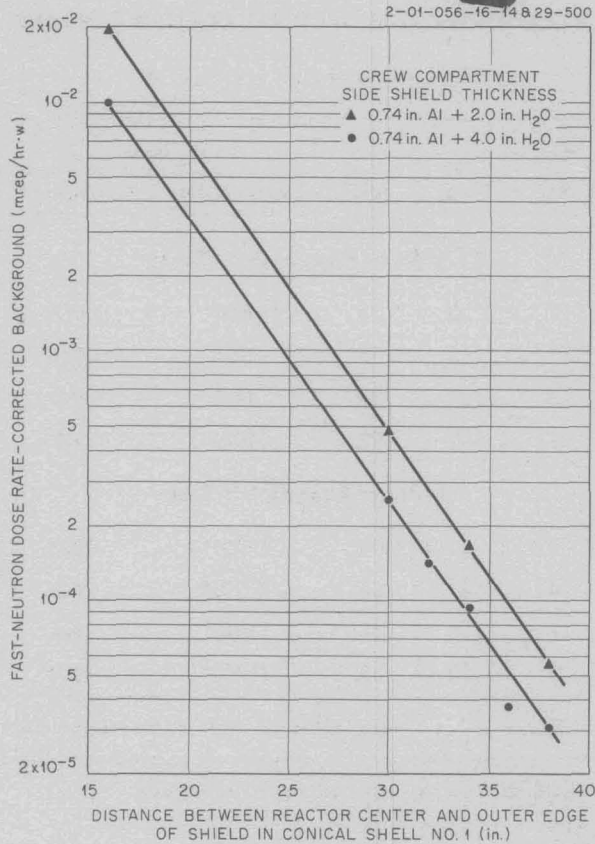


Fig. 6.2.45. Compartmentalized Crew-Compartment Tank.



**Fig. 6.2.46. Fast-Neutron Dose Rate in Boeing Crew-Compartment Mockup Resulting from Radiation from Conical Shell No. 1 as a Function of Shield Thickness in Shell No. 1.**

compartment side shield thickness of 12 cm (10 cm of water plus 2 cm of aluminum). A comparison of the measured and calculated values of  $\lambda_s^S$  is presented in Table 6.2.1. With the exception of the values for cone 1, the data are considered to be in good agreement. Values for  $\lambda_s^S$  cannot be calculated for the completely drained condition by using the above equation, since  $T_n$  is not constant over the entire conical shell owing to the intersection with the cylindrical standpipe. A calculation procedure which includes the effect of the standpipe is presented in the following section ("Analysis of Experimental Data").

In order to calculate relaxation lengths for comparison with those obtained from the experimental data shown in Figs. 6.2.46 through 6.2.53, an "over-all" relaxation length  $\lambda_0(T_n + T_s, \theta)$  was

**TABLE 6.2.1. COMPARISON OF EXPERIMENTAL AND CALCULATED RELAXATION LENGTHS OF AIR-SCATTERED FAST NEUTRONS IN THE SIDE OF BOEING CREW COMPARTMENT**

$$T_s = 10 \text{ cm of H}_2\text{O} + 2 \text{ cm of Al}$$

Cone No.	$\theta_n$ (deg)	$T_n$ (cm)	$\lambda_s^S$ (cm)	
			Experimental	Calculated
<b>At Outer Edge of 2-in. Tanks</b>				
1	0	74	8.3	7.1
4	83*	56	6.0	6.1
7	128**	38	5.0	4.7
8	180	29	4.6	4.2
<b>At Outer Edge of Standpipe</b>				
1	0		7.4	
4	83*		4.9	
7	128**		4.5	
8	180		4.4	

\*The value of  $\lambda_s^S$  for  $\theta = 90$  deg in Fig. 6.2.63 was used in the calculation.

\*\*The value for  $\theta = 135$  deg in Fig. 6.2.63 was used in the calculation.

defined by

$$\int_0^{T_n+T_s} \frac{dt}{\lambda_0(\theta, t)} = \int_0^{T_n} \frac{dt}{\lambda_d(t)} + \int_0^{T_s} \frac{dt}{\lambda_s^S(\theta, T_n, t)}$$

The partial derivative of this expression with respect to  $T_n$  yields

$$\lambda_0(T_n + T_s, \theta) = \left\{ \frac{1}{\lambda_d(T_n)} + \int_0^{T_s} \frac{\partial [1/\lambda_s^S(\theta, T_n, t)]}{\partial T_n} dt \right\}^{-1}$$

Values of the over-all relaxation lengths were calculated for cones 1, 4, 7, and 8 in which the shield was assumed to extend to the outer edge of the 2-in. tanks. The results are compared in Table 6.2.2 with values taken from the experimental data. The fact that the measured values are higher than those calculated is attributed to the geometrical effect of the cylindrical standpipe intersecting the

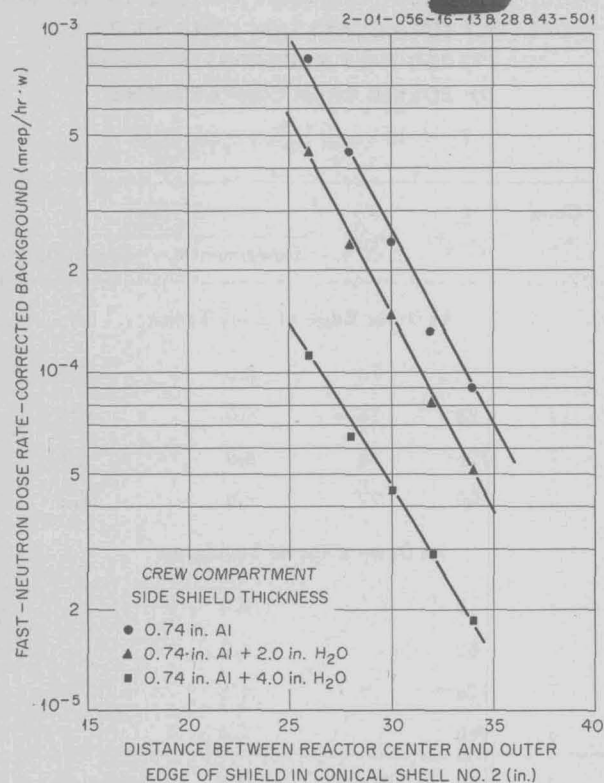


Fig. 6.2.47. Fast-Neutron Dose Rate in Boeing Crew-Compartment Mockup Resulting from Radiation from Conical Shell No. 2 as a Function of Shield Thickness in Shell No. 2.

conical shells. When the experimental data are extrapolated to the outer edge of the 1-ft compartments, lower relaxation lengths are obtained which are in good agreement with the calculated values.

A comparison of the integral dose rate in the crew compartment with the summation of the differential dose rates is shown in Fig. 6.2.64 for a crew-compartment side shield consisting of 10 cm of water and 2 cm of aluminum. The consistently lower results obtained from the summation of the differential data are attributed to the interference of adjacent shells when a partially filled conical shell is between two completely filled conical shells. The ratio of the integral dose rate to the summation of the differential dose rates as a function of layers drained is tabulated in Fig. 6.2.64. Analysis of the data from the integral measurements has not been started.

TABLE 6.2.2. COMPARISON OF EXPERIMENTAL AND CALCULATED OVER-ALL RELAXATION LENGTHS

$$T_s = 10 \text{ cm of H}_2\text{O} + 2 \text{ cm of Al}$$

Cone No.	$\theta_n$ (deg)	$T_n$ (cm)	$\lambda_0$ (cm)	
			Experimental	Calculated
At Outer Edge of 2-in. Tanks				
1	0	74	10.0	10.2
4	83	56	12.5	10.1
7	128	38	11.1	9.2
8	180	29	10.4	9.0
At Outer Edge of 1-ft Tanks				
1	0	104	(~10)*	10.3
4	83	86	(~10)*	10.3
7	128	68	(~10)*	10.4
8	180	59	(~10)*	10.2

\*These values were obtained from extrapolated data and are shown only for comparison with calculated values; they should not be used as measured values.

#### Analysis of the Experimental Data

In order to account for the long relaxation lengths apparent in Figs. 6.2.46 through 6.2.53, a calculation of dose rate inside the crew compartment as a function of distance through the reactor shield was attempted for cone 4 with the use of a calculation procedure similar to that used in the TSF neutron shield optimization study.<sup>13</sup> To simplify the calculation, the following initial assumptions were made:

1. A vertical section through the shield tank at  $\theta_n = 90$  deg is equivalent to a section through cone 4 at  $\theta_n = 82\frac{3}{4}$  deg.

2. The probability of neutrons being scattered by air into the sides of the crew compartment,  $l^2 P_s^s(\theta)$ , is constant from  $\theta_n = 90$  deg to  $\theta = 75\frac{1}{2}$  deg.

3. The dose rate outside the crew compartment ( $l = 64$  ft) can be expressed in terms of a reactor surface source strength with cosine distribution.

<sup>13</sup>M. F. Valerino and F. L. Keller, ANP Quar. Prog. Rep. Sept. 10, 1955, ORNL-1947, p 205.

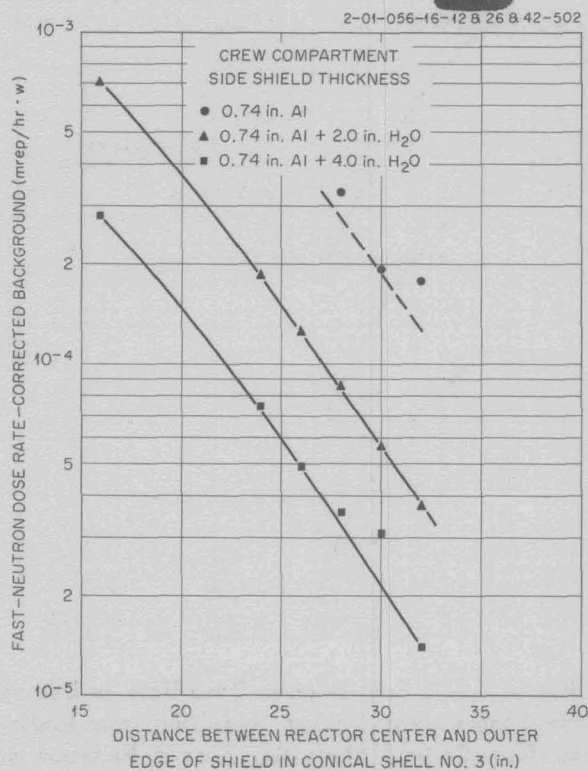


**Fig. 6.2.48. Fast-Neutron Dose Rate in Boeing Crew-Compartment Mockup Resulting from Radiation from Conical Shell No. 3 as a Function of Shield Thickness in Shell No. 3.**

A vertical section through cone 4 is presented in Fig. 6.2.65 to illustrate the geometry used for the calculations. For each compartment in cone 4, the procedure consists of attenuating through the shield tank from the reactor surface to a point in space far outside the shield tank (so that all lines from the reactor are nearly parallel), multiplying by the probability of scattering into the crew compartment at a distance of 64 ft, and finally attenuating through the side of the crew compartment. A numerical integration is carried out with respect to (1) the reactor surface source strength (cosine distribution) seen from a point in space, (2) the polar angle  $\phi$ , and (3) the conical shell angle  $\theta_n$ .

$$D_m = \Delta_n \cos \theta \, l^2 P_s^s(\theta_n) f_s^s \frac{1}{l^2} \sum_{i=0}^6 \sum_{j=0}^{\pi/2} \frac{\cos \phi_j \sin \theta_n}{\pi} \bar{P}_i \lambda_{cij} \Delta A_i \Delta \phi_j \frac{cV}{C} \times$$

$$\times \exp - \int_0^{T_s} \frac{dt}{\lambda_s^s(T_{ij}, \theta_n)} \exp - \int_0^{T_{ij}} \frac{dt}{\lambda_d}$$

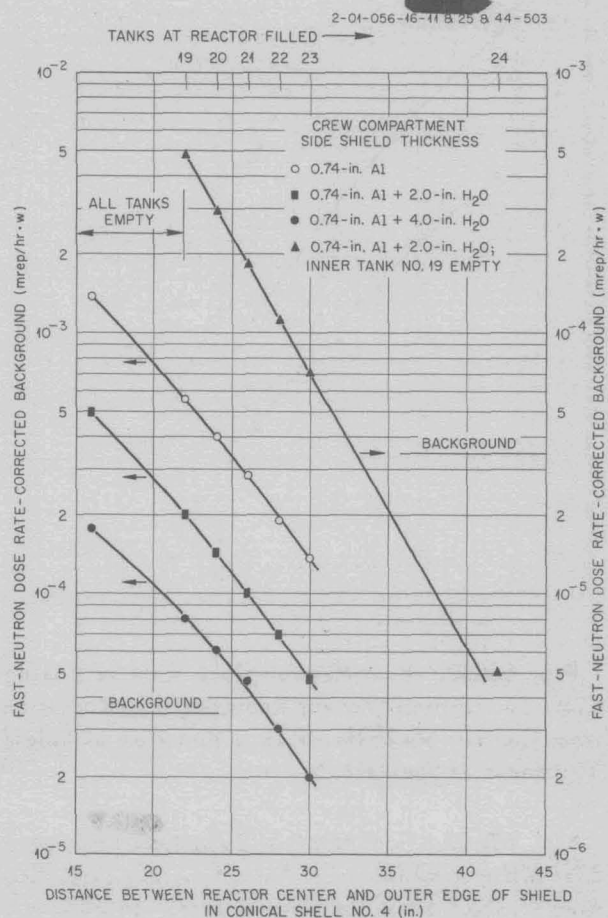


**Fig. 6.2.49. Fast-Neutron Dose Rate in Boeing Crew-Compartment Mockup Resulting from Radiation from Conical Shell No. 4 as a Function of Shield Thickness in Shell No. 4.**

In order to simplify the calculation procedure,  $\theta_n$  was held constant, and the side face power distribution taken from Fig. 6.2.66 was averaged over the projected conical shell width (about  $1\frac{1}{2}$  fuel elements) of compartment 19. This value was taken as 0.925 of the peak value. The expression for the relative fast-neutron dose rate in terms of the surface source strength (cosine distribution) is given by

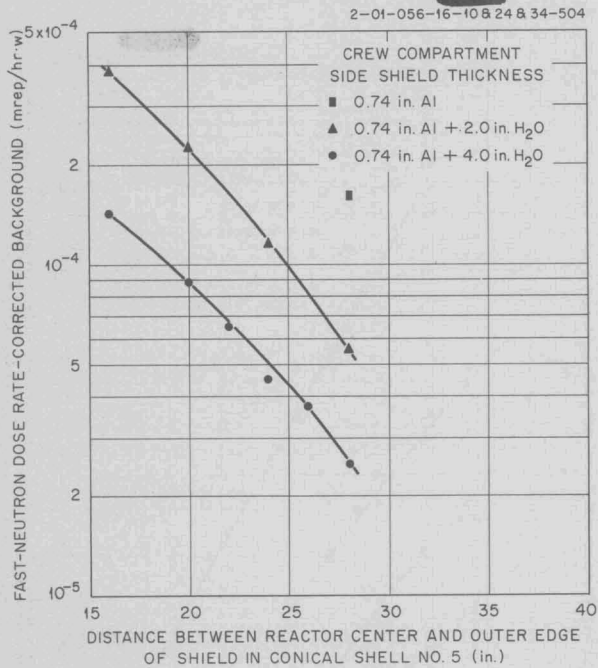


Fig. 6.2.50. Fast-Neutron Dose Rate in Boeing Crew-Compartment Mockup Resulting from Radiation from Conical Shell No. 5 as a Function of Shield Thickness in Shell No. 5.

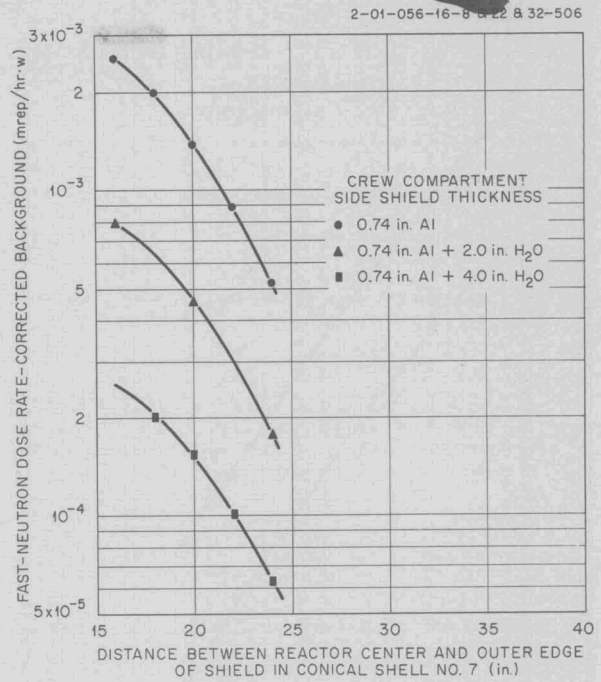


Fig. 6.2.52. Fast-Neutron Dose Rate in Boeing Crew-Compartment Mockup Resulting from Radiation from Conical Shell No. 7 as a Function of Shield Thickness in Shell No. 7.

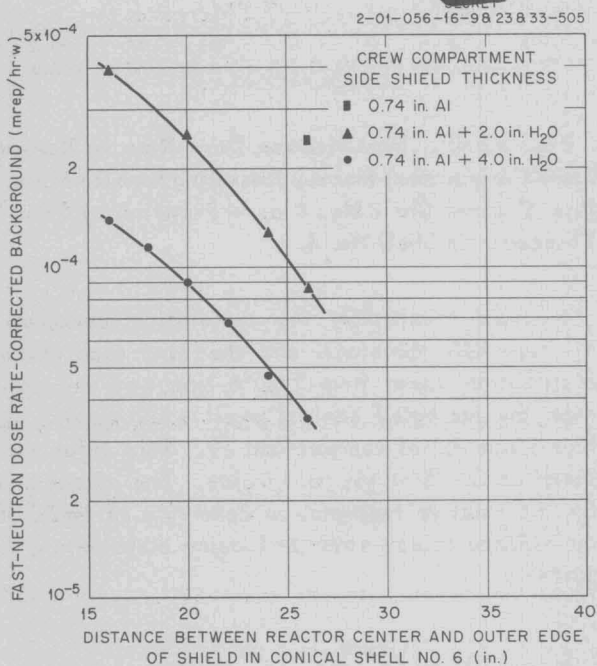


Fig. 6.2.51. Fast-Neutron Dose Rate in Boeing Crew-Compartment Mockup Resulting from Radiation from Conical Shell No. 6 as a Function of Shield Thickness in Shell No. 6.

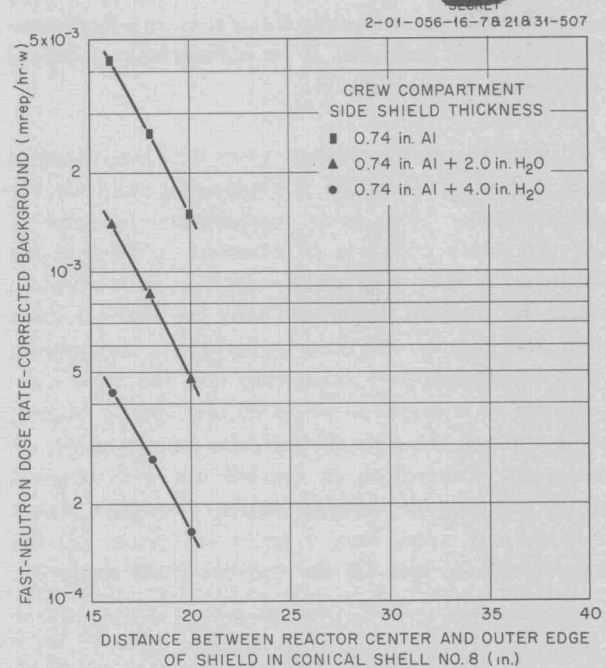


Fig. 6.2.53. Fast-Neutron Dose Rate in Boeing Crew-Compartment Mockup Resulting from Radiation from Conical Shell No. 8 as a Function of Shield Thickness in Shell No. 8.

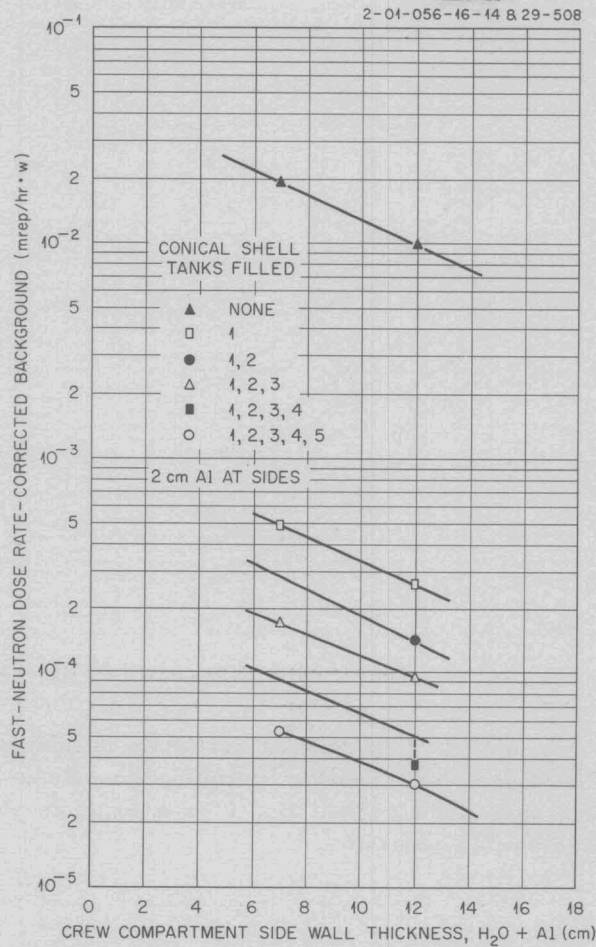


Fig. 6.2.54. Fast-Neutron Dose Rate in Boeing Crew-Compartment Mockup Resulting from Radiation from Conical Shell No. 1 as a Function of Crew-Compartment Side Wall Thickness.

where

$D_m$  = dose rate inside the crew compartment arising from compartment  $m$  in cone 4,

$\Delta_n \cos \theta l^2 P_s^s(\theta_n) f_s^s$  = fraction of the total radiation from a conical shell scattering into the center of the crew compartment,

$\frac{\cos \phi_j \sin \theta_n}{\pi} \bar{P}_i \lambda_{cij} \frac{c\nu}{C}$  = cosine-distributed surface source strength per unit area per unit solid angle,

$\Delta A_i$  = incremental area of solid angle,

$\bar{P}_i$  = relative average power density over  $\theta_n$  based on power distribution data of Fig. 6.2.67 (w/cm<sup>3</sup>),

$\lambda_c$  = core relaxation length (cm),

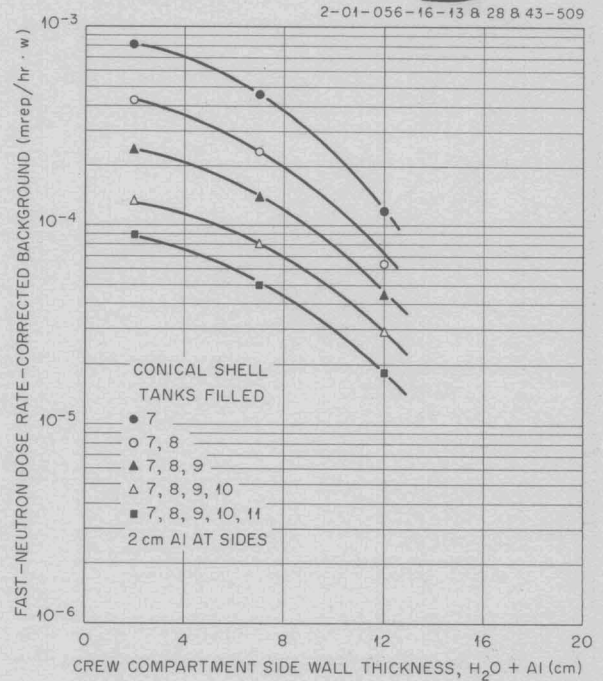


Fig. 6.2.55. Fast-Neutron Dose Rate in Boeing Crew-Compartment Mockup Resulting from Radiation from Conical Shell No. 2 as a Function of Crew-Compartment Side Wall Thickness.

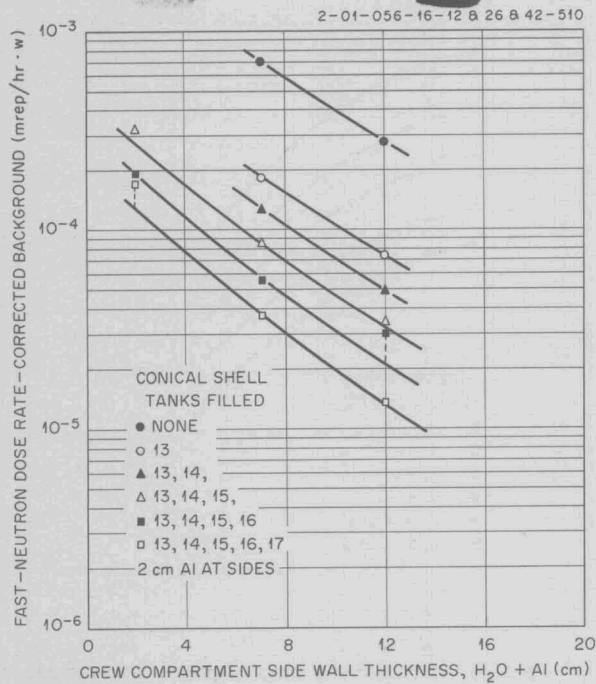


Fig. 6.2.56. Fast-Neutron Dose Rate in Boeing Crew-Compartment Mockup Resulting from Radiation from Conical Shell No. 3 as a Function of Crew-Compartment Side Wall Thickness.

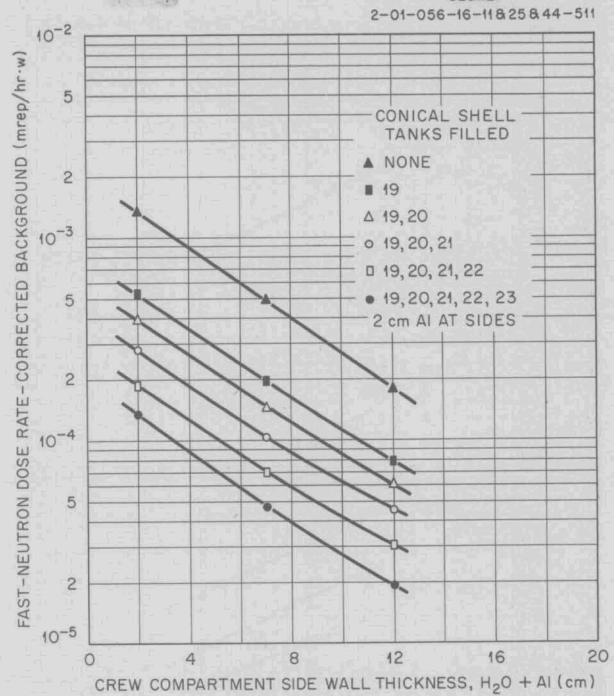


Fig. 6.2.57. Fast-Neutron Dose Rate in Boeing Crew-Compartment Mockup Resulting from Radiation from Conical Shell No. 4 as a Function of Side Wall Thickness.

$$c\nu = (\text{neutrons/w}\cdot\text{sec}),$$

C = conversion from number flux to dose rate,

$$\exp - \int_0^{T_{ij}} \frac{dt}{\lambda_d} = \text{attenuation through the } m\text{th compartment in the reactor shield,}$$

$$\exp - \int_0^{T_s} \frac{dt}{\lambda_s^s(T_{ij}, \theta_n)} = \text{attenuation through the side of the crew compartment.}$$

Elimination of all the constants from the equation yields

$$D_m \propto \sum_{i=0}^6 \sum_{j=0}^{\pi/2} \cos \phi_j \bar{P}_i \lambda_{cij} \Delta A_i \Delta \phi_j \exp - \int_0^{T_{ij}} \frac{dt}{\lambda_d} \exp - \int_0^{T_s} \frac{dt}{\lambda_s^s(T_{ij})} .$$

Results of the calculation for cone 4 are shown in Fig. 6.2.68. The lack of agreement between the measured and calculated relaxation lengths for the inner compartments is attributed to neglecting the effect of slant leakage into cone 4 from cones 3 and 5. Note that the calculated curve has a shape which is similar to the upper curve of Fig. 6.2.49

(compartment 19 empty). The calculation is being repeated by integrating over  $\theta$  in the horizontal plane (Fig. 6.2.44) in the same manner as that used for integrating over  $\phi$  in the vertical plane (Fig. 6.2.65).

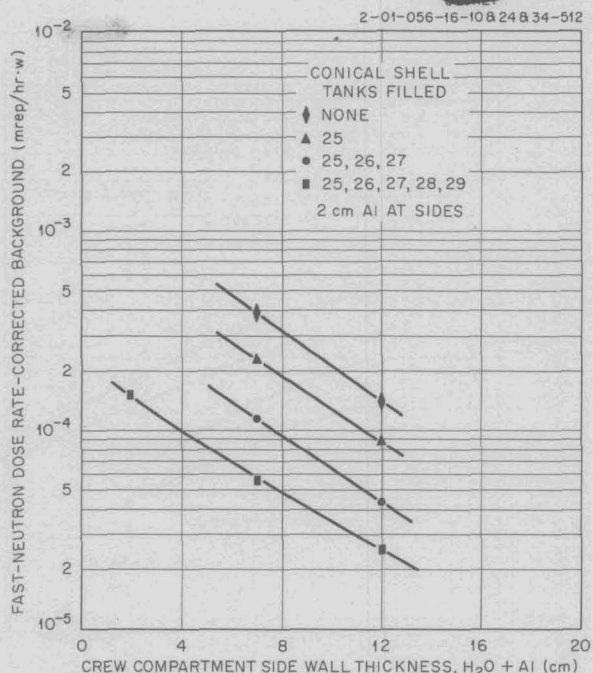


Fig. 6.2.58. Fast-Neutron Dose Rate in Boeing Crew-Compartment Mockup Resulting from Radiation from Conical Shell No. 5 as a Function of Crew-Compartment Side Wall Thickness.

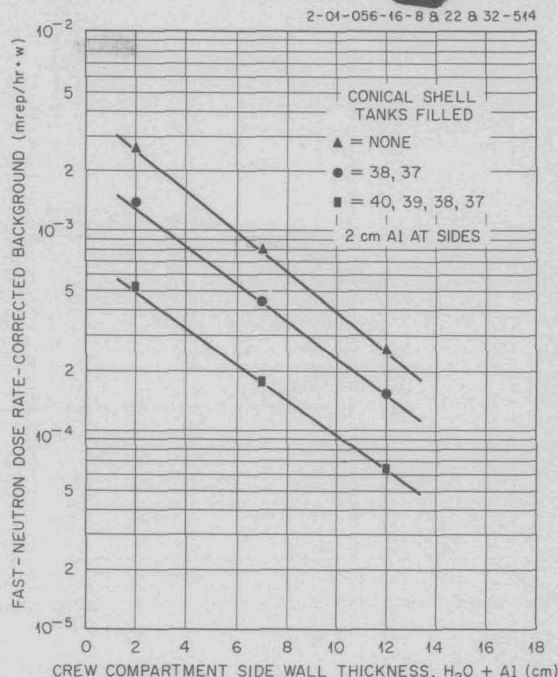


Fig. 6.2.60. Fast-Neutron Dose Rate in Boeing Crew-Compartment Mockup Resulting from Radiation from Conical Shell No. 7 as a Function of Crew-Compartment Side Wall Thickness.

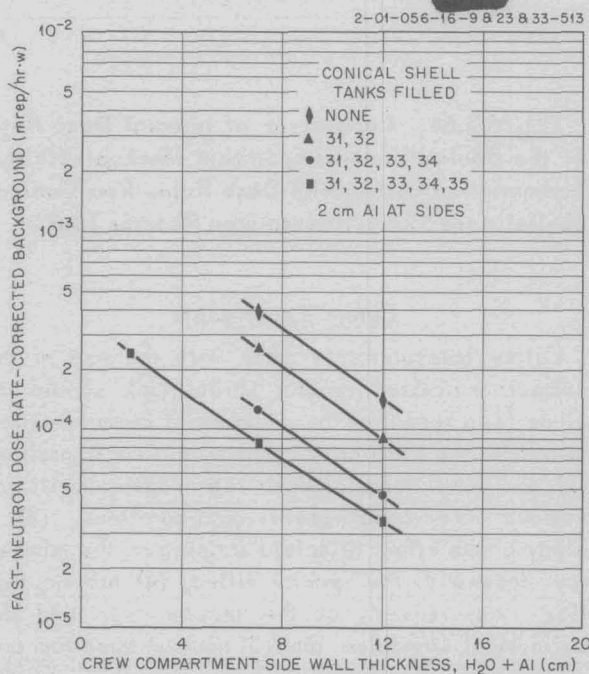


Fig. 6.2.59. Fast-Neutron Dose Rate in Boeing Crew-Compartment Mockup Resulting from Radiation from Conical Shell No. 6 as a Function of Crew-Compartment Side Wall Thickness.

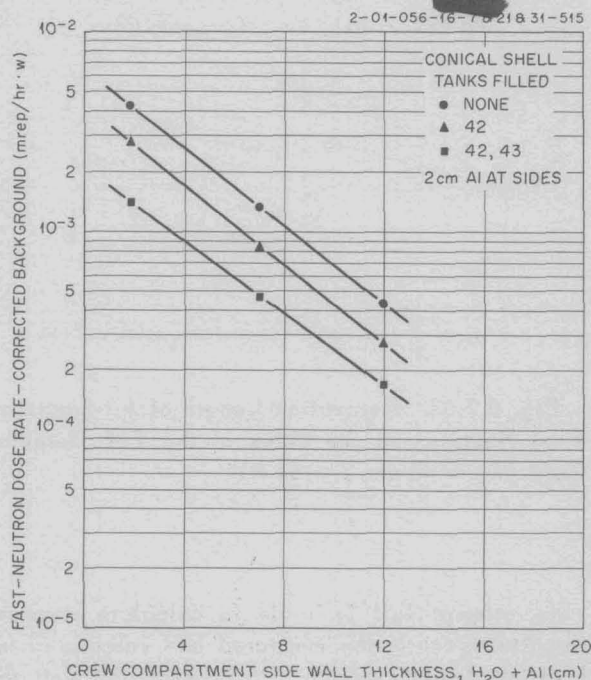


Fig. 6.2.61. Fast-Neutron Dose Rate in Boeing Crew-Compartment Mockup Resulting from Radiation from Conical Shell No. 8 as a Function of Crew-Compartment Side Wall Thickness.

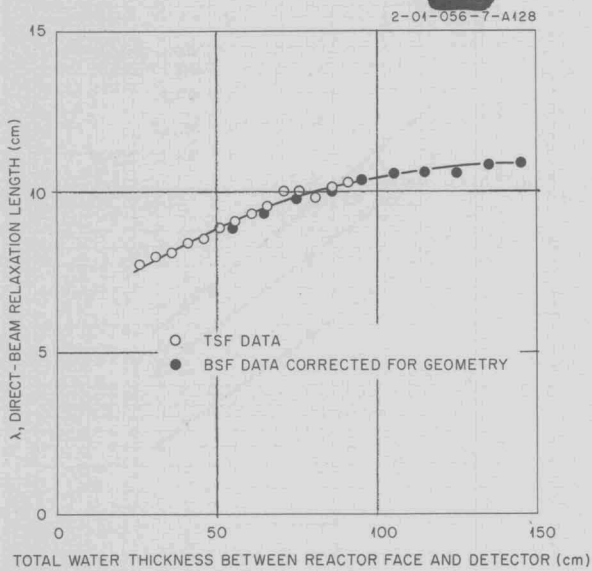


Fig. 6.2.62. Direct-Beam Relaxation Lengths for Fast Neutrons in the Water Surrounding the BSF and TSF Reactors.

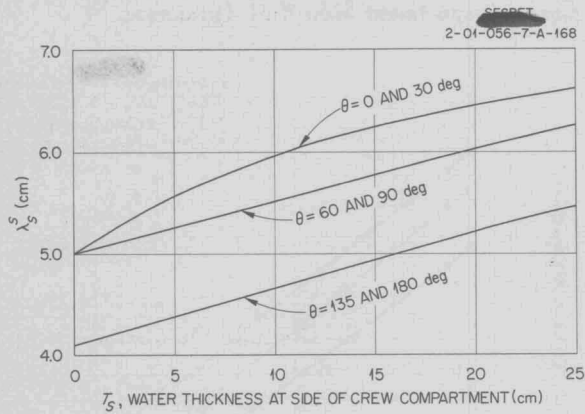


Fig. 6.2.63. Relaxation Length of Air-Scattered Fast Neutrons in the Sides of the TSF Detector Tank ( $T_n = 45$  cm,  $l = 64$  ft).

No attempt will be made to calculate absolute magnitudes until the measured and calculated relaxation lengths agree. It is expected that the magnitudes will be in good agreement, since the power distribution of the reactor (400 kw) is known.

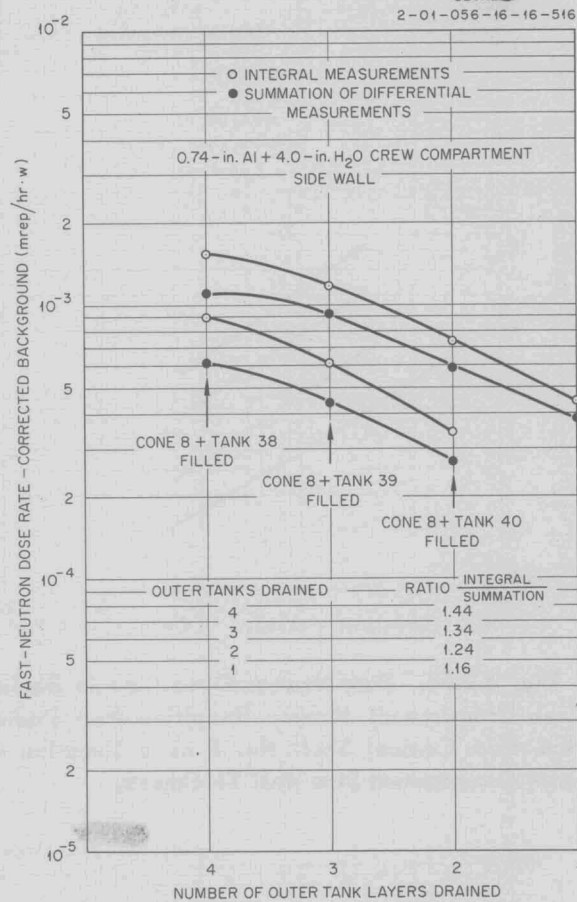


Fig. 6.2.64. Comparison of Integral Dose Rate in the Boeing Crew-Compartment Mockup with the Summation of Differential Dose Rates from Conical Shells in the Compartmentalized Reactor Tank.

Future Experiments

Future measurements made with the use of the compartmentalized reactor shield tank should include (1) a repeat of the differential beam measurements for the third crew-compartment configuration, (2) additional integral dose rate measurements for various crew-compartment configurations, (3) a study of the effect of shield shaping on the gamma-ray dose with the reactor filled, (4) fast-neutron flux measurements at the reactor face and the cylindrical standpipe, and (5) neutron spectrum and surface angular distribution measurements at the reactor shield tank and inside the crew compartment.

2-01-056-16-D-519

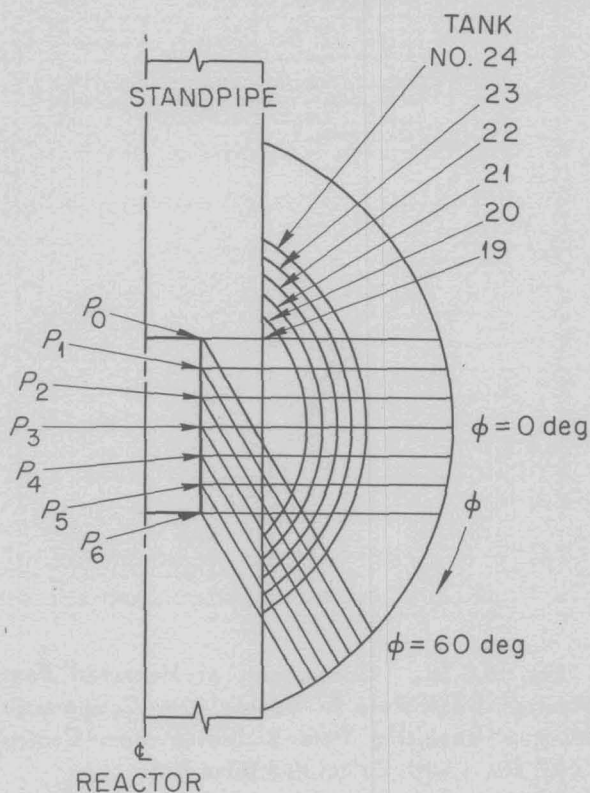


Fig. 6.2.65. Vertical Section Through Conical Shell No. 4 ( $\theta = 82\frac{3}{4}$  deg) Showing Geometry Used for a Surface Source Reactor Tank Attenuation Calculation.

DETERMINATION OF GAMMA-RAY DOSE RATES AND SPECTRA FROM SOIL AND CONCRETE SAMPLES AFTER IRRADIATION AT THE TSF

F. J. Muckenthaler      W. R. Champion<sup>14</sup>  
 J. L. Hull                  V. R. Cain

Samples of concrete and soil from Marietta, Georgia, were irradiated at the Tower Shielding Facility in order to determine the degree of activation to be expected at the Lockheed Radiation Damage Facility. Specifically, it was hoped that sufficient information would be obtained to pre-

<sup>14</sup>On assignment from Lockheed Aircraft Corp.

2-01-056-9-4-517

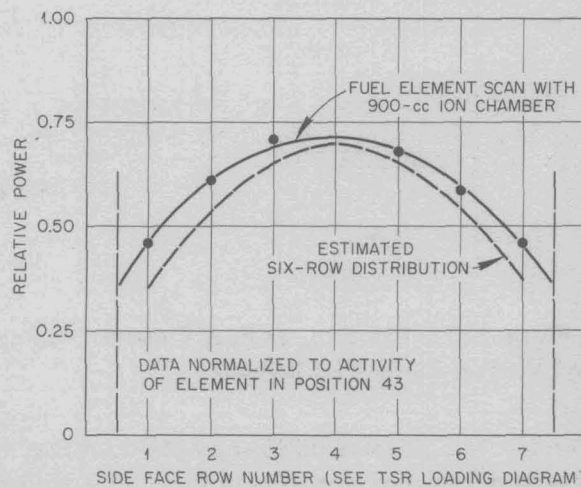
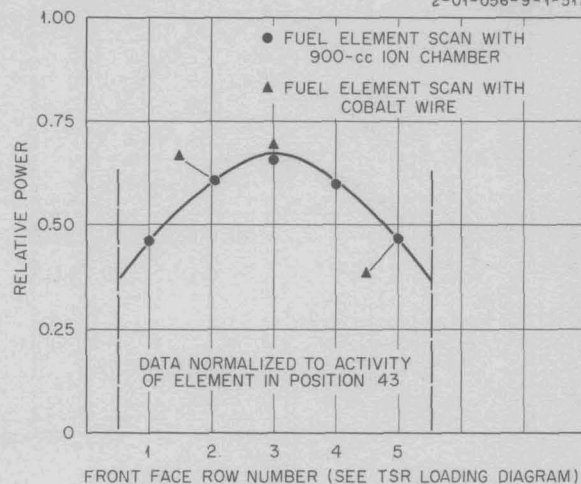


Fig. 6.2.66. Front- and Side-Face Power Distribution of the TSF Reactor.

dict the gamma-ray dose rates from such samples after they had been irradiated for as much as 100 hr.

Each sample was a 3 by 3 by 1 ft block, there being one soil sample and four concrete samples. The concrete samples consisted of plain concrete, barytes concrete, and one of each type containing an admixture of 1% boron. They were exposed for 20 hr to the radiation from the TSF reactor operating at a power of 400 kw (Fig. 6.2.69). The reactor had only 13.7 cm of water and 1/2 in. of boral as a shield, and the fast-neutron dose rate measured on top of the soil sample was 0.986 ergs/g·hr·w. The dose rate measured on top of one of the concrete



UNCLASSIFIED  
2-01-056-17-D-483

UNCLASSIFIED  
2-01-056-17-D-484

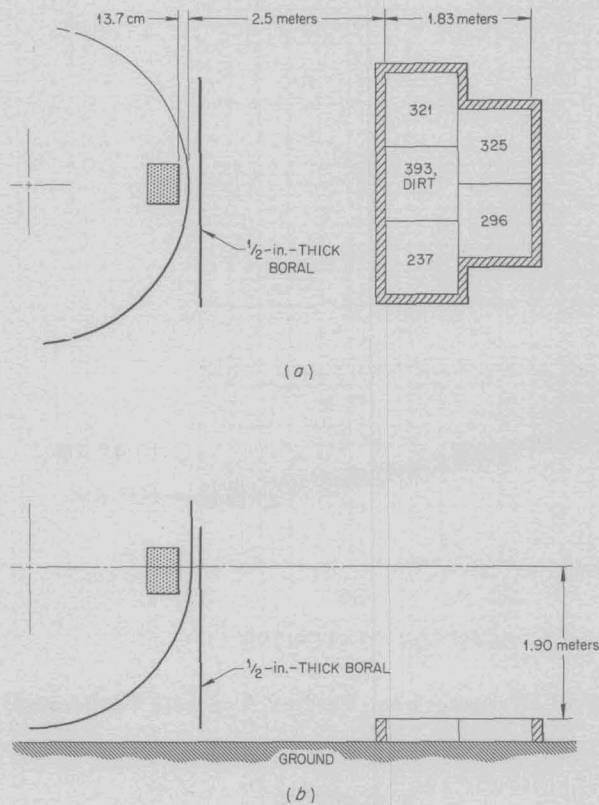


Fig. 6.2.69. Geometry for Irradiation of Concrete and Soil Samples. (a) Top view, (b) side view.

It was hoped that from these results the contribution from each element could be calculated. Owing to a very long half-life, estimated at several hundred

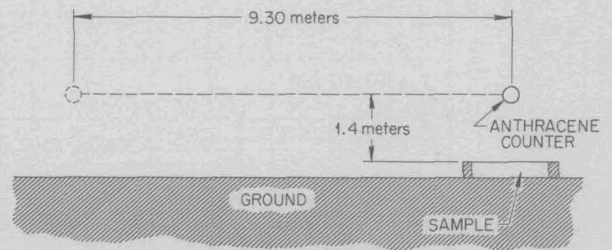


Fig. 6.2.70. Geometry for Measurement of Gamma-Ray Intensity from Irradiated Concrete and Soil Samples.

days, this analysis is not complete. It should be mentioned, however, that this long half-life appears only in the barytes concrete and soil samples.

A 3 by 3-in. NaI crystal and a 20-channel analyzer were used to measure a pulse-height spectrum of the gamma rays from the irradiated samples of plain concrete containing boron. A  $Zn^{65}$  gamma-ray source was used for calibration of the detector. The geometry for this measurement is shown in Fig. 6.2.77; the gamma-ray intensity from the sample determined the separation distance between the crystal and sample. The resulting pulse-height spectrum (Fig. 6.2.78) again indicated that, for energies above 1 Mev, the thermal  $n-\gamma$  reaction in  $Na^{23}$  is the main contributor to the gamma-ray dose rate 24 hr after shutdown.

UNCLASSIFIED  
1-01-056-17-1-(-3)-445

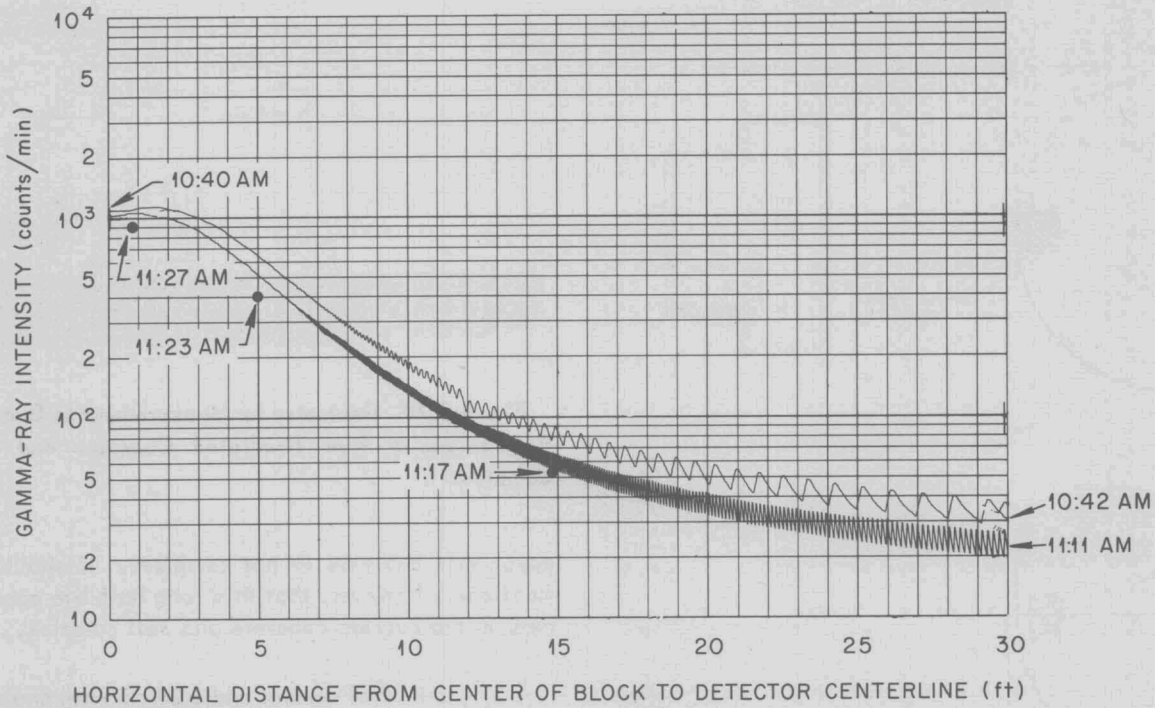


Fig. 6.2.71. Gamma-Ray Intensity as a Function of Distance from Barytes Concrete (Unborated) Sample No. 237.

UNCLASSIFIED  
1-01-056-17-5-(2)-449

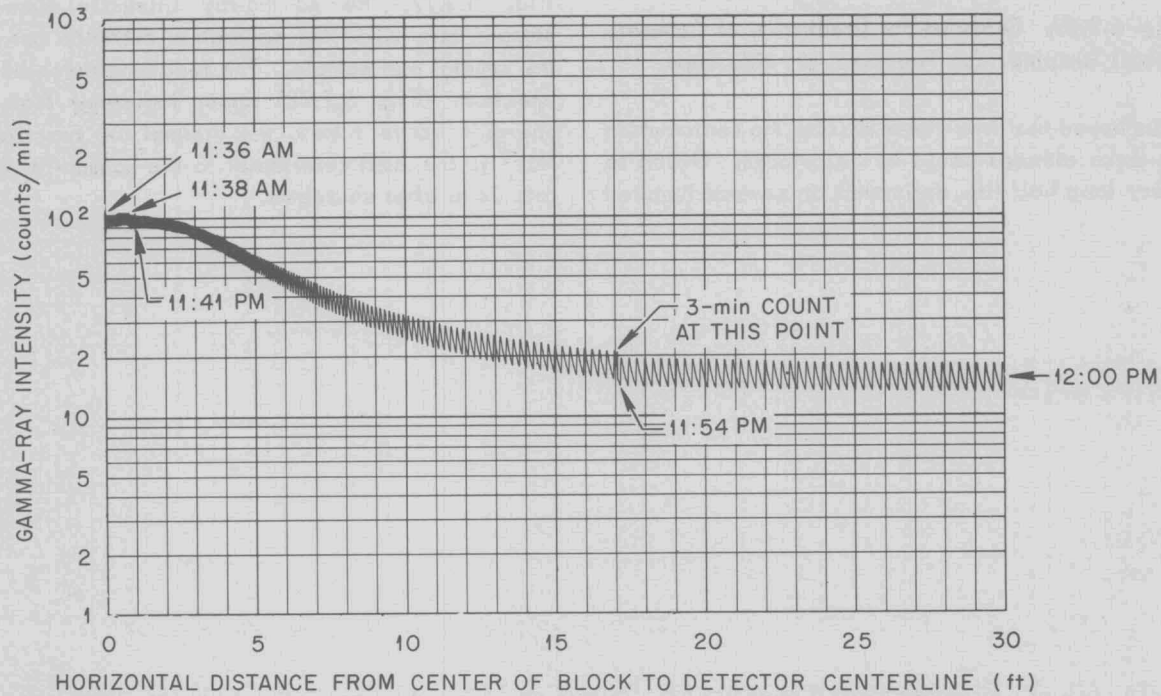


Fig. 6.2.72. Gamma-Ray Intensity as a Function of Distance from Borated Barytes Concrete Sample No. 296.

UNCLASSIFIED  
1-01-056-17-4-(2)-448

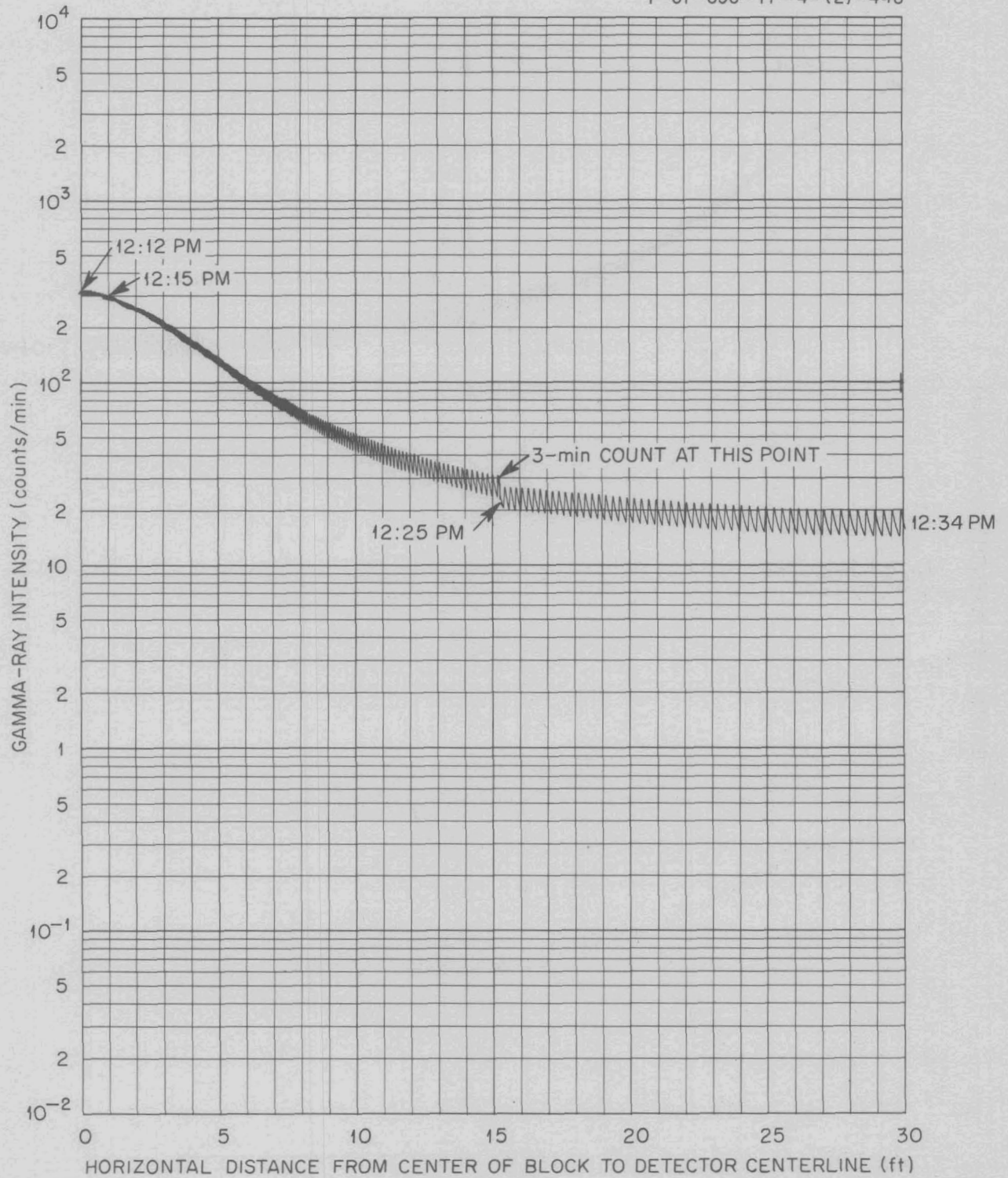


Fig. 6.2.73. Gamma-Ray Intensity as a Function of Distance from Soil Sample No. 393.

UNCLASSIFIED  
1-01-056-17-3-(-3)-447

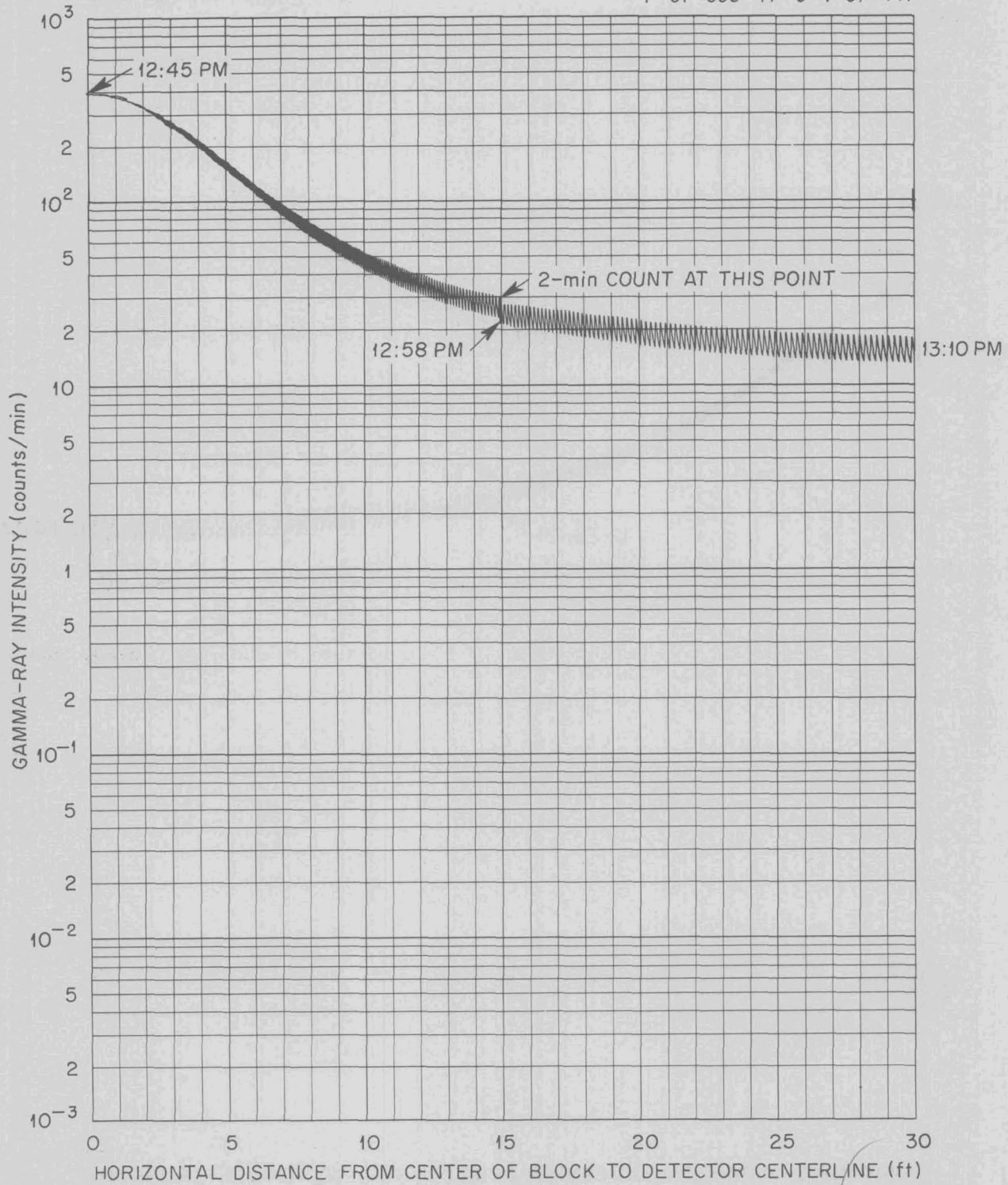


Fig. 6.2.74. Gamma-Ray Intensity as a Function of Distance from Plain Concrete (Unborated) Sample No. 321.

UNCLASSIFIED  
4-01-056-17-2-(2)-446

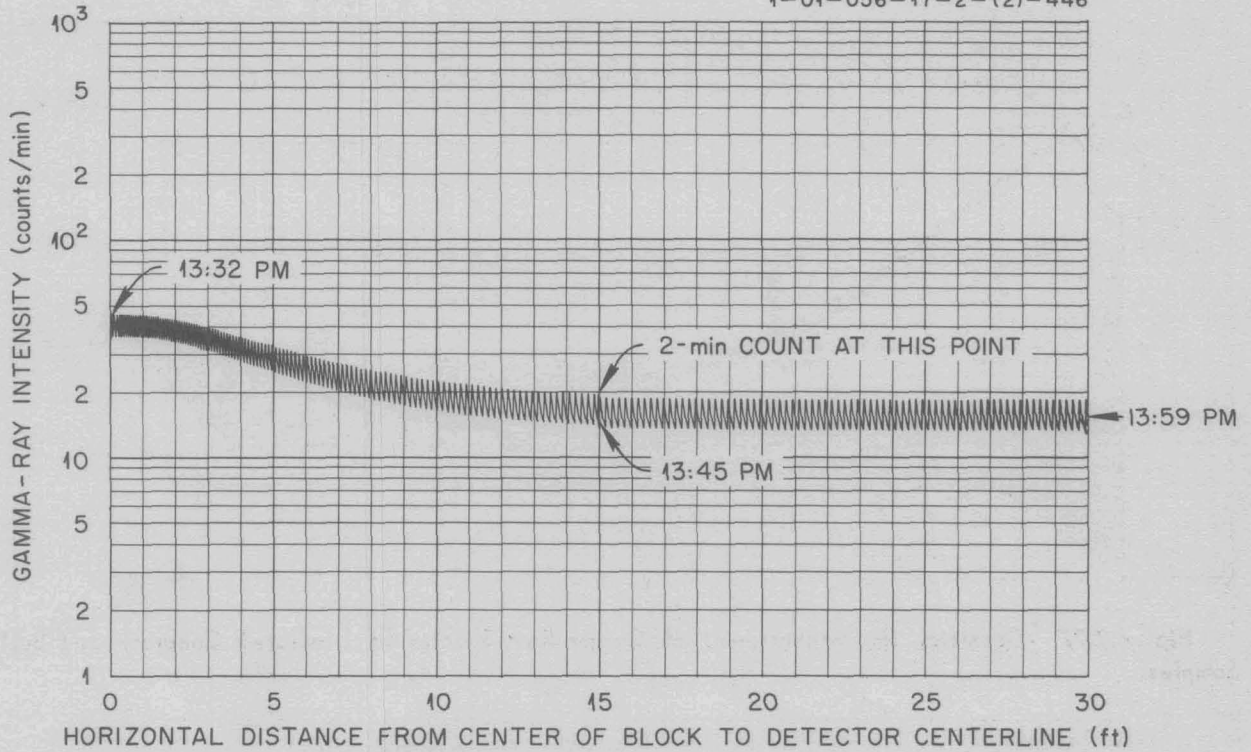


Fig. 6.2.75. Gamma-Ray Intensity as a Function of Distance from Borated Plain Concrete Sample No. 375.

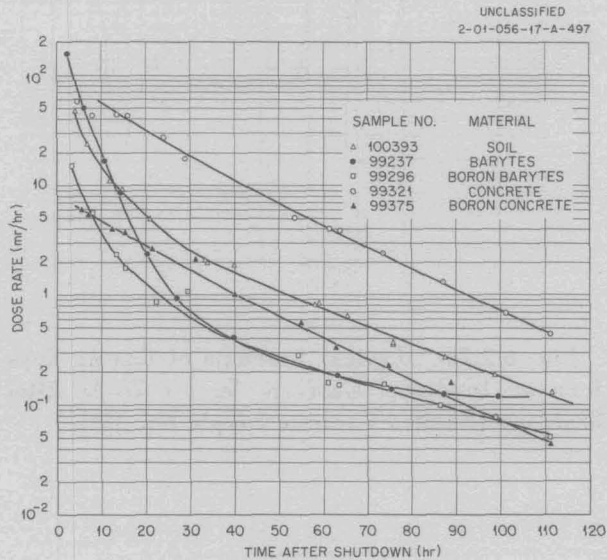


Fig. 6.2.76. Gamma-Ray Dose Rates Directly Above Irradiated Samples as a Function of Time After Shutdown.

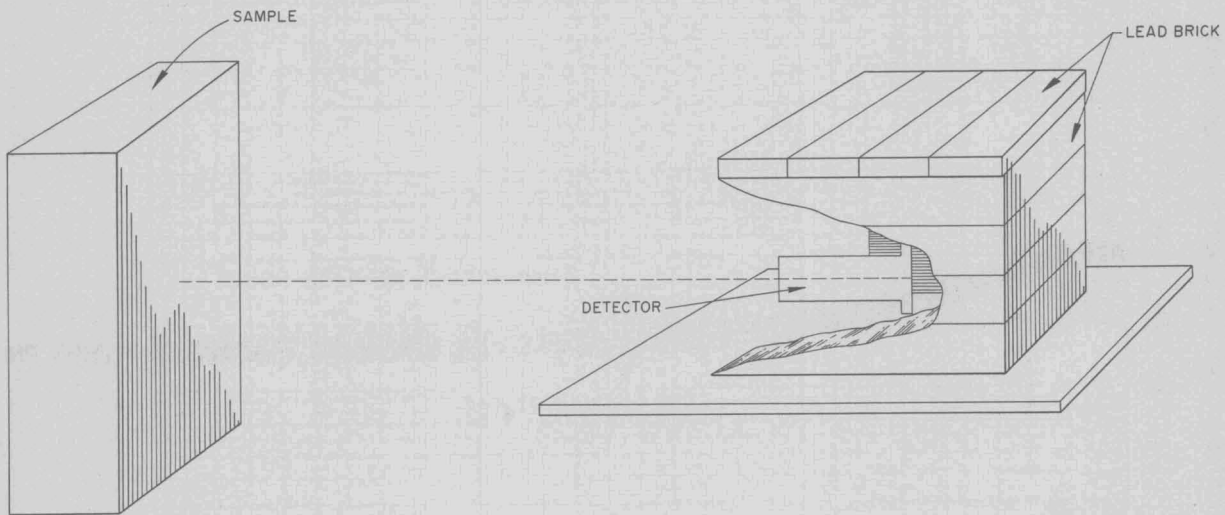


Fig. 6.2.77. Geometry for Measurement of Gamma-Ray Spectra of Irradiated Concrete and Soil Samples.

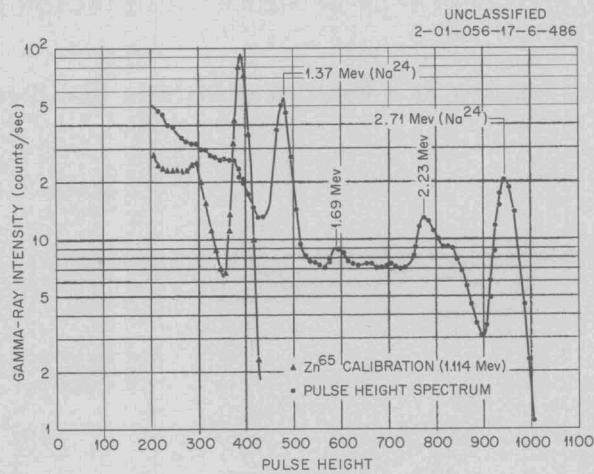


Fig. 6.2.78. Typical Spectrum of Gamma Rays from an Irradiated Concrete Sample 28 hr After Shutdown (Borated Concrete Sample No. 375).

**SECRET**

**RESTRICTED DATA**

This document contains Restricted Data as defined in the Atomic Energy Act of 1954. The unauthorized disclosure of its contents in any manner to an unauthorized person is prohibited.

**SECRET**

1

111